ABSTRACT

LACROIX, ANDREW THOMAS. Evaluation of Different Methods for Populating the LTPP Materials Database with Dynamic Modulus. (Under the direction of Dr. Y. Richard Kim).

The *NCHRP 1-37A Guide for Mechanistic-Empirical Design of New and Rehabilitated Design Structures* introduces the dynamic modulus (|E*|) as the material property to characterize asphalt concrete. This is a significant change from the resilient modulus (M_R) used in the previous AASHTO Pavement Design Guide. One of the challenges of changing the material characterization is that databases, such as the Long Term Pavement Performance (LTPP) Materials Database, contain older material characterization information. Therefore, databases must be updated to the currently accepted standard. This thesis evaluates two methods to populate the LTTP database with |E*| values: 1) determine the |E*| from different geometries (i.e., cores and prisms) and 2) predicting the |E*| from the measured M_R values in the database.

Acquiring the |E*| from existing pavements is difficult due to the standardized dimensions of the test specimen. Other geometries, indirect tension specimens and prismatic specimens, have been tested to determine if the measured |E*| is statistically different from the modulus obtained from the AASHTO TP 62 protocol. This study provides a comparison of the effects of a non-uniform state of stress and anisotropy. These effects are isolated by comparing specimens prepared by Superpave gyratory compaction and vibratory steel-wheel compaction. The results in the thesis are verified using four 12.5 mm surface course mixtures with different aggregate types and binder types, and one 25.0 mm base mixture. The results are verified using volumetric variations such as different percentage of aphalt cement and air voids. The results show that the

difference between the |E*| values obtained from different geometries is statistically insignificant. The results provide justification for using alternative methods for acquiring the |E*| experimentally, specifically from previously constructed pavements.

Practioners prefer a mathematical model since measuring the |E*| is a time and labor intensive. The second section of this thesis presents an artificial neural network (ANN) to predict the |E*| from the measured M_R. The first step is an analytical method of calculating the M_R from the |E*|. It involves the application of multiaxial linear viscoelastic theory to linear elastic solutions for the indirect tension test developed by Hondros (1959). The results show that the predicted and measured M_R values are in close agreement. The results provide a forward model for the back-calculation of the |E*| from M_R. Using this forward model, a database of measured dynamic moduli is populated with corresponding predicted resilient moduli to train an ANN. The trained ANN is the back calculation model used to predict |E*| from measured M_R. The dynamic moduli predicted from the measured resilient moduli using the trained ANN are found to be reasonable compared to the measured dynamic moduli.

Evaluation of Different Methods for Populating the LTPP Materials Database with the Dynamic Modulus

By
Andrew Thomas LaCroix

A thesis submitted to the Graduate Faculty of
North Carolina State University
In partial fulfillment of the
Requirements for the Degree of
Master of Science

Civil, Construction, and Environmental Engineering

Raleigh, North Carolina

2007

APPROVED BY:

_____	_____
Dr. Murthy N. Guddati	Dr. Roy H. Borden

_____
Dr. Y. Richard Kim
Chair of Advisory Committee

DEDICATION

This thesis is a testament to many people who have constantly encouraged me to stretch and grow as I have journied along my academic career.

The primary influence on my academic career is my parents, Michael and Carol LaCroix, who have shown me the joys of learning a multitude of topics. Probably the most important lessons were about my faith in God, which has given me the strength to keep moving even when it seemed all was lost.

Professors Fr. Thomas McShane and Dr. Michael Cherney in the Department of Physics at Creighton University have encouraged me to succeed and explore new topics such as cellular automata and encouraged me to branch out into engineering.

Dr. E. Terence Foster, a professor of Construction Systems in the College of Engineering at the University of Nebraska at Omaha who provided me with the encouragement and guidance to use my physics background as a firm grounding for the applications of civil engineering.

The final influence has been Dr. Y. Richard Kim since he was willing to take a chance to train a physics student to research transportation materials.

BIOGRAPHY

Andrew LaCroix was born in Greensboro, North Carolina to Michael and Carol LaCroix. After nine months there, his family moved to Albemarle, North Carolina, where they lived for nine years. Then the family moved to Reading, Pennslyvania, living there three years. His family then moved to Omaha, Nebraska, where he lived for ten years. Living in the Heartland of America strongly shapes who he since he completed sixth through the completion of his undergraduate degree in Omaha. The attitude of someone from the Heartland is honesty, directness, and simplicity. His attitude toward life is generally relaxed with the belief that God will provide all his needs. He graduated from Omaha Central High School in May 2001 with honors. He then remained in Omaha to attend Creighton University to earn a Bachelor of Science in Physics magna cum laude in May 2005.

After graduating from Creighton, Andrew returned to North Carolina to start graduate school at North Carolina State University. The return to North Carolina reinforced an important aspect of Andrew's life: the Korean connection. Andrew's grandparents were education missionaries to Korea from the 1950's to 1990. At North Carolina State University, Andrew found himself in good company since his advisor, Dr. Kim, and several lab partners were Korean. Also, Andrew's wife, Amanda, was adopted from Korea. The Korean connection is strong and may influence where Andrew works in the future.

ACKNOWLEDGEMENTS

The most important person to acknowledge is my wife, Amanda. Without her encouragement, patience with long and crazy hours, helping sieve, and watching movies at the CFL, the research for this thesis would not be possible. I also acknowledge my parents for their encouragement and understanding when I vented about the number of differents tasks I have done over the years.

A special thanks to Christopher Capp and Jessica Allison of Duke University for being my adopted brother and sister, especially the first year of graduate school.

The most critical group of people for accomplishing the research were my lab partners. Shane Underwood has been a great mentor, especially by challenging me to think about the problem differently and solving many mechanical problems, many times by opening the right drawer. Sangyum Lee has been a great friend who could make me smile when it was what I needed most. The graduate students of Dr. Kim's, Tae Young Yun, Cheol Min Baek, Jae Jun Lee, Ju Sang Lee, Fadi Jadoun, and Ardalan Mosavi Khandan, are appreciated for providing encouragement and coffee throughout the research process.

Several professors were instrumental in teaching me. Dr. Kim provided the needed guidance, encouragement, and big picture to complete the study. Dr. Ranji S. Ranjithan taught me the concept of ANN. Dr. Arellano guided me in using statistics to determine conclusions from a large database with several interactions.

This research is sponsored by the Federal Highway Administration under the project No. DTFH61-05-RA-00108. Its support is gratefully acknowledged.

TABLE OF CONTENTS

LIST OF FIGURES

LIST OF TABLES

CHAPTER 1 INTRODUCTION

In mechanistic or mechanistic-empirical pavement design and analysis methods, it is essential to know the properties of the layer materials. These material properties define a basic relationship between the stresses and strains in the various layers. The 1993 AASHTO Pavement Design Guide employs the resilient modulus (M_R) as the material property representing the stiffness characteristics of layer materials. The M_R is defined as the ratio between applied stress (σ_a) and recoverable strain (ε_r); that is,

$$M_R = \frac{s_a}{e_r}. \tag{1.1}$$

Several testing standards have been developed for the determination of the M_R of asphalt concrete using the indirect tensile (IDT) test method (ASTM D4123, NCHRP 1-28, SHRP P-07, NCHRP 1-28A).

One of the major changes in the recently developed *NCHRP 1-37A Guide for Mechanistic-Empirical Design of New and Rehabilitated Design Structures*, compared to the 1993 AASHTO Guide, is that the dynamic modulus (|E*|) is used as the material property to characterize asphalt concrete. This transition from M_R to |E*| may make a significant amount of the M_R data that have been collected in state highway agencies obsolete, unless a method to measure the |E*| from existing pavements is developed or a method to convert M_R values to |E*| is developed. One good example of a database with M_R values obtained from numerous cores taken from in-service pavements is the Long Term Pavement Performance (LTPP) Materials Database. This thesis evaluates two methods to populate the LTPP database with |E*| values: 1) determine the |E*| from

different geometries (*i.e.*, cores and prisms) and 2) predicting the |E*| from the measured M_R values in the database.

1.1 Measuring Dynamic Modulus with Different Geometries

The first major challenge to populating the LTPP materials database with |E*| is acquiring the material property from existing pavements. For example, the LTPP materials database has cores from many different pavements, but many cannot be cut and cored to the standard dimensions for measuring |E*|. The AASHTO TP-62 standard decribes a method to determine the |E*| and phase angle of hot mix asphalt (HMA) specimens using an axial compression load. In the standard, a specimen is a cylinder 150 mm (about 6.0 in.) tall and 100 mm (about 4.0 in.) in diameter. The height is greater than some thin pavements, which means the specimen cannot be cored from the surface of the pavement. Also, thicker asphalt concrete pavements are usually composed of several layers (such as base, intermediate, and surface layers). These layers may have different |E*| values, so the ability to characterize the |E*| for each layer from these cores is questionable.

Kim *et al*. (2004) evaluates the possibility of using IDT testing to measure the |E*| of existing asphalt concrete pavements by comparing the |E*| values from the IDT tests against those from axial compression tests on standard cylinders. Twelve asphalt mixtures were used in the verification study. Considering the fact that IDT specimens are 38 mm (1.5 in.) in thickness and can be cored from a pavement, IDT tests are a viable option for testing material properties of existing pavements. However, IDT specimens are not the only option for testing materials from pavements. Pavements can be trench cut,

and the resulting cross sections can be cut or cored into specimens similar to the axial specimens used in the AASHTO TP-62 standard. In light of this fact, a prismatic column (prism) geometry is also considered in this study.

Several challenges are addressed in Chapter Five to evaluate the possibility of accepting IDT and/or prism testing as an alternative to standard cylinder. Kim *et al.* (2004) recognized that two main differences exist between IDT and axial compression tests. One difference is the uniaxial stress state in axial compression versus the biaxial state of stress in IDT. The other difference is the relative directions of compaction and stress-strain analysis. For axial compression tests on specimens compacted by the Superpave gyratory compactor (SGC), the directions of compaction and stress-strain analysis are identical. On the other hand, SGC-produced IDT specimens are tested perpendicular to the compaction direction. In an anisotropic mixture, the aggregate within a mixture tends to have certain orientations based on the method of compaction (Hunter *et al.*, 2004, Tashman *et al.*, 2004). The anisotropic aggregate structures resulting from SGC compaction could affect the stress-strain analysis. Another source of anisotropy is the effect of SGC versus field compaction, because specimens for measuring |E*| for existing databases are removed from pavements in the field. The total difference between the field IDT and laboratory axial compression measurements could be due to the effect of anisotropy because of the differences in state of stress, different directions between the compaction and the stress-strain analysis, and/or the compaction method.

For this study, these differences are investigated along with the differences between axial and prism compression testing. The comparisons in this section are based on

recommendations in a white paper by Schwartz (2004). Chapter Five of the thesis presents experimental results to determine whether the |E*| can be measured from different geometries and compaction methods, as well as possible limitations that might exist for implementing this method as a standardized test.

1.2 Predicting Dynamic Modulus from Resilient Modulus

The LTPP materials database can be populated with |E*| values in a less rigorous, though less accurate method than measuring |E*|. Practioners desire a model to predict |E*| since measuring |E*| is a time and labor-intensive process. Currently, several predictive models of |E*| exist, such as the Witczak model (Bari and Witczak, 2007) and the Hirsch model (Christensen *et al.*, 2003). These models use a variety of inputs such as binder properties, HMA volumetrics, and aggregate information. One of the measured mixture properties available in the LTPP materials database is M_R. Therefore, is important to develop a relationship between M_R and |E*| to populate the LTPP material database with reasonably accurate values of |E*|. Such a method has further benefit since some asphalt materials and pavement analysis methods still require the M_R as an input.

M_R provides a snapshot of the material behavior under one loading history (i.e., a 0.1 second haversine loading followed by a 0.9 second rest period) at different testing temperatures (normally three temperatures at 5°, 25°, and 40°C). Most attempts to develop the relationship between M_R and |E*| so far have been empirical in nature, such as setting a correlation between |E*| and M_R values at a frequency of 5.2 Hz (Loulizi *et al.*, 2006). Other relationships involve trying to predict the material property using mechanical theory, such as two-phase micromechanical relationships (Li and Metcalf,

2005). Zhang (1996) explored the possibility of characterizing the viscoelastic properties from M_R tests using Fourier analysis. It was concluded that this type of analysis is impractical due to: 1) the difficulty in solving a large number of variables and, 2) the limited range of results, providing slightly more time-temperature characterization than M_R data. Another challenge is that Fourier analysis requires a loading and deformation history for optimizing the viscoelastic parameters, which most databases do not contain. Therefore, any attempt to predict the |E*| from the M_R is, at best, empirical in nature. The hypothesis of this study is the prediction of the M_R from the |E*| can be made using the theory of viscoelasticity.

The sixth chapter of the thesis presents an analytical approach to predict the M_R from the |E*|. Experimental results provide evidence that the concept is valid. Because the M_R of asphalt concrete is normally determined using the IDT test, analytical, viscoelastic solutions are developed for the IDT test configuration. It involves the application of multiaxial linear viscoelastic theory to linear elastic solutions for the IDT test developed by Hondros (1959). Since the ultimate purpose of this study is to populate the LTPP materials database with |E*| values, the linear viscoelastic solution is used as a forward model (*i.e.*, |E*| is used to predict M_R) for the back-calculation of |E*| from M_R.

Using the forward solution method, a database of measured dynamic moduli, such as the Witczak database, is populated with corresponding predicted resilient moduli to train an artificial neural network (ANN). Once a database is populated with predicted M_R values, predictive relationships can be developed using optimization techniques, such as the artificial neural network (ANN). The trained ANN is the back calculation model used

to predict |E*| from measured M_R. Further information regarding the use of neural networks in pavement applications can be found in Xu *et al.* (2002).

CHAPTER 2 MATERIAL PROPERTIES

2.1 Dynamic Modulus (|E*|)

|E*| is one of the three fundamental material properties that can be used in the linear viscoelastic constitutive relationship. E* is the complex modulus, which is composed of the storage and loss modulus, as shown in Figure 2.1.

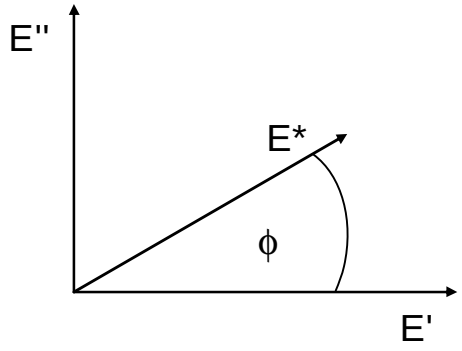

Figure 2.1 Graphical Represenation of E*.

The complex modulus, E*, is represented as follows:

$$E^* = E' + iE'', \tag{2.1}$$

where

|E*| = magnitude of E*;

E' = storage modulus = |E*| cos ϕ;

E'' = loss modulus = |E*| sin ϕ.

The storage modulus represents the storage (elastic) component of energy of the response. The loss modulus represents the damping and energy loss of the system during the material response. The other two material properties are creep compliance, D(t), and

the relaxation modulus, E(t). Due to their fundamental nature, theoretical relationships exist among these three material properties that have been proven valid for the characterization of asphalt concrete (Kim and Lee, 1995). The storage modulus (E'), can be represented in terms of a Prony series as seen in Equation (2.2). Knowing E' is important for predicting the stress response to a given strain history.

$$E'(w_r) = E_\infty + \sum_{i=1}^{n} \frac{w_r^{\,2} r_i^{\,2} E_i}{w_r^{\,2} r_i^{\,2} + 1}, \tag{2.2}$$

where

E_∞ = elastic modulus (MPa);

ω_r = angular reduced frequency;

E_i = modulus of the i^{th} Maxwell element; and

ρ_i = relaxation time of the i^{th} Maxwell element.

Since most |E*| tests are load-control tests, D(t) is needed to predict the strain response from a stress history. An exact conversion to D(t) can be obtained by solving the following equations:

$$[A]\{D\} = \{B\}, \text{ or } A_{kj} D_j = B_k \tag{2.3}$$

$$A_{kj} = E_\infty \left(1 - e^{-(t_k / t_j)}\right) + \sum_{i=1}^{m} \frac{r_i E_i}{r_i - t_j} \left(e^{-(t_k / r_i)} - e^{-(t_k / r_i)}\right) \qquad r_i \neq t_j, \tag{2.4}$$

and

$$B_k = 1 - \left(E_\infty + \sum_{i=1}^{m} E_i e^{-(t_k / r_i)}\right) \Big/ \left(E_\infty + \sum_{i=1}^{m} E_i\right). \tag{2.5}$$

where,

A_{kj} = matrix element in the k^{th} row and j^{th} column of matrix A;

B_k = vector element in the k^{th} row of vector B;

E_∞ = equilibrium modulus (MPa);

E_i = modulus of the i^{th} Maxwell element;

r_i = relaxation time of the i^{th} Maxwell element determined *a priori*;

t_j = retardation time of the j^{th} Voigt element determined *a priori*

t_k = time of interest; and

m = number of Prony coefficients.

By solving for D_j, the Prony series representation for D(t) can be determined. Equation (2.4) does not show a solution for $\rho_i = \tau_i$ since the error increases when such a case exists (Park and Schapery, 1999).

Since the behavior of viscoelastic materials is dependent on time, rate of loading, and temperature, these material properties are determined at multiple rates of loading and multiple temperatures (in degrees Celsius) as seen in Figure 2.2.

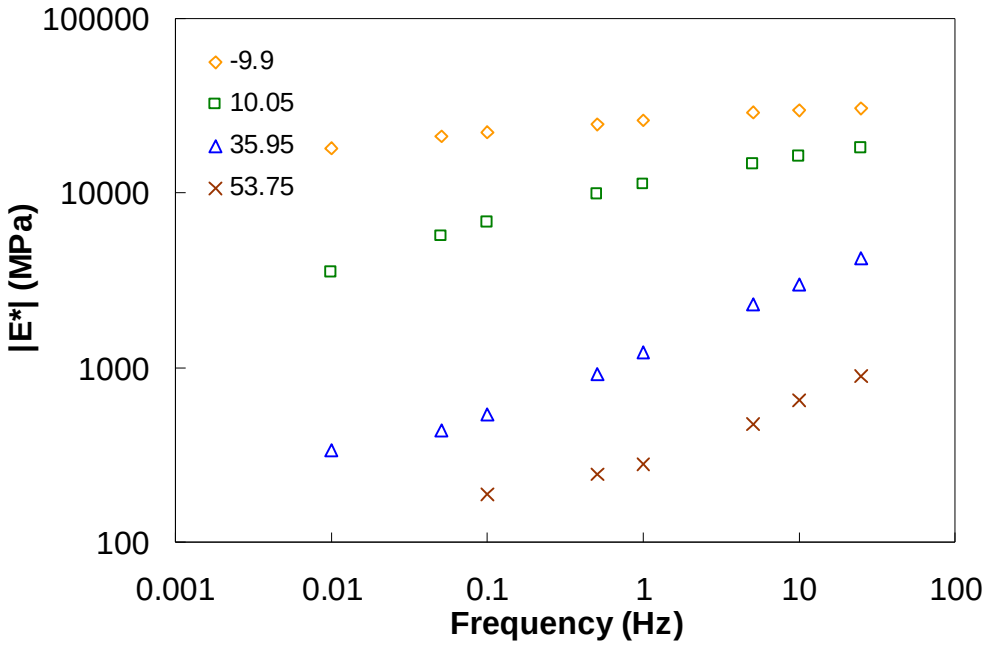

Figure 2.2 Example of measured |E*| values at different frequencies and temperatures.

A single, continous curve is developed using the time-temperature superposition principle. The principle states that rheologically simple materials, such as HMA, can be shifted in the time or frequency domain (i.e., the horizontal axis) to produce a single, continuous curve. The equation for the shifted frequency, known as the reduced frequency, is:

$$f_r = a_T f \tag{2.6}$$

where

f = frequency (Hz); and

f_r = reduced frequency.

$$\log(a_T) = a_1 T^2 + a_2 T + a_3 \tag{2.7}$$

where

a_1, a_2, and a_3 = coefficients; and

T = temperature.

The |E*| values are shifted according to Equations (2.6) and (2.7) to produce a continuous curve called a mastercurve. Before shifting, a reference temperature is selected such that $\log(a_T)$ is zero. The result is a curve that provides the relationship between shift factors and temperature as seen in Figure 2.3 with a reference temperature of 10°C.

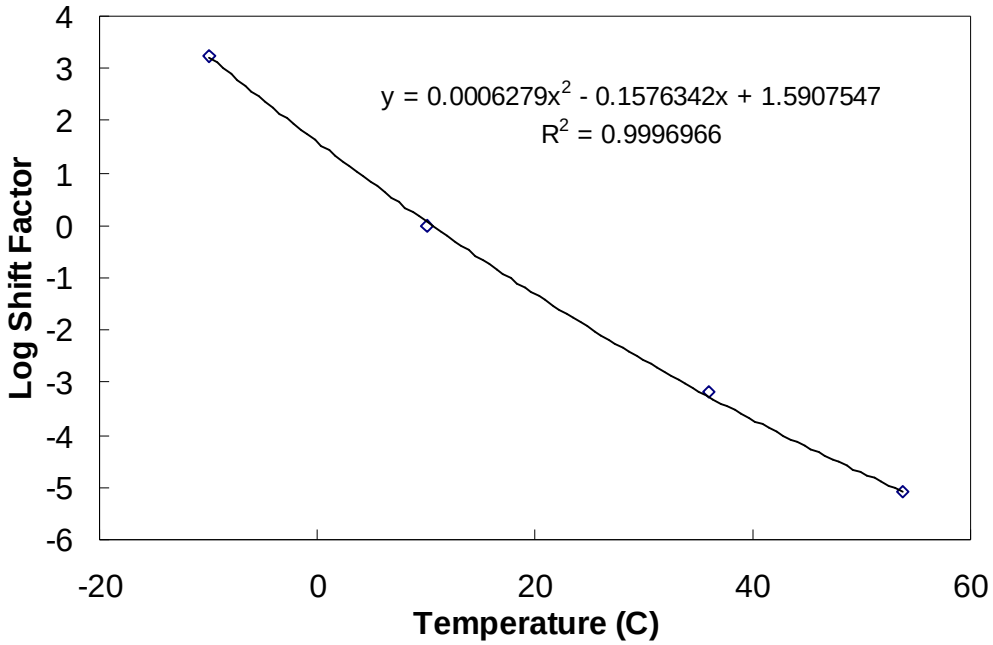

Figure 2.3 Example of a temperature shift factor curve.

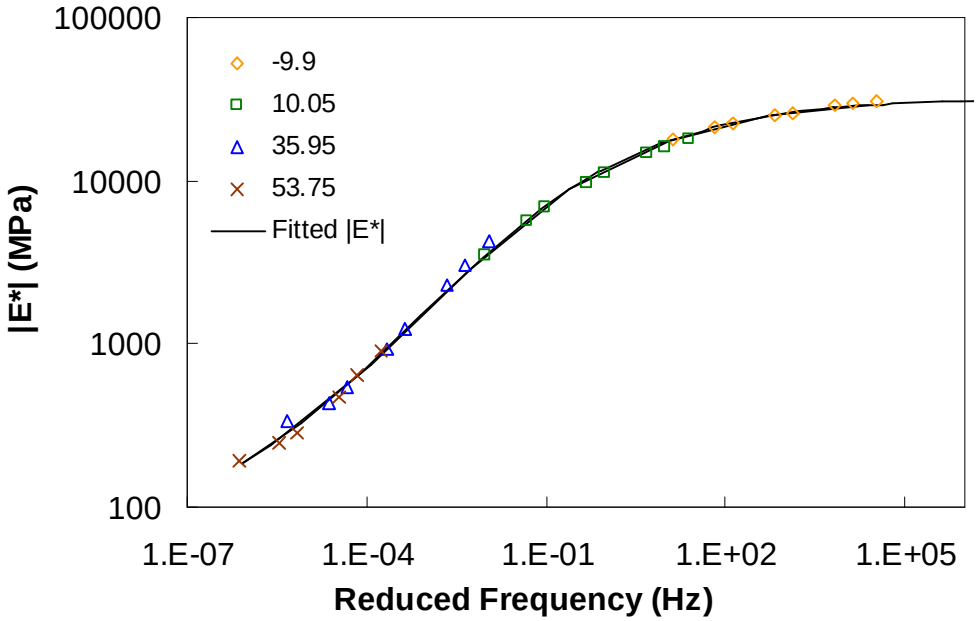

Figure 2.4 Time-temperature shifted |E*| mastercurve.

As seen in Figure 2.4, the horizontal shifting of the |E*| values in Figure 2.2 produces a mastercurve. The mastercurve is represented by a sigmoidal function, Equation (2.8), which was selected to compensate for variability that might be present in the data.

$$\log|E^*| = a + \frac{b}{1+\frac{1}{e^{c+d*\log(f_r)}}}, \tag{2.8}$$

where

a, b, c, d = constants; and

f_r = reduced frequency.

The reduced frequency represents the testing frequency needed to produce the |E*| value at the reference temperature. The benefit of time-temperature superpoisiton is the ability to predict the material response at temperatures and frequencies other than the measured values. To determine the |E*| at a different temperature and/or frequency, calculate the reduced frequency to find |E*| from the mastercurve sigmoidal equation.

2.1.1 |E| Using Axial Compression*

Axial compression is a uniaxial state of stress in the plane of loading. Axial and prism specimens are loaded in the uniaxial manner. Equation (2.9) shows the simple formulation of calculating the |E*| from uniaxial measurements.

$$|E^*| = \frac{s_o}{e_o}, \tag{2.9}$$

where

σ_o = steady-state stress amplitude; and

ε_o = steady-state strain amplitude.

The steady-state response of the material is a result of repeated sinusoidal loading. The following equation is used to calculate the steady-state response for stress and strain.

$$f(t) = a + bt + c\cos(wt + f) \tag{2.10}$$

where

f = stress of strain time history;

ω = angular frequency (radians/s);

ϕ = phase angle (radians); and

a, b, and c = fitting coefficients such that *c* is the stress or strain amplitude.

Figure 2.5 shows a steady-state response for a stress and strain time histories. The dynamic modulus test described in AASHTO TP-62 is a load-controlled test, therefore the measured response is the deformation. The last five cycles are sampled to measure the amplitude and the phase angle between the stress and strain curves

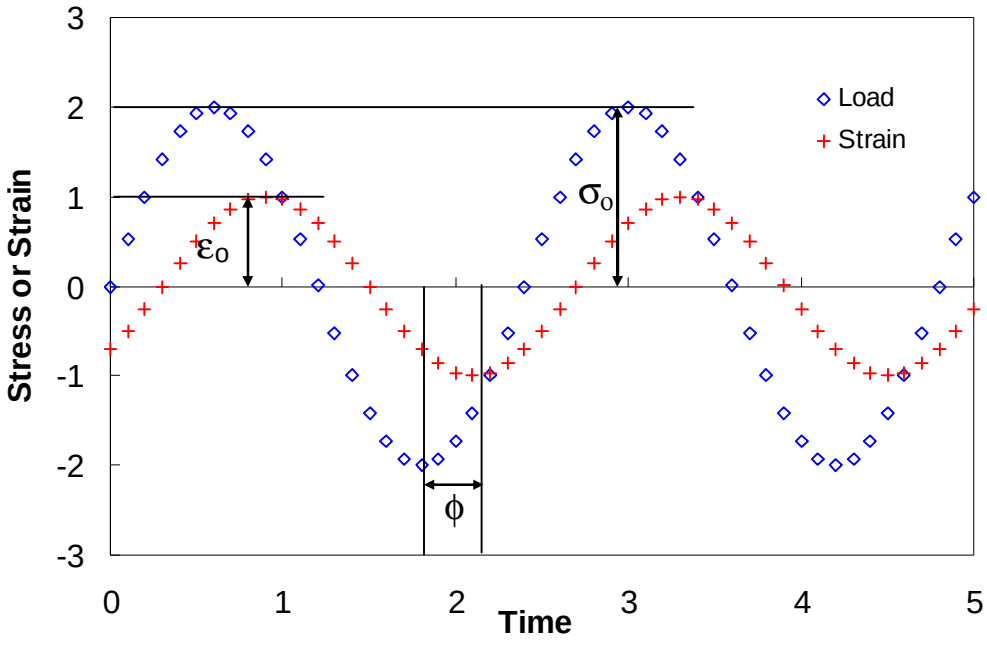

Figure 2.5 Idealized steady-state stress and strain curves with phase angle.

2.1.2 |E| Using the IDT Test*

IDT testing causes a biaxial state of stress in the plane of loading and the plane perpendicular to it on the face of the specimen. Therefore, determination of |E*| from the IDT test requires a more complex formulation than uniaxial testing (e.g., AASHTO TP-62) requires. Drescher et al. (1997) and Zhang et al. (1997) applied the theory of viscoelasticity to linear elastic solutions, developed by Hondros (1959), to develop linear viscoelastic solutions for stresses, strains, complex compliances, phase angle, and Poisson's ratio from the IDT test. The three-dimensional analysis includes calculations for deviatoric or shear stresses and volumetric stresses and strains (Drescher et al., 1997). To validate the solutions, the creep compliance from a creep test was used to calculate the horizontal and vertical displacements from a pulsed loading test, i.e., the MR test. Zhang et al. (1997) conclude that the viscoelastic solution predicted the displacements reasonably well; they recommend a further step to validate the solution, which is to test more replicates at different temperatures.

Kim *et al*. (2004) analyzed the viscoelastic material behavior under sinusoidal loading in the IDT test with the objective of developing explicit solutions for the |E*|. The developed solutions were successfully verified by comparing the |E*| values from the IDT tests against those from the axial compression tests performed in accordance with the AASHTO TP-62. Twelve asphalt mixtures were used in the verification study. Equations (2.11) and (2.12) show these solutions for |E*| and Poisson's ratio, ν. The derivation assumes a plane stress condition, which means that the specimen is thin and, therefore, the stresses along the thickness direction are zero everywhere in the specimen. This study furthers the research done by Zhang *et al*. (1997) by predicting the M_R at

multiple temperatures from the |E*| determined by the IDT test. In this study, the |E*| is calculated using the two-dimensional IDT derivation of Kim *et al.* (2004) since the M_R is calculated from two-dimensional elastic analysis.

$$|E^*| = -\frac{2P_o}{pad}\frac{b_1 g_2 - b_2 g_1}{g_2 V_o - b_2 U_o} \text{ and} \tag{2.11}$$

$$n = \frac{b_1 U_o - g_1 V_o}{-b_2 U_o + g_2 V_o}, \tag{2.12}$$

where

P_o = applied load amplitude (N);

a = loading strip width (m);

d = thickness of specimen (m);

V_o = amplitude of sinusoidal vertical displacement (m);

U_o = amplitude of sinusoidal horizontal displacement (m); and

β_1, β_2, γ_1, γ_2 = geometric coefficients.

Table 2.1 Geometry Coefficients

IDT |E*|	β_1	β_2	γ_1	γ_2
	-0.0134	-0.0042	0.0037	0.0116
M_R	k_3	K_4	k_1	k_2
	-0.00067	0.000209	-0.00018	0.000578

The coefficients in Equations (2.11) and (2.12) are listed in Table 2.1. These coefficients are based on a 152.4 mm (6.0 in.) diameter specimen with a 50.8 mm (2.0 in.) gauge length, which are the geometries used in this study. The sign convention for load, strains, and displacements is positive for tension and negative for compression.

Therefore, in the IDT test, horizontal displacements are positive while vertical displacements and compressive loads are negative.

2.2 Resilient Modulus (M_R)

M_R can be calculated by several different methods, including the ASTM D 4123-82, the NCHRP 1-28 method , the SHRP P07 protocol, AASHTO TP-31 standard, or the Roque and Buttlar equation (1992), which accounts for the bulging effects of the specimen. The NCHRP 1-28 elastic solutions are used in this paper. The equations for calculating M_R and Poisson's ratio are given as follows:

$$M_R = \frac{P}{Ud}(k_1 - k_2 n) \text{ and} \tag{2.13}$$

$$n = \frac{k_3 + k_1(V/U)}{k_4 + k_2(V/U)}, \tag{2.14}$$

where

M_R = resilient modulus (MPa);

P = applied load (N);

d = thickness of specimen (m);

U = recoverable horizontal displacement (m);

V = recoverable vertical displacement (m); and

k_1, k_2, k_3, k_4 = constants.

Equations (2.13) and (2.14) can be combined to yield the following relationship:

$$M_R = \frac{P}{Ud}\left[k_1 - k_2 \frac{k_3 + k_1(V/U)}{k_4 + k_2(V/U)}\right]. \tag{2.15}$$

These equations are based on the linear elastic solutions, developed by Hondros (1959), after accounting for the non-uniform stress and strain distributions in the IDT specimen, shown in Figure 2.6. The constants in Equations (2.13) and (2.14) are listed in Table 2.1. Note that these constants are different from the constants for |E*|, because the coefficients for M_R are derived using linear elastic theory whereas those for |E*| are derived using linear viscoelastic theory.

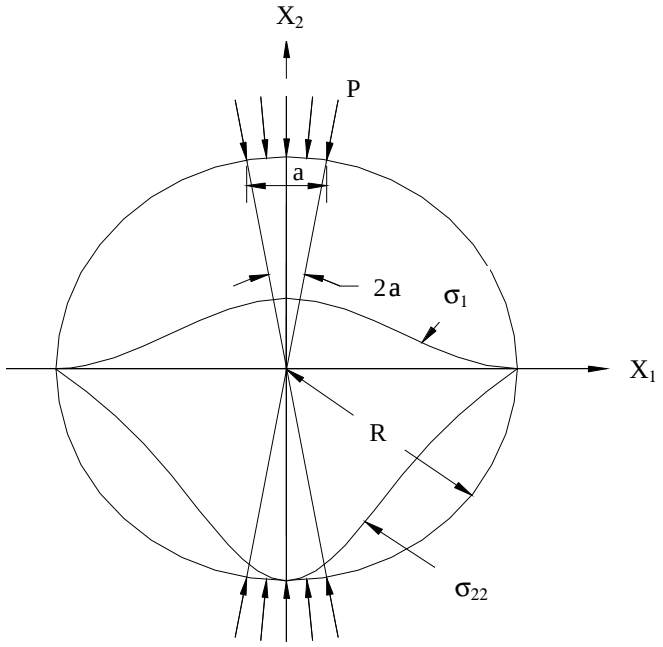

Figure 2.6 Stress distribution in the IDT specimen subjected to a strip load.

CHAPTER 3 MATERIALS AND SPECIMEN FABRICATION

The specimens in this study comprise ten different mixtures listed in Table 3.1. Five of these mixtures, S12.5C, S12.5CM, S12.5FE, S12.5F and B25.0C, have been provided by the North Carolina Department of Transportation. The first mixture is a surface mixture that has a 12.5 mm (0.5 in.) nominal maximum aggregate size (S12.5C) and coarse aggregate gradation. The granite aggregate came from a quarry in eastern Alamance County, North Carolina. The B25.0C mixture is a 25.0 mm (1 in.) nominal maximum

aggregate base mixture designed with the same aggregate and binder as S12.5C. The S12.5FE mixture was designed to match the gradation of the S12.5C but used a slate aggregate obtained from Asheboro, North Carolina. The main difference is that the slate aggregate contains a large percentage (7.7%) of the aggregate characterized as flat and elongated (S12.5FE) compared to 2.7% for the S12.5C mixture. Based on the large percentage of flat and elongated particles in the S12.5FE mixture, it is assumed that this mixture has a larger degree of anisotropy than the more cubical reference mixture (***e.g.*** S12.5C). The S12.5F mixture was a fine mixture with a large percentage (47%) by weight of aggregate of fines. The S12.5CM mixture has same gradation as S12.5C but uses a SBS modified binder with a PG grade of 76-22 from Citgo Savannah. The other five mixtures were used to evaluate systemic volumetric variations. In these cases, the reference mixture for this project, S12.5C, was adjusted to add or subtract air void (AV) or asphalt content (AC).

Table 3.1 Summary of Asphalt Mixtures

<table>
<tr><th>Mix</th><th>% AV</th><th>% AC</th><th>Asphalt Grade</th><th>NMSA</th><th>Gradation</th></tr>
<tr><td>S12.5C</td><td>4</td><td rowspan="3">5.5</td><td rowspan="4">PG 64-22</td><td rowspan="8">12.5 mm</td><td rowspan="7">Coarse</td></tr>
<tr><td>S12.5C-AV+2</td><td>6</td></tr>
<tr><td>S12.5C-AV-2</td><td>2</td></tr>
<tr><td>S12.5C-AC+1</td><td>4</td><td>6.5</td></tr>
<tr><td>S12.5C-AC-1</td><td>4</td><td>4.5</td></tr>
<tr><td>S12.5CM</td><td>4</td><td>5.5</td><td>PG 76-22</td></tr>
<tr><td>S12.5FE</td><td>4</td><td rowspan="2">5.7</td><td rowspan="3">PG 64-22</td></tr>
<tr><td>S12.5FE-AV+3</td><td>7</td></tr>
<tr><td>S12.5F</td><td>4</td><td>4.8</td><td>Fine</td></tr>
<tr><td>B25.0C</td><td>4</td><td>4.9</td><td>25.0 mm</td><td>Coarse</td></tr>
</table>

The target air voids for most of the mixtures was 4% ± 0.5%. The binder for all mixtures, except S12.5CM, is a PG 64-22 acquired from Citgo in Wilmington, North Carolina. The mixing temperature is 158°C (316°F) and the compaction temperature is 145°C (293°F). The S12.5CM uses a SBS-modified binder with a PG grade of 76-22 from Citgo in Savannah. The mixing and compaction temperatures are the same as those of the other binder.

An important component of this study is the evaluation of different compaction methods, as seen in Table 5.1. For a majority of the specimens, the mixtures were compacted using the SGC. Three different specimen geometries were produced using the SGC: cylindrical specimens according to AASHTO TP-62 specifications (axial), prismatic column specimens (prism), and short cylinders for IDT testing. The initial specimen geometries were cut to the final dimensions listed in Table 5.1. The prism dimension of 70 mm corresponds to a side of a square that has a diagonal of 100 mm. The diagonal length was chosen to eliminate the need to produce or modify metal endplates for 100 mm diameter axial specimens. This decision is important for acceptance by practitioners because equipment such as the Simple Performance Tester (SPT) are readily available. Also, the thickness allows the specimen to be easily removed from a 100 mm (4.0 in.) layer, which is a typical thickness for thin pavements. Two IDT specimens, each with a diameter of 150 mm and a thickness of 38 mm (1.5 in.), were cut from the initial specimen. The thickness of the specimens was selected to balance the need for 1) a thin specimen to meet the plane stress assumption in the viscoelastic |E*| solutions and 2) a RVE in the diametral direction needed to test mixtures with large

aggregates. Roque and Buttlar (1992) suggest 25 mm as the ideal thickness of IDT specimens based on three-dimensional finite element analysis. However, 25 mm is not thick enough to meet the conventionally accepted RVE requirement of the minimum dimension to maximum aggregate size ratio of three for even 12.5 mm mixes. 38 mm is higher than the ideal thickness necessary to satisfy the plane stress condition, but was selected in this study based on the consideration of the RVE requirement.

The other compaction procedure was to compact a slab to reproduce the field environment. The mold was a steel frame with the dimensions of 61 by 60 cm placed on top of a sheet of plywood covered with a ¼ in. sheet of aluminum. The mold was divided into six sections in order to extract one IDT and prism sample from each section. The compactor was a steel wheel compactor with a vibratory rear wheel.

Several differences exist between the slab produced by the steel wheel compactor and the standard method (AASHTO T 312) of preparing and compacting a specimen using the SGC. To produce a large quantity of mixture (≈ 100 kg) for a slab, the mixture was divided into smaller equal batches of approximately 6.5 kg for production. Each batch was aged for 4 hours at 135°C (275°F) and combined into 8 pans of specific masses. After mixing, the slab materials were cooled and stored in pans covered with aluminum foil and plastic wrap to reduce further aging. Once enough mixture was produced, the 8 pans were heated from room temperature to the compaction temperature (149°C) for 3 hours. The S12.5FE mixture was compacted a few days after mixing, whereas the S12.5C mixture was stored in sealed pans for almost two months before compaction.

To prepare for compaction, the mold was placed inside the building to reduce environmental effects such as the intensity of the sun and the temperature. The first layer was placed in the cool mold by pouring the material into the pre-marked quadrants. After pouring the mixture into the mold, a hand rake was vigorously worked into the mixture to settle and level the mixture. Compaction began immediately after mixture placement. The first layer was lightly compacted to stabilize the structure and prevent shoving. While the top layer was scarified to produce a continuous layer, the second layer mold and ramps were added to compact the second layer. The second layer was placed like the first layer while the first layer was still hot (> 100°C). The first and second lift heights were both 5 cm (about 2.0 in.). The total structure height after placing the second lift was 10 cm (about 4.0 in.). Due to the difficulty in compacting a thick, continuous layer, the air voids of the slabs were not equal to 4%. The S12.5C and S12.5FE slabs had samples with 6% and 7% air voids, respectively.

CHAPTER 4 TESTING PROGRAM

4.1 Geometry Comparisons

The testing procedure for the axial and prism specimens was similar, but slightly different from the IDT |E*| testing. In both cases, loose-core type LVDTs were mounted to the specimen surface to record specimen deformations. The LVDTs for the axial specimens were placed 90° apart from each other. For the prism specimens, the LVDTs were placed at the center of each face. Both axial and prism specimens had a gauge length of 100 mm (about 4.0 in.). Measurements of both horizontal and vertical deformations were taken on the front and back faces of the IDT test specimens. Two LVDTs were mounted on the

front surface, one vertically in the plane of the center of the loading strip and one rotated 90° from the vertical plane at a gauge length of 50.8 mm (2.0 in.). The same set-up was repeated on the back of the specimen but with the position of the horizontal LVDT flipped 180° so that both horizontal wires extended from the specimen on the same side, as seen in Figure 4.1.

The other difference between the two tests is the difference in loading device. Testing the axial and prism specimens requires contacting the loading plates and applying sinusoidal loading up to 25 Hz. IDT testing requires a device to hold the specimen and apply strip loading. Once the specimen has been prepared, the specimen is placed in the Load Guide Device (LGD), developed from the Strategic Highway Research Program (SHRP). The NCHRP 1-28 study recommends using the SHRP LGD because its two columns provide stability to prevent the specimen from rocking without causing significant friction between the guide posts and the upper loading plate (Barksdale ***et al.***, 1997). The first step of the set-up procedure is to align the rod to prevent unequal loading of the front versus the back. Experience showed that allowing the rod to align itself while applying a load to an aluminum specimen was the best solution. A centering device was used to ensure consistent results in the alignment of the specimens with the loading strips.

(a)

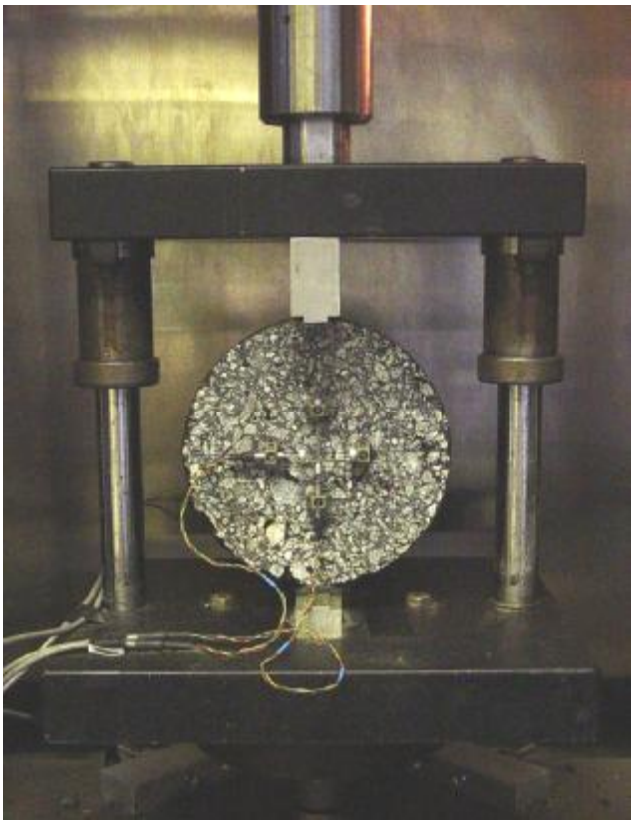

(b)

Figure 4.1 (a) Surface-mounted LVDTs and (b) IDT test setup with SHRP LGD.

The testing was carried out using a closed-loop servo-hydraulic machine with a 25 kN (5.62 kip) load cell. A temperature chamber with refrigeration and heat was used to

control the temperature during the tests. A dummy asphalt concrete specimen with the same dimensions as the test specimens was used to monitor the temperature of the test specimens. The loading histories for the |E*| of all tests consisted of eight frequencies (25, 10, 5, 1, 0.5, 0.1, 0.05, 0.01 Hz) at three temperatures (-10, 10, and 35°C). Axial and prism specimens were also tested at the first six frequencies at 54°C. IDT testing did not include this temperature due to increased punching shear under the loading strip. The load levels were adjusted to keep the strains below 75 microstrains for the axial and prism specimens. In the IDT |E*| test, the target for horizontal strains was 30 microstrains which resulted in 60 to 100 microstrains vertical strains depending upon the temperature and Poisson's ratio. It is important to note that the strain levels chosen to limit the material to a linear viscoelastic response are based on experience. Other studies have tested specimens at higher strain levels, which might produce different results.

4.2 Comparison Between |E*| and M_R

IDT |E*| testing and IDT M_R testing were both conducted following the same set-up procedure. The difference between the two tests is the difference in loading sequence and temperatures. The loading histories for the |E*| and M_R tests are summarized in Table 4.1. Testing the |E*| at different temperatures than the M_R demonstrates the strength of time-temperature superposition. It is noted that the recommended gauge length used for acquiring the deformations is varies standard to standard. Therefore, the geometry constants in the |E*| and M_R equations must be recalculated for the gauge length that is specified in each standard.

Table 4.1 Comparison of Loading Histories for IDT |E*| and M_R

Test Type	Test Temperatures (^oC)	Loading History	Frequency (Hz)
|E*|	-10, 10, 35	Sinusoidal	25, 10, 5, 1, 0.5, 0.1, 0.05, 0.01
M_R	5, 25, 40	Haversine Pulse	10 Hz (0.1s) Pulse, 0.9 s rest period

In the IDT |E*| test, the load amplitude used at the beginning of this research was adjusted to target 60 to 80 microstrains in the horizontal direction (i.e., ε_{11}) of the center of the specimen. However, this load resulted in a large vertical displacement, which caused a slight shear deformation under the loading strip. Therefore, the load level was reduced to induce 60 to 100 microstrains in the vertical direction (i.e., ε_{22}) of the center of the specimen. This reduced load level, however, yielded a smaller horizontal strain and a lower signal-to-noise ratio that made the analysis more difficult. It is interesting to note that the resulting |E*| mastercurves obtained from these two different load levels are not statistically different. In the IDT M_R test, the load levels that yield vertical strains between 60 to 80 microstrains were used.

The data were acquired using LabVIEW software and a National Instruments board. The data acquisition rate was one thousand points per second. The rate was chosen to have 100 points for the 0.1 second haversine pulse in M_R testing.

CHAPTER 5 MEASURING DYNAMIC MODULUS WITH DIFFERENT GEOMETRIESEQUATION CHAPTER (NEXT) SECTION 1

5.1 Method

To evaluate the challenges set out in the Introduction, several comparisons are necessary to account for interaction effects. The questions to answer are:

1. Do IDT and axial testing procedures produce the same |E*| mastercurve?
2. What is the magnitude of anisotropic effects?
3. What are the geometry influences for prism versus axial specimens?
4. What are the differences in IDT |E*| measured from SGC versus slab specimens?
5. Do the non-uniform stress and strain fields in IDT testing influence the measured |E*| values?
6. Are prism and IDT specimens of adequate size to test large aggreage mixtures?

Table 5.1 provides an overview of the mixtures, geometries, and compaction methods used in this study for the comparisons.

Table 5.1 Summary of Completed Test and Specimen Fabrication Methods

	Test Type				
	Axial Compression |E*|			IDT |E*|	
Test Specimen Geometry	Cylinder	Prismatic Column		Disk	
Specimen Type	Axial	Prism		IDT	
Original Specimen Geometry	Cylinder	Cylinder	Slab	Cylinder	Slab
Original Specimen Dimensions	150 mm diameter, 178 mm height		600 mm by 600 mm by 100 mm	150 mm diameter, 120 mm thickness	600 mm by 600 mm by 100 mm
Specimen Final Dimensions	100 mm diameter, 150 mm height	70 mm length, 70 mm width, 150 mm height		150 mm diameter, 38 mm thickness	
Compaction Method	SGC		Rolling-Wheel	SGC	Rolling Wheel
Mixture Type	Number of Replicates				
S12.5C	4	5	-	4	-
S12.5C-AV+2	3	-	3	3	3
S12.5C-AV-2	4	-	-	3	-
S12.5C-AC+1	3	-	-	4	-
S12.5C-AC-1	3	-	-	3	-
S12.5CM	3	-	-	4	-
S12.5FE	3	3	-	5	-
S12.5FE-AV+3	-	-	3	4	4
S12.5F	4	-	-	3	-
B25.0C	3	3	-	4	-
Total	30	11	6	37	7

Mixture types described in Table 3.1

5.2 Discussion of Results

Several comparisons mentioned earlier are necessary to determine if IDT and prism specimens are acceptable alternatives to the standard axial specimen. The evaluations are categorized as: 1) geometry, 2) non-uniform stresses and strains, 3) anisotropy, and 4) representative volume element (RVE). Throughout this section, the labels of each specimen and geometry type are represented by two letters. The first letter represents the compaction method, i.e., (S)GC and (R)olling-wheel; and the second letter represents the geometry, i.e., (A)xial, (P)rism, and (I)DT.

Theoretically, testing specimens with different geometries should produce the same values, provided the material is tested in the range of linear viscoelastic behavior and has the appropriate RVE. The study by Kim et al. (2004) presents a comparison of IDT and axial mastercurves. The conclusion is that IDT and axial geometries produce similar mastercurves a majority of the time. Therefore, the expected outcome of this study is a similarity between the mastercurves generated by the two different geometries.

Due to the specimen-to-specimen variability, statistical methods are used to determine if the mixtures are similar or different. The statistical test chosen for the comparison is the equal variance two-tailed paired t-test. The null hypothesis is that the axial and IDT mastercurves are the same. The test is performed at six testing conditions, (10 and 0.1 Hz at -10, 10, and 35°C), to evaluate different regions of the curve. These frequencies are denoted as fq1 – fq6, representing 0.1 Hz at 35°C to 10 Hz at -10°C (*i.e.*, smallest to largest reduced frequency). The data were generated by fitting the measured data for each

replicate with a sigmoidal curve based on a shift factor curve referenced to 10°C. Then, the |E*| values for the six frequncies were predicted using the conditions above.

One problem with using multiple t-tests to evaluate data is an increased probability of finding significance when significance does not exist or finding Type I error in the statistics. Therefore, the data were evaluated using a multiple test p-value adjustment method, which helps adjust the p-values of the t-test for Type I errors. The method used in this study is the stepdown bootstrap method. This method involves generating a pseudo data set by sampling from the input data. The dataset is evaluated using the paired t-test. These steps are repeated many times to generate a population of comparisons. The adjusted p-value is the proportion of the population of comparisons that is less than or equal to the original p-values (SAS Institute, 2004). Of the multiple test methods, this stepdown bootstrap method is most likely to show significance, indicating a difference between sample groups. One challenge with using this method is that it determines significance based on the pooled variances of all the inputs. Some comparisons involve one set of data with low variability at one frequency and high variability at another frequency, such as seen in Figure 5.1 and Figure 5.2. These graphs allow observations of the variability of the data, and any difference between IDT and axial values. Overall, the variability is similar between geometries except for a few cases such as S12.5FE IDT (Figure 5.2b). This difference means that some p-values would be more precise than others.

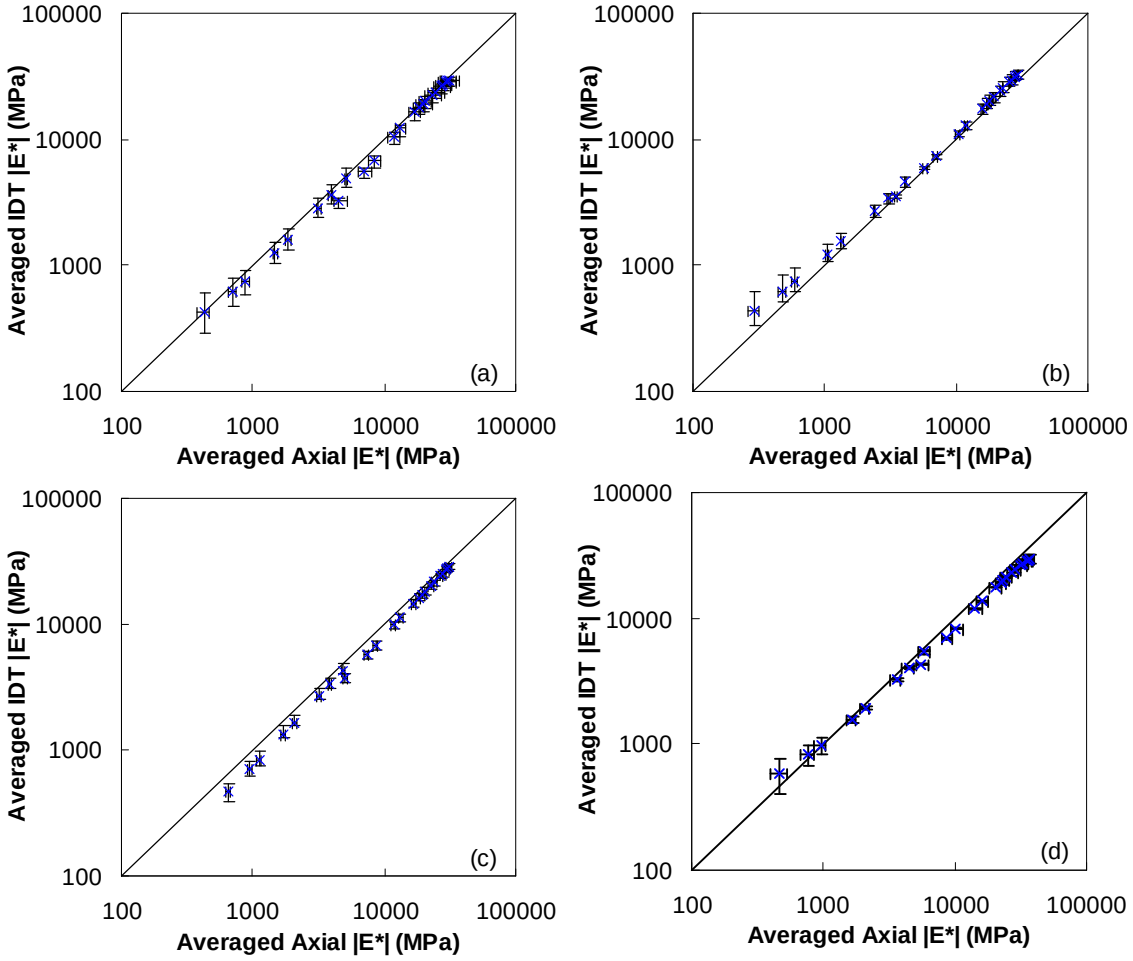

Figure 5.1 Log-log line-of-equality of SA and SI |E*| values for (a) S12.5C, (b) S12.5FE, (c) S12.5CM, and (d) S12.5C-AV-2.

To compensate for this effect, the standard deviation was determined for each frequency. The standard devations from each mixture for a given specimen geometry were averaged. The assumption is a given testing method has a normal variability. Sometimes the variability between replicates is small, other times it is large, but the variability of the test method should not change. The statistical tests were performed on the averaged value plus/minus one averaged standard deviation. The standard deviation was largest to smallest: axial, IDT, prism. The averaged standard deviation is approximately a 15% deviation from the average. The following discussion focuses mainly on whether a

statistically significant difference exists between the methods. Graphical comparisons are presented to support the statistical results.

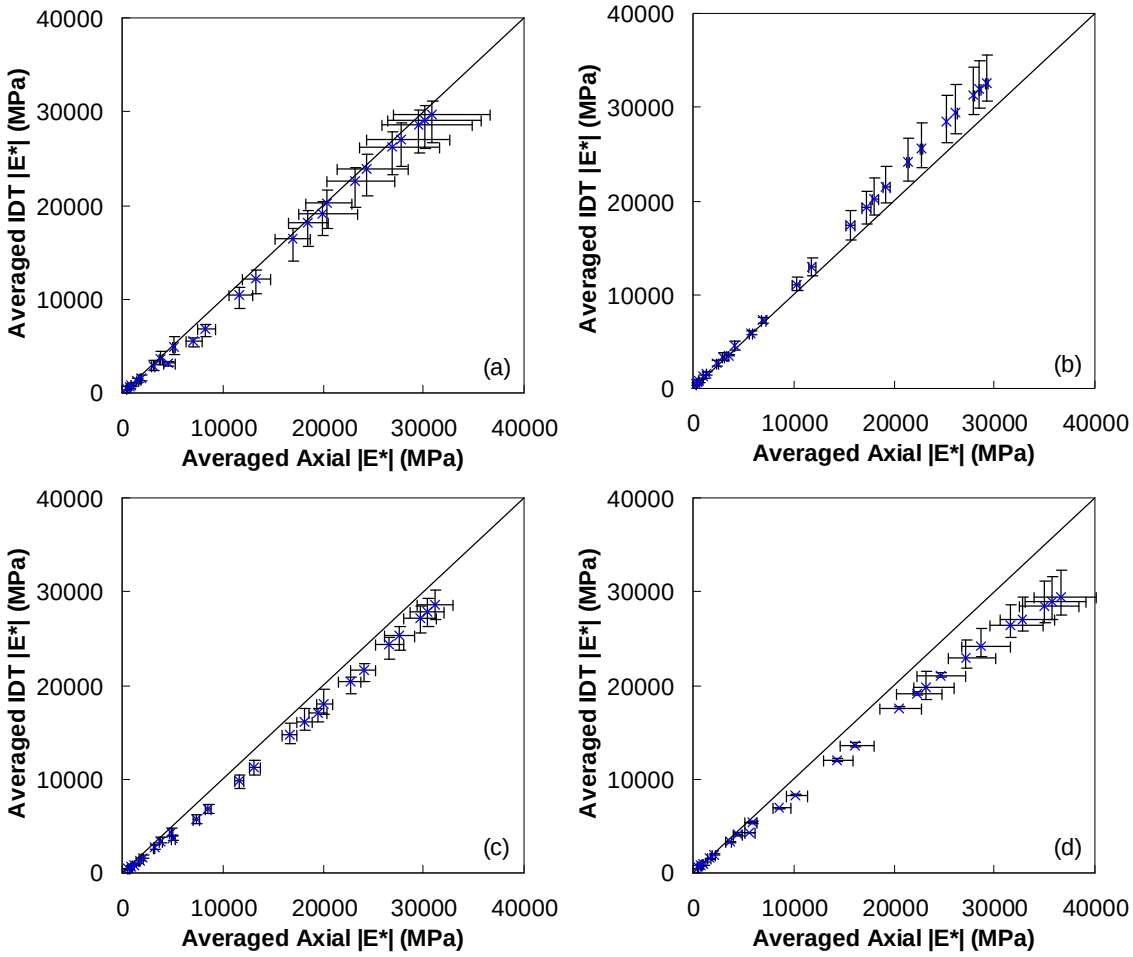

Figure 5.2 Line-of-equality of SA and SI |E*| values for (a) S12.5C, (b) S12.5FE, (c) S12.5CM, and (d) S12.5C-AV-2.

Figure 5.1 and Figure 5.2 provide evidence that axial compression and IDT measurements produce similar |E*| values. In these graphs, note that the data series represents the averaged values. Since data points were not measured at exactly the same temperature, the points are the average of linearly interpolation from the different reduced frequencies corresponding to the measured temperatures. The error bars

represent the maximum and minimum |E*| values from these replicates. The number of replicates used is shown in Table 5.1.

5.2.1 Geometry Comparisons

Table 5.2 Statistical Results for Geometry Comparisons

			Stepdown Bootstrap p-value					
Evaluation	Comparison	Mixture	fq1	fq2	fq3	fq4	fq5	fq6
IDT Procedure	SA vs SI	S12.5C	0.60	0.83	0.20	0.81	0.92	0.69
		S12.5C-AV+2	0.11	0.32	0.20	0.15	0.070	0.13
		S12.5C-AV-2	0.85	0.34	0.066	0.065	0.067	0.041
		S12.5C-AC+1	0.55	0.44	0.11	0.15	0.041	0.041
		S12.5C-AC-1	0.31	0.31	0.065	0.20	0.13	0.067
		S12.5CM	0.16	0.23	0.065	0.20	0.26	0.29
		S12.5FE	0.24	0.14	0.27	0.067	0.071	0.18
		S12.5F	0.92	0.88	0.27	0.43	0.12	0.18
		B25.0C	0.028	0.11	0.54	0.92	0.74	0.45
Prism	SA vs SP	S12.5C	0.92	0.59	0.92	0.15	0.239	0.740
		S12.5FE	0.27	0.80	0.91	0.92	0.92	0.800

Note: * Compaction (first letter): (S)GC or (R)olling Wheel
Geometry (second letter): (A)xial, (P)rism, or (I)DT

IDT versus Axial

Table 5.2 shows the p-values from t-tests comparing IDT and axial values for different mixtures. Overall, most p-values show no statistical difference. From this table it is observed that the S12.5C, S12.5FE, S12.5F, and B25.0C mixtures show no significant difference between IDT and axial mastercurves. B25.0C is significant at high temperature and low frequency. The IDT |E*| value is higher than axial, which is expected. At high temperatures, the material is soft and easily deforms. In IDT testing the RVE is small (*e.g.*, 2), therefore any large particle could reduce the deformations over the gauge length, which increase the |E*| value. The general finding from these particular mixtures is important because they cover a range in mixture types and provide evidence that IDT

testing is suitable for a wide range of mixtures. Measurements with the S12.5CM mixture show statistical insignificance at low reduced frequencies (fq1-fq4). Also of note is the S12.5-AV-2 mixture, where the results show p-values near the 0.05 threshold, except for fq2. A closer analysis of these results suggests that the data from IDT and axial compression are indeed different. The reason fq2 for S12.5-AV-2 is highly insignificant is the IDT curve crosses the axial curve at this point. This is an undesirable result because it indicates that the shapes of the curves are different. Even though some mixtures show a significant difference, most of the mixtures show insignificance. Based on statistical information, IDT and axial mastercurves are concluded to be similar.

Axial versus Prism

Another geometry comparison of interest is that of axial and prismatic specimens. It is expected that prismatic and axial specimens should be similar because the compaction and loading directions and state of stress are the same as for axial specimens. The only difference is a smaller cross-sectional area in prismatic specimens to apply the load.

The data in Table 5.2 show that comparisons between prism and axial specimens have no statistically significant difference. The variability of prism testing is the smallest of all three geometries. The average variability of the data points is approximately 10% of the averaged |E*| value. Based on this evidence, comparisons between prism and IDT specimens can be considered similar to comparisons between axial and IDT specimens.

RVE

While evaluating different geometries for measuring the |E*|, it is important to consider the possible limitations of each geometry. The RVE comparison in Table 5.3 shows that

the difference between axial, IDT, and prism specimens is statistically insignificant for all frequencies except for the previously mentioned small reduced frequency in the SA versus SI comparison. Given the large aggregate size, and the small RVE (≈ 2), this observation provides evidence that the IDT gauge length of 2 inches and the thickness of 1.5 inch are adequate to capture the response of the mixture. Kim *et al.* (2004) show an increase in the difference between axial and IDT specimens for increasing nominal maximum size of aggregate (NMSA) values, but this study shows a similarity. Caution should be exercised when comparing IDT and axial mastercurves at low reduced frequencies. Large variability occurs in this region. This variability is to be expected because the lower |E*| value corresponds to 35°C, the temperature at which the material is rather soft and the large aggregate would disproportionately affect the deformation over the gauge length (i.e., larger stiffness gradient between constituent phases).

Table 5.3 Statistical Results for RVE and Non-uniform Stress

			Stepdown Bootstrap p-value					
Evaluation	Comparison	Mixture	fq1	fq2	fq3	fq4	fq5	fq6
RVE	SA vs SI	S12.5C	0.60	0.83	0.20	0.81	0.92	0.69
		B25.0C	0.03	0.11	0.54	0.92	0.74	0.45
	SA vs SP	S12.5C	0.92	0.59	0.92	0.15	0.23	0.74
		B25.0C	0.17	0.85	0.92	0.87	0.84	0.57
Non-uniform stress	RP vs RI	S12.5-AV+2	0.62	0.88	0.07	0.07	0.07	0.07
		S12.5FE-AV+3	0.09	0.04	0.92	0.47	0.14	0.15

5.2.2 Non-uniform State of Stress

An important comparison between IDT and axial mastercurves is seen in evaluating the effects of the different states of stress. As discussed previously, only the specimens obtained from the compacted slabs may be used to fairly assess this factor. Table 5.3 shows the results that demonstrate non-uniform state of stress does not produce a

significant difference. In the case of the S12.5C-AV+2 mixture, a nearly significant difference is observed. Significance is seen in the S12.5FE-AV+3 mixture at low reduced frequencies. IDT testing at low reduced frequencies is more variable due to the high strain levels and damage to the specimen at high temperatures. To gain further insight into these observations, Figure 5.3 illustrates the results of the testing in both semi-log and log-log space for the two mixtures.

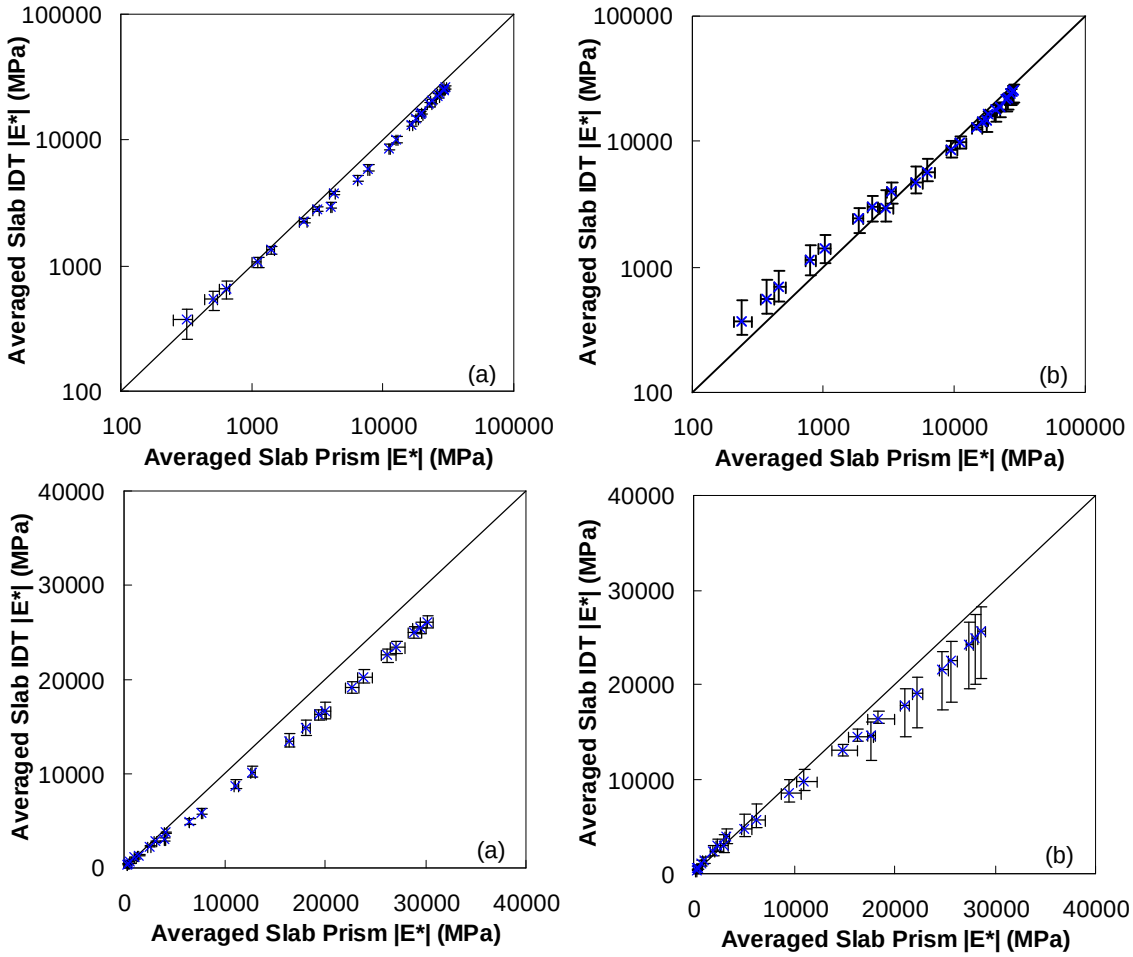

Figure 5.3 Line-of-equality of RI and RP |E*| values for (a) S12.5C-AV+2 and (b) S12.5FE-AV+3.

In Figure 5.3, for the S12.5C-AV+2 mixture, the RI mastercurve is lower than the RP mastercurve except at the lowest modulus value. For the S12.5FE mixture, the RP and RI mastercurves are similar except in the lower modulus range (i.e., low reduced frequencies). Once again, the inconsistency in variability for the same geometry is shown, though in this case the RI specimens tend to have larger variability than RP specimens do. Recall that the S12.5C-AV+2 mixture contains cubical aggregates, which research suggests should result in less inherent anisotropy than mixtures with flat and elongated aggregate (Saadeh, 2002). It is, therefore, unexpected that this mixture shows more significance with regard to stress state than the S12.5FE-AV+3 mix, so it is assumed the state of stress does not cause the difference shown. The conclusion is the state of stress does not effect the |E*| values due to the stastical analysis.

5.2.3 Anisotropy

Anisotropy is a difficult parameter to quantify. It is potentially influenced by compaction and loading direction as well as the physical characteristics of the aggregate particles. In this study, the comparison is further complicated due to differences in air voids and aging that were present both between mixes and between the different test configurations within mixtures. A statistical comparison of the air voids was performed to determine if the effect of air voids is significant. The difference in air voids is statistically insignificant for axial and IDT geometries and S12.5C and S12.5FE mixtures over the tested range (2 – 7%). Other studies have made similar observations for air voids in this range (Kim *et al.*, 2005, Mirza *et al.*, 2006). Based on this conclusion, the effect of air voids was shown to be insignificant; however, the interaction between air voids and other factors may not be insignificant. By collating the information in Table 5.1 and Table 3.1 with the necessary

comparisons from Table 5.3, the challenges of interpreting the data with differences in aging and air voids is observed.

Both compaction and anisotropy comparisons have aging effects and differences in air voids, which are inconsistent. For example, for comparisons of anisotropic effects, each comparison for the S12.5C-AV+2 mixture can be made with the same air voids, but the comparisons for the S12.5FE mixture require data with air voids of 4% (SA) and 7% (RP and RI). In addition, both mixtures contain aging effects due to differences in fabrication. The slab mixture was cooled and reheated instead of immediately proceeding to compaction like the SGC specimens. The greater aging of the rolling-wheel specimens should produce a higher stiffness. Therefore, the aging effect may account for the smaller distance to the line-of-equality because the S12.5C mixture sat in pans for two months instead of a few days. The difference in aging alone, though, does not explain the reason that the SI and SP mastercurves are higher than those of the RI and RP. Therefore, it should be understood that the following conclusions are drawn with less confidence than if the materials had the same air voids and if there had been no aging effects.

SGC versus Field Compaction

Rehabilitation design requires forensic work and field specimens for testing. The mechanistic-empirical models in the MEPDG software are based on laboratory data. Therefore, it is important to know if any difference exists between the material property measured from laboratory specimens and specimens acquired from the field. In this study, both prism and IDT samples were removed from a slab to simulate field samples.

To compare the effects of compaction on anisotropy, comparisons should be made between the SI and RI. The results in Table 5.4 show the difference in S12.5C is insignificant, but in S12.5FE is significant. It is important to note that the rolling-wheel specimens have higher air voids than the SGC specimens, which could be the source of the difference. But as previously mentioned, air voids showed no statistical difference. Because the effects of compaction based on IDT were inconclusive, a comparison was made with prism specimens (SP vs. RP). This comparison removes any interaction effects from the different states of stress. The results of this comparison show that the difference between mastercurves is significant for the S12.5C. The reason for the difference is the smaller standard deviation used to prism specimens than IDT or axial. If the standard deviation for the IDT testing had been used, the mixture would have no statistical difference.

Table 5.4 Statistical Results for Compaction and Anisotropy

			Stepdown Bootstrap p-value					
Evaluation	Comparison	Mixture	fq1	fq2	fq3	fq4	fq5	fq6
SGC vs Field Compaction [b]	SI vs RI	S12.5-AV+2 [a]	0.17	0.07	0.17	0.27	0.165	0.17
		S12.5FE [a]	0.20	0.81	0.17	0.04	0.04	0.066
	SP vs RP	S12.5-AV+2	0.008	0.008	0.008	0.008	0.041	0.065
		S12.5FE	0.42	0.66	0.16	0.27	0.42	0.27
Anisotropy [b]	SA vs SI	S12.5-AV+2	0.11	0.32	0.20	0.15	0.07	0.13
		S12.5FE [a]	0.24	0.14	0.27	0.07	0.07	0.18
	SA vs RP	S12.5-AV+2	0.09	0.07	0.21	0.29	0.12	0.12
		S12.5FE [a]	0.08	0.04	0.19	0.26	0.86	0.88
	SA vs RI	S12.5-AV+2	0.71	0.18	0.04	0.04	0.03	0.04
		S12.5FE [a]	0.40	0.45	0.27	0.19	0.17	0.19

Note: [a]air void difference * Compaction (first letter): (S)GC or (R)olling Wheel
[b]aging difference Geometry (second letter): (A)xial, (P)rism, or (I)DT

Because previously mentioned difficulties complicate a definitive conclusion regarding compaction method, it is beneficial to examine the possible sources of differences

between the comparisons. The known differences between the two curves, SI and RI, are the method of compaction and the aging. Only the aging condition is inconsistent between the mix types. As previously mentioned, the effect of aging does not entirely account for the SGC specimens being stiffer than the rolling-wheel specimens. Even though the statistics reveal insignificant influence from the compaction method, a numerical investigation seems to suggest an increase in |E*| values from the SGC. The increase may be a result of the air distribution within a gyratory specimen, since the center of the specimen is known to be denser in the center where the LVDT's measure deformations than the outside, which could increase the |E*| values. Based on statistics, the values are not different.

Effect of Anisotropy on Field to Laboratory Values

To evaluate the magnitude of the effect of anisotropy, Table 5.4 displays results that show, in general, the effects are insignificant. However, the S12.5FE rolling-wheel specimens had 7% air voids. Due to the limitations of materials, axial specimens had 4% air voids. Therefore, comparisons are made based on the assumption that air voids do not produce different |E*| values. The comparison between SA and RP shows an insignificant difference, providing further evidence that prism and axial specimens produce the same results. This result implies that compaction does not create a significant difference because previous evidence suggests that measurements from axial and prism specimens produce the same |E*| mastercurves. Recall that the comparisons between SA and SI specimens show, in general, insignificant statistical difference. Because compaction may not significantly affect the mastercurves, these results imply that the differences in

compaction and stress-strain analysis do not have an effect. In the comparison of SA and RI, a significant difference occurs at high reduced frequencies or at high modulus values. In the S12.5C-AV+2 mixture, the SA values are higher than S12.5C, which is unexpected since S12.5-AV+2 has greater air voids and is less dense, the |E*| values should remain the same or decrease. This difference could explain why S12.5C-AV+2 is different but S12.5FE is not. The results seem to imply that the magnitude of anisotropy is not as great a factor as might be expected. Because the material's property is measured at low strain levels, which generally does not mobilize the aggregate, this conclusion is reasonable. Results suggest that the compaction direction and stress-strain analysis generally do not have an effect.

5.3 Conclusions

Based on the results presented in this chapter, the following conclusions can be drawn:

1. The statistical difference between IDT and axial specimens is insignificant for a variety of mixture gradations at low strain levels.
2. Sources of anisotropy and its effects are difficult to isolate. Based on the data, compaction and loading direction have an insignificant effect.
3. Prism specimens provide a good alternative for axial specimens in forensic work. Prisms have statistically similar |E*| values for SGC and rolling-wheel specimens.
4. The effects of non-uniform stress in IDT testing is insignificant compared to prism specimens.
5. The prism and IDT geometries provide an adequate alternative for measuring the |E*| for asphalt concrete mixtures with NMSA up to at least 25.0 mm. The IDT

test method has a small RVE, which is adequate except at small reduced frequencies (high temperatures and long loading times), due to the gauge length.

6. The alternative geometries explored in this study appear to reduce the specimen-to-specimen variability.

Based on these conclusions and the observations in this chapter, the |E*| can be acquired through several geometries with minimal concerns about differences stemming from the RVE, non-uniform states of stress, and anisotropy.

CHAPTER 6 PREDICTING DYNAMIC MODULUS FROM RESILIENT MODULUS USING AN ARTIFICAL NEURAL NETWORK

6.1 Method

This study has three stages for investigating whether M_R data can be used to predict the |E*| using the ANN: 1) developing a database with corresponding |E*| and M_R values; 2) training the ANN; and 3) verifying the accuracy of the predictions.

Developing a database with |E*| and M_R values can be a lengthy task if the properties are measured in the laboratory, especially for a database comprehensive enough to encompass a large range of mixture variables, such as binders, gradations, NMSA, voids in mineral aggregate, voids filled with asphalt, air voids, etc. The proposed method is to use a comprehensive |E*| database, and then populate the database with M_R values using the method presented.

As previously mentioned, several M_R formulations exist. The M_R solution used in this study is the NCHRP 1-28 (Barksdale *et al.*, 1997) elastic formulation, shown in Equation (6.1).

$$M_R = \frac{P}{Ud}(k_1 - k_2 n), \quad (6.1)$$

where

M_R = resilient modulus (MPa);

P = applied load (N);

U = recoverable horizontal displacement (m);

d = thickness of specimen (m);

ν = Poisson's ratio; and

k_1, k_2 = (-0.00018, 0.000578).

The unknowns in the equation are the load, the horizontal displacement, and the Poisson's ratio. The Poisson's ratio is assumed to be constant for a given temperature (0.2, 0.35, and 0.45 for 5°, 25°, and 40°C, respectively). To determine the horizontal displacement amplitude, a two-dimensional viscoelastic formulation is needed to predict a strain history from a given loading history for a biaxial state of the stress. Equation (6.2) shows the formulation for calculating the horizontal strains needed for Equation (6.1). Equation (6.2) is based on the generalized Hooke's Law in conjunction with the viscoelastic correspondence principle and the plane stress formulations of Hondros (1959):

$$U = \frac{2(g_1 + n g_2)}{p\,ad}\int_0^t D(t-t)\frac{\partial P}{\partial t}dt, \quad (6.2)$$

where

D = compliance

a = loading strip width (m);

d = thickness of specimen (m); and

γ_1, γ_2 = geometric coefficients for a gauge length of 50.8 mm (0.0037, 0.0116).

To predict the horizontal displacement, a representative loading history (*i.e.* a repeated 0.1 second haversine pulse followed by a 0.9 second rest period) is introduced to Equation (6.2). Once the horizontal strains are calculated, the M_R can be calculated by using Equation(6.1).

After the database has been populated, the next step is to train the ANN. The ANN is a model composed of nonlinear transfer functions, typically a sigmoidal function, between inputs and outputs. The ANN is trained using the feedfoward, backpropagation method. The feedforward portion of the training involves presenting the inputs and the desired outputs (targets) so that the computer program can make the appropriate connections with the transfer functions. The backpropagation portion involves predicting the output using a given input, which is the ultimate purpose of the ANN. The program evaluates the error between the targeted and predicted outputs based on the weighted transfer functions. Using the Levenberg-Marquardt optimization algorithm, the computer selects new weighted values and repeats this process until the program reaches a maximum number of iterations or the minimum error desired. Further information regarding the use of neural networks in pavement applications can be found in Xu *et al.* (2002).

Once the network has been trained, the next process is to verify the accuracy of the network. Some trained networks may show small errors between targeted values given for the feedforward method and predicted values used in training, but may not have the predictive capabilities desired when new data are presented to it. Some data from the training dataset are reserved for use as verification of the predictions after training. In training the ANN, the user selects how many degrees of freedom the network has to fit

the data. If the network has too many degrees of freedom, the data can predict the training data well, but may not be able to interpolate for new inputs, which is the ultimate purpose of training the network.

In order to verify the accuracy of the predictions, an independent database containing both measured |E*| and M_R values is used. The measured |E*| values allow for a comparison between predicted and measured values. The M_R data are necessary to determine if the greater variability in measured M_R affects the ANN results.

6.2 Theoretical Background

6.2.1 Determination of Displacements Using the Multiaxial Convolution Integral

For linear elastic materials, the stress-strain relationship is represented by the generalized Hooke's law. Assume the rectangular coordinate of x_1 in the horizontal direction, x_2 in the vertical direction, and x_3 in the depth direction of the IDT specimen. Two strains that are of interest are ε_{11} and ε_{22}. According to the generalized Hooke's law, these two strains are related to stresses as follows:

$$e_{11} = \frac{1}{E}(s_{11} - n s_{22}) = D(s_{11} - n s_{22}); \tag{6.3}$$

$$e_{22} = \frac{1}{E}(s_{22} - n s_{11}) = D(s_{22} - n s_{11}), \tag{6.4}$$

where

E = Young's modulus and

D = compliance.

Application of the elastic-viscoelastic correspondence principle to these linear elastic solutions results in the following linear viscoelastic stress-strain relationships:

$$e_{11} = \int_0^t D(t-t)\frac{\partial}{\partial t}[s_{11} - n(t-t)s_{22}]dt \quad \text{and} \tag{6.5}$$

$$e_{22} = \int_0^t D(t-t)\frac{\partial}{\partial t}[s_{22} - n(t-t)s_{11}]dt \ . \tag{6.6}$$

The Hondros equations used to calculate the resulting stresses in the horizontal and vertical directions are:

$$s_{11} = \frac{2P}{p\,ad}[f(x) - g(x)] \quad \text{and} \tag{6.7}$$

$$s_{22} = -\frac{2P}{p\,ad}[f(x) + g(x)], \tag{6.8}$$

where

$$f(x) = \frac{(1 - x^2/R^2)\sin 2a}{1 + (2x^2/R^2)\cos 2a + x^4/R^4} \tag{6.9}$$

$$g(x) = \tan^{-1}\left[\frac{1 - x^2/R^2}{1 + x^2/R^2}\tan a\right]; \tag{6.10}$$

R = radius of specimen (m);

x = horizontal distance from center of specimen (m); and

α = radial angle (radians).

Combining Equations (6.5), (6.6), (6.7), and (6.8) results in the following expressions for the horizontal and vertical strains:

$$e_{11}(x_1, t) = \frac{2}{p\,ad}\int_0^t D(t-t)\frac{\partial P}{\partial t}\{[f(x) - g(x)] + n(t-t)[f(x) + g(x)]\}dt \ ; \tag{6.11}$$

$$e_{22}(x_2, t) = -\frac{2}{p\,ad}\int_0^t D(t-t)\frac{\partial P}{\partial t}\{[f(x) + g(x)] + n(t-t)[f(x) - g(x)]\}dt \ . \tag{6.12}$$

The displacements at the gauge length can be calculated by integrating the non-uniform strains in Equations (6.11) and (6.12) along the gauge length, i.e., *-l* to *+ l*:

$$U = \int_{-l}^{l} e_{11}(x_1, t)dx; \tag{6.13}$$

$$V = \int_{-l}^{l} e_{22}(x_2, t)dx; \tag{6.14}$$

or

$$U = \frac{2}{p\,ad}\int_0^t D(t-t)\frac{\partial P}{\partial t}\left(\int_{-l}^{l}[f(x)-g(x)]dx + n(t-t)\int_{-l}^{l}[f(x)+g(x)]dx\right)dt\ ; \tag{6.15}$$

$$V = \frac{2}{p\,ad}\int_0^t D(t-t)\frac{\partial P}{\partial t}\left(-\int_{-l}^{l}[f(x)+g(x)]dx + n(t-t)\int_{-l}^{l}[g(x)-f(x)]dx\right)dt\ . \tag{6.16}$$

For the gauge length of 50.8 mm (2.0 in.), Equations (6.15) and (6.16) reduce to:

$$U = \frac{2}{p\,ad}\int_0^t D(t-t)\frac{\partial P}{\partial t}\{g_1 + n(t-t)g_2\}dt\ ; \tag{6.17}$$

$$V = \frac{2}{p\,ad}\int_0^t D(t-t)\frac{\partial P}{\partial t}\{b_1 + n(t-t)b_2\}dt\ , \tag{6.18}$$

where the values of β_1, β_2, γ_1, and γ_2 are shown in Table 2.1.

Equations (6.17) and (6.18) require two time-dependent material properties, i.e., creep compliance and Poisson's ratio. It has been proven that the creep compliance of asphalt concrete can be predicted from the |E*| using theoretical relationships (Kim and Lee, 1995). In this study, the approach is used to convert the |E*| mastercurve to the creep compliance is presented in Section 2.1.

The second time-dependent material property in Equation (6.17) is Poisson's ratio. The time-dependent nature of Poisson's ratio has been reported in Kim *et al.* (2004). Poisson's ratio values for the S12.5C mixture are shown in Figure 6.1 against the reduced time to show a typical trend. These Poisson's ratio values are calculated from Equation (2.12) using the data from the IDT |E*| test. As can be seen in this figure, there is a large

sample-to-sample variability in Poisson's ratio values. Another difficulty involved in Poisson's ratio is that Equation (6.17) is difficult to solve because there are two time-dependent properties in the equation. If Poisson's ratio in Equation (6.17) and (6.18) is assumed to be constant, Equations (6.17) and (6.18) reduce to the following:

$$U = \frac{2(g_1 + n g_2)}{p\,ad} \int_0^t D(t-t) \frac{\partial P}{\partial t} dt \quad \text{and} \tag{6.19}$$

$$V = \frac{2(b_1 + n b_2)}{p\,ad} \int_0^t D(t-t) \frac{\partial P}{\partial t} dt \ . \tag{6.20}$$

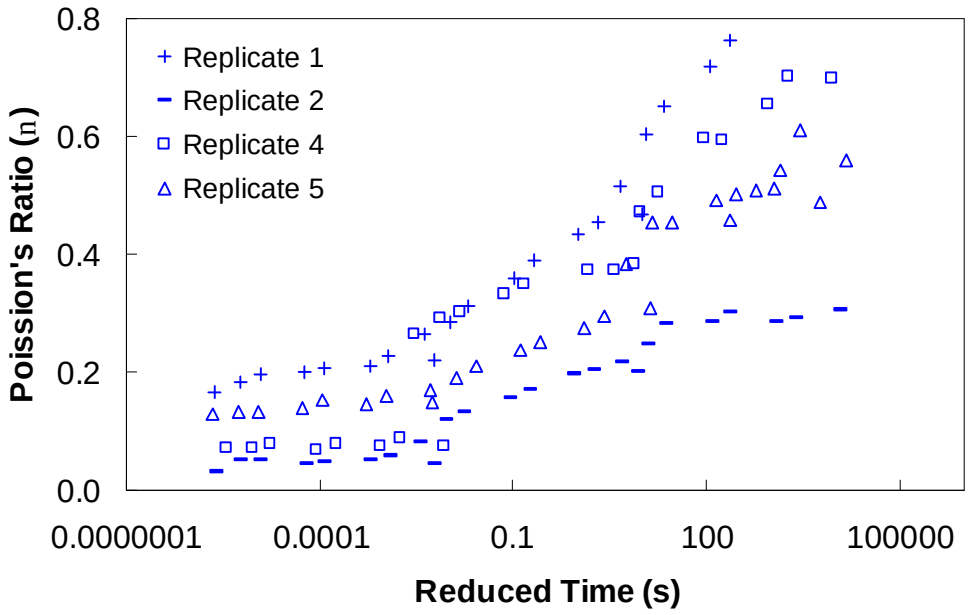

Figure 6.1 Poisson's ratio versus reduced time for S12.5C.

Figure 6.1 presents the measured Poisson ratio's using Equation (2.12). Since the material is viscoelastic, the reduced time is inverse of the reduced frequency multiplied by 0.1. Therefore. small reduced time represents high frequency and low temperature data. The Poisson's ratio is smaller at low temperatures and larger at high temperatures. The measured Poisson's ratio exceeds the theoretical limits of 0.0 to 0.5. A high

Poisson's ratio occurs at large reduced times when the temperature is high and/or the loading time is long. Some Poisson's ratios are higher than 0.5, indicating that damage has occurred in the specimen (Fairhurst et al, 1990, Barksdale *et al.*, 1997). Damage is possible at 35°C, since shear is observable under the loading strips at high stresses. The biggest challenge in determining Poisson's ratio in the IDT test is to induce a large enough horizontal displacement to overcome the electronic noise in the testing system without causing damage in the specimen. Mirza *et al*. (1997) provide a method to evaluate the quality of the data using a deflection ratio.

The effect on M_R, when a constant Poisson's ratio is assumed, is evaluated by using three different Poisson's ratios at each temperature of each mixture and calculating the percentage difference in the predicted M_R values. Poisson's ratio values used in this comparison are 0.15, 0.2, and 0.25 for 5°C, 0.25, 0.3, and 0.35 for 25°C, and 0.4, 0.45, and 0.5 for 40°C. It was found that the difference in M_R values is negligible when Poisson's ratio, which is used to predict the displacements, is used for calculating the M_R. A more in-depth analysis of Equations (2.13) and (6.17) along with the geometry coefficients in these equations, which are shown in Table 2.1 (i.e., k_1, k_2, γ_1, and γ_2), reveals that the effect of change in Poisson's ratio on the term $(k_1 - k_2 n)$ in the numerator of Equation (2.13) is about the same as that on the horizontal displacement calculated from Equation (6.17), which appears in the denominator of Equation (2.13). Therefore, it is concluded that the effect of Poisson's ratio on the M_R calculation is minimal. Vinson drew a similar conclusion that a Poisson's ratio of 0.15 to 0.45 does not affect M_R much, based on theoretical finite-element analysis (1989). For the remainder of this chapter,

Equation (6.19) with constant Poisson's ratios of 0.2, 0.35, and 0.45 for 5°, 25°, and 40°C, respectively, are used.

Because the numerical integration of Equation (6.19) requires calculating all the previous time steps to arrive at the current time step, calculation times can grow exponentially (Underwood *et al.*, 2005). To reduce the calculation time, the state variable approach described in Equations (6.21) to (6.23) is used in this study:

$$e^{n+1} = \int_0^{t^{n+1}} D(t^{n+1} - t)\frac{ds}{dt}dt = h_o^{n+1} - \sum_{i=1}^{n} h_i^{n+1}, \tag{6.21}$$

where

$$h_o^{n+1} = (D_o + \sum_{i=1}^{m} D_i)(s^{t^{n+1}} - s^{t^o}) \text{ and} \tag{6.22}$$

$$h_i^{n+1} = e^{-\frac{\Delta t}{t_o}} h_i^n + e^{-\frac{\Delta t}{2t_o}} [s^{t^{n+1}} - s^{t^n}] D_i . \tag{6.23}$$

6.3 Material Information

6.3.1 Measuring Material Properties

The specimens in this study comprise seven different mixtures with four percent air voids listed in Table 3.1. Note the wide range of mixtures necessary to explore the wide range of possible |E*| values. All the specimens for this study were compacted using a SGC. The |E*| and M_R were measured from these specimens and used as verification of the ANN.

6.3.2 Database

For this study, the database used to train the ANN was the Witczak |E*| database. The database consists of over 8000 |E*| data points from a variety of mixtures. The Witczak

database was selected because it contains 346 mixtures with a large range of values, especially at high values of the |E*|. For training the ANN, the database was reduced to 210 mixtures because 136 of the mixtures do not have the mixture phase angle data, which are necessary for the forward modeling process (i.e., predicting the M_R from the |E*|). The data points for the 210 mixtures were evaluated using internally developed software. The software fits a sigmoidal mastercurve to the |E*| data for each mixture, then calculates creep compliance. The creep compliance is necessary for Equation (6.2). A few more mixtures were removed due to curve fitting issues, reducing the database to 206 |E*| and M_R pairs. After obtaining the creep compliance, the response to a M_R loading history was simulated (***e.g.***, using a 10 Hz haversine pulse with a 0.9 second rest period) at three temperatures. From this simulated response history, the M_R was determined. Then, the resilient moduli were calculated for each mixture. Of the 206 available mixtures, ten were randomly removed from the training database. After training the ANN, these ten mixtures were used to evaluate the predictive capabilities of the trained ANN of data with similar variability as the training set. After verifying the predictive capabilities, the predictive accuracy of the ANN was verified by using measured data acquired for the mixtures previously listed.

6.4 Developing Forward Model

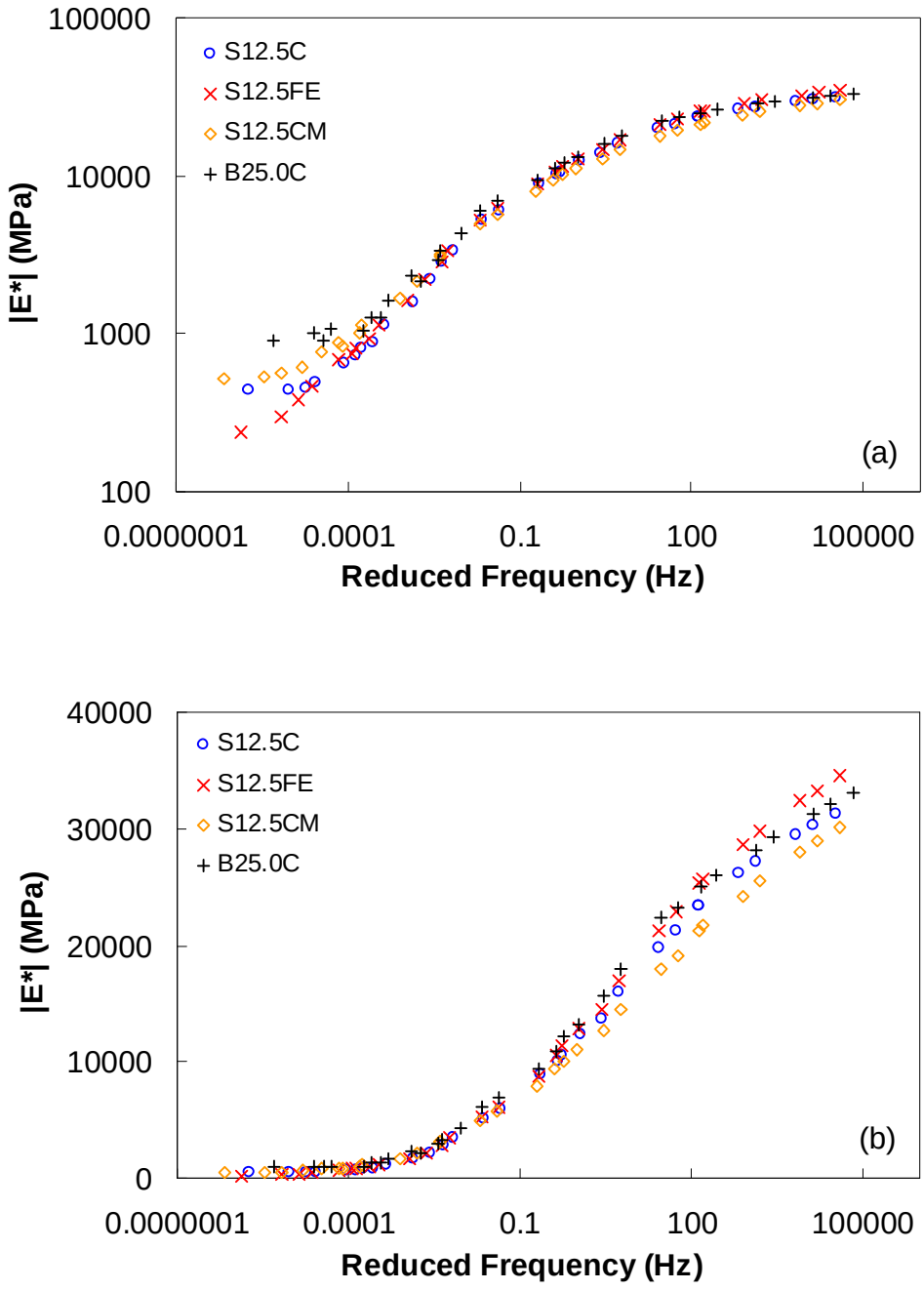

Figure 6.2 Average |E*| mastercurves: (a) in log-log scale and (b) in semi-log scale.

The |E*| mastercurves for the four mixtures are plotted in Figure 6.2. It can be seen in Figure 6.2(b) that |E*| of the S12.5FE mixture is slightly higher than B25.0C which is slightly higher than the S12.5C mixture at high reduced frequencies. At low reduced frequencies, these S12.5C and S12.5FE mixtures exhibit essentially the same stiffness characteristic as shown in Figure 6.2(a). The variation of the stiffness at high reduced frequencies (i.e., low temperatures) appears to be the result of sample-to-sample variability in the averaging of each mixture. The same dynamic moduli at small reduced frequencies (i.e., high temperatures) indicate that the effect of flat and elongated aggregate particles in the S12.5FE mixture on the |E*| is minimal. This observation suggests that the |E*| testing with small strain amplitudes cannot capture the effect of the aggregate structure.

The slightly higher |E*| of B25.0C at small reduced frequencies than those of the 12.5 mm mixtures may be due to the pronounced effect of larger aggregates at high temperatures. Comparison of the |E*| mastercurves from S12.5C and S12.5CM reveals the effects of binder modification on |E*| values. At high reduced frequencies (i.e., low temperatures), the SBS modified mixture is less stiff. At low reduced frequencies (i.e., high temperatures), the binder modification makes the mixture stiffer, which demonstrates the benefit of the SBS modification of the binder.

The horizontal strain is predicted from Equation (6.11) using the measured IDT |E*| shown in Figure 6.2 and a constant Poisson's ratio for each temperature. Time histories of the predicted and measured horizontal strains are plotted in Figure 6.3 through Figure 6.5. In these figures, vertical strains have a minus sign because they are in compression

whereas the horizontal tensile strains have a plus sign. There are two parameters to compare in Figure 6.3; one is the mean strain, and the other is the strain amplitude. It can be seen in Figure 6.3 that the prediction is quite good at 5°C for both the mean strain and strain amplitude for both vertical and horizontal strains. However, at 25° and 40°C in Figure 6.4 and Figure 6.5, the prediction of the strain amplitudes is reasonable as seen by comparing the shifted measured strain versus the predicted strain. The shifted strain was calculated by subtracting the difference between the measured and predicted strains at relative time of zero from the measured strain.

As can be seen in Figure 6.4 and Figure 6.5, the mean strain prediction is poor. At 25° and 40°C, the measured mean strains are much greater than the predicted mean strains for both vertical and horizontal strains. This difference indicates that the IDT |E*| testing causes a significant permanent deformation, which cannot be predicted from the proposed approach in this paper using the theory of linear viscoelasticity. The fact that the strain amplitude prediction is reasonable even with a significant permanent deformation supports the earlier observation made from the same |E*| between the S12.5C, S12.5FE, and B25.0C mixtures; that is, the small stresses and strains used in the |E*| testing do not capture the effect of changes in the aggregate structure.

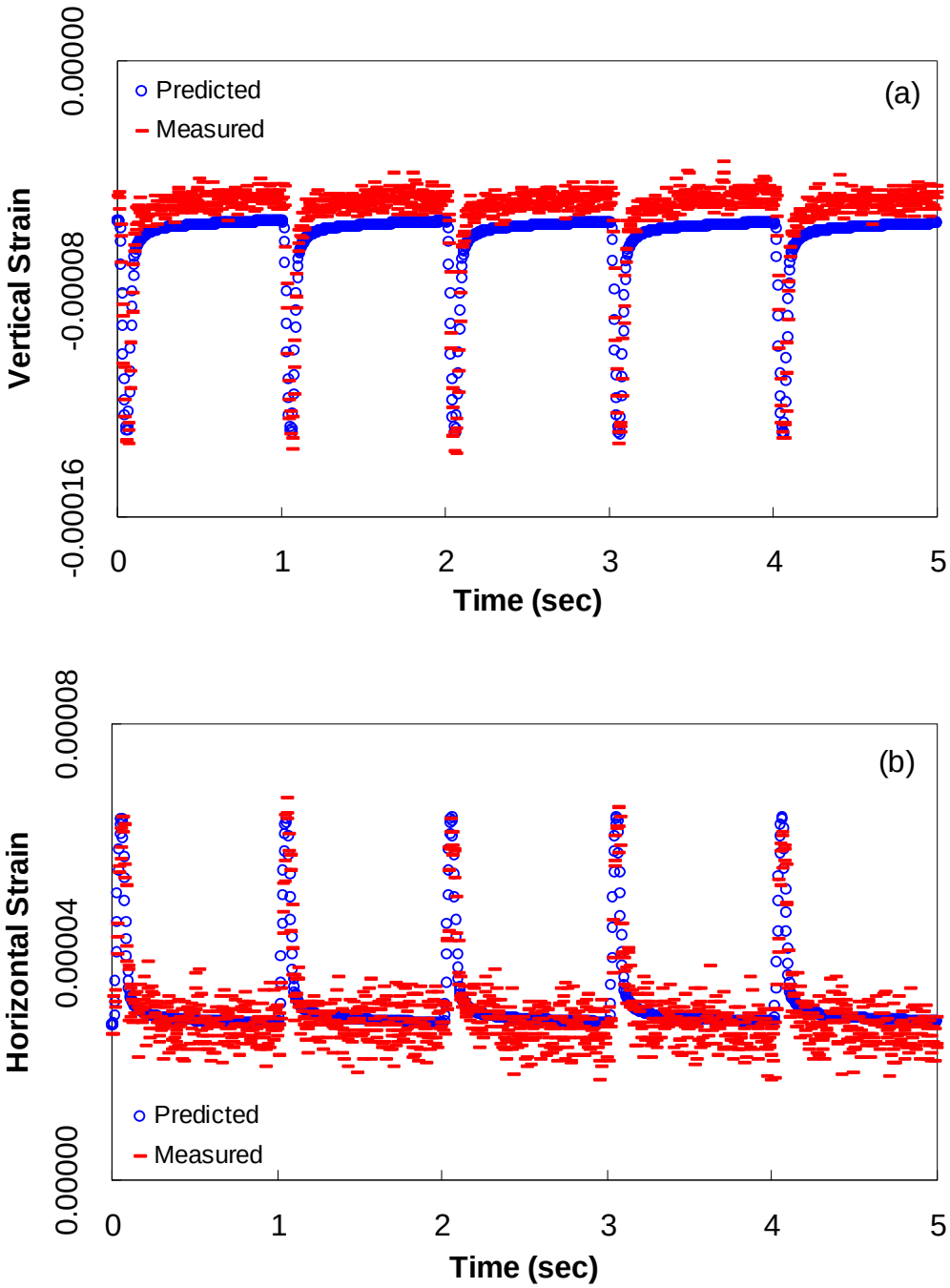

Figure 6.3 Strain comparison for ν = 0.20 at 5°C: (a) vertical and (b) horizontal.

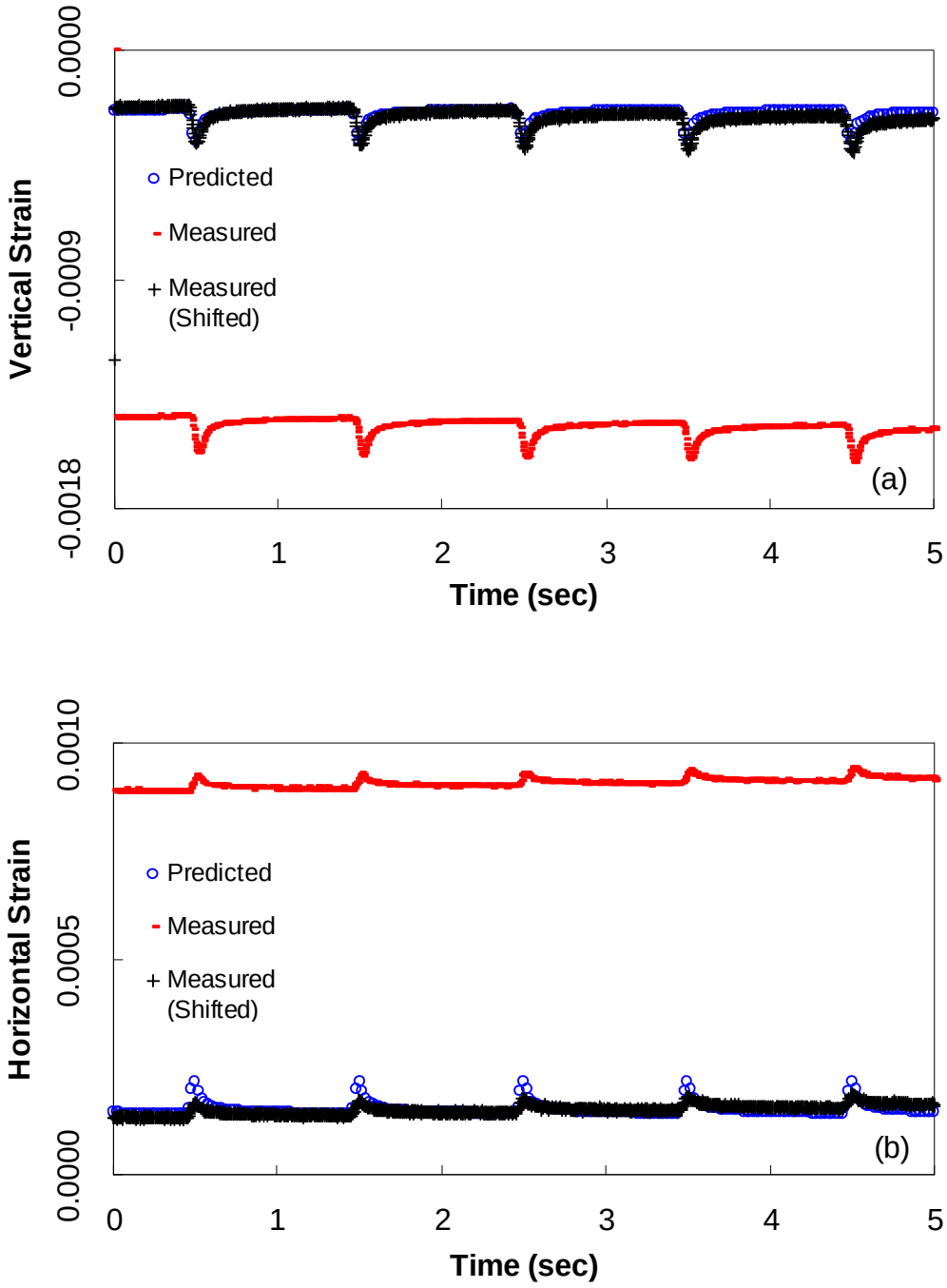

Figure 6.4 Strain comparison for ν = 0.35 at 25°C: (a) vertical and (b) horizontal.

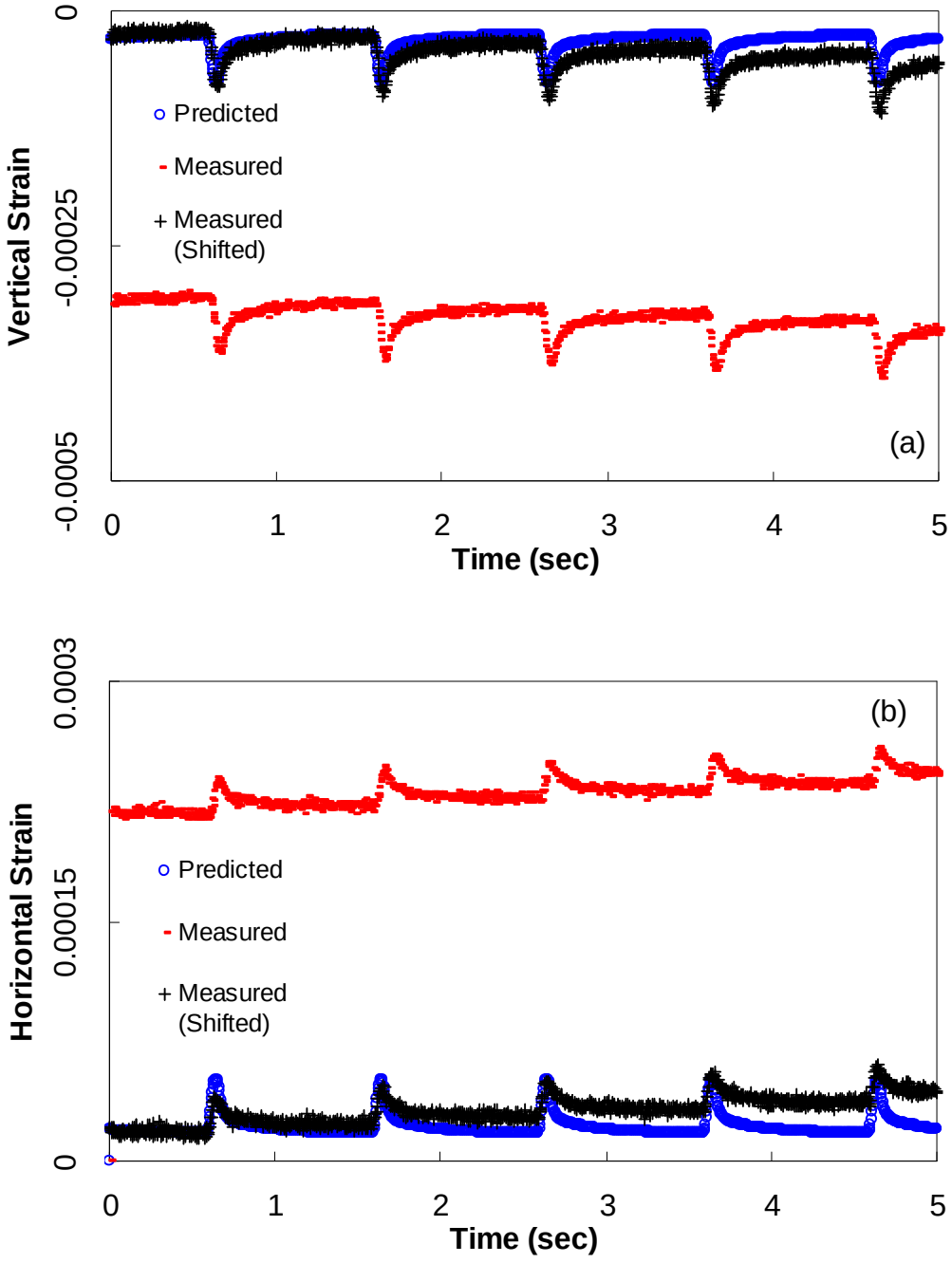

Figure 6.5 Strain comparison for ν = 0.45 at 40°C: (a) vertical and (b) horizontal.

Table 6.1 Comparison of Predicted and Measured M_R Values

S12.5C				
	Measured M_R (MPa)		Predicted M_R (MPa)	
Temperature (°C)	Mean	Standard Deviation	Mean	Standard Deviation
5	20,300	1,800	20,100	280
25	5,460	320	5,980	100
40	2,100	410	1,880	100
S12.5CM				
	Measured M_R (MPa)		Predicted M_R (MPa)	
Temperature (°C)	Mean	Standard Deviation	Mean	Standard Deviation
5	18,360	1,560	17,700	370
25	5,990	940	5,470	60
40	1,540	160	1,640	50
B25.0C				
	Measured M_R (MPa)		Predicted M_R (MPa)	
Temperature (°C)	Mean	Standard Deviation	Mean	Standard Deviation
5	21,200	1,340	21,600	20
25	6,200	270	6,560	110
40	1,640	80	2,270	60
S12.5FE				
	Measured M_R (MPa)		Predicted M_R (MPa)	
Temperature (°C)	Mean	Standard Deviation	Mean	Standard Deviation
5	20,700	2,540	20,600	410
25	5,800	1,050	5,810	260
40	1,740	350	1,630	60

Since the ultimate objective of task one is to evaluate the prediction accuracy of the proposed approach to M_R determination, Equation (6.19) is used to predict the M_R for each specimen. In this prediction, the load history specific to each specimen is used. Also, Poisson's ratio values of 0.2, 0.35, and 0.45 are used for 5°, 25°, and 40°C analysis, respectively. Table 6.1 presents the mean and standard deviation of the measured and predicted M_R values for all the conditions tested in this study. All the predictions except

40°C data from B25.0C are within two standard deviation of the measured average value, which means the predicted value has a 95% probability of falling within a normal distribution of the measured data.

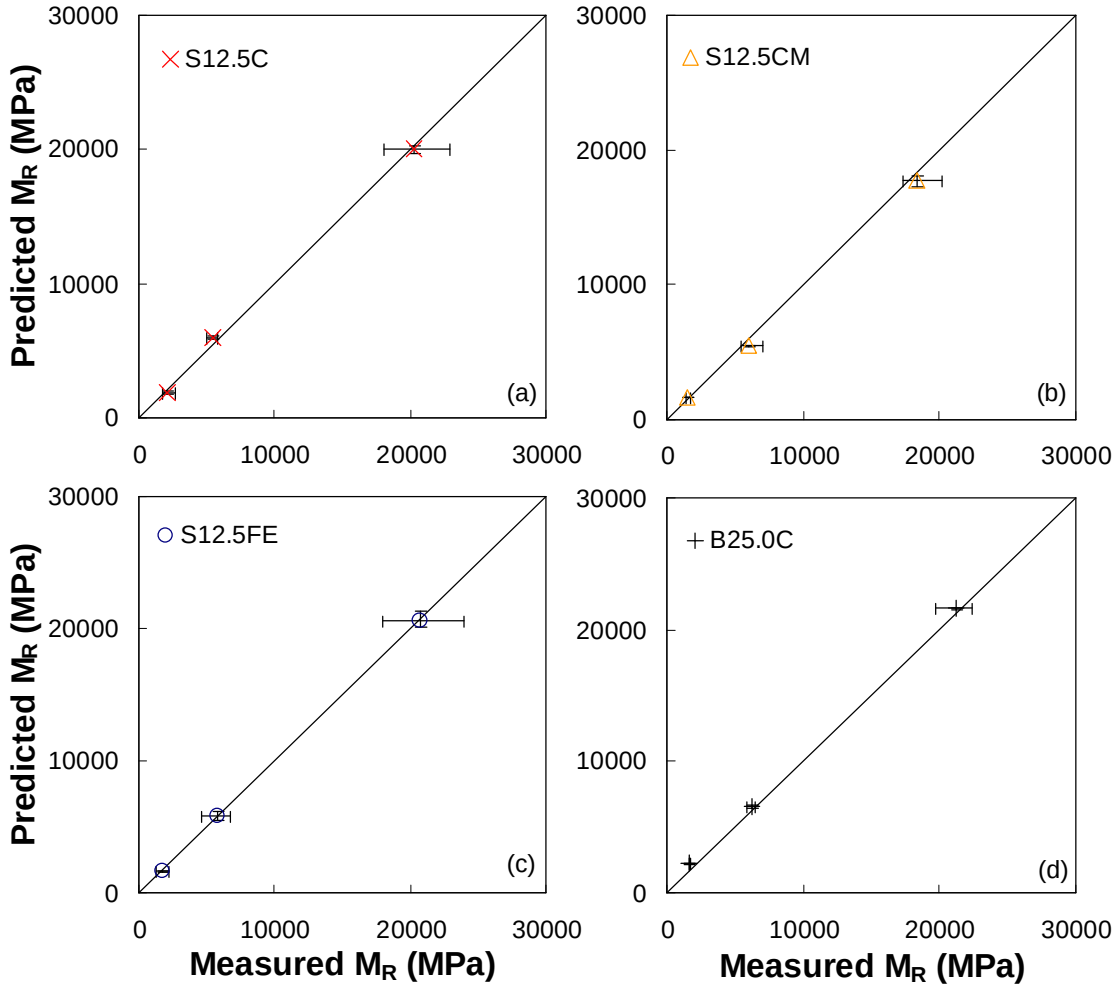

Figure 6.6 Comparison of predicted and measured M_R values: (a) S12.5C, (b) S12.5CM, (c) S12.5FE, and (d) B25.0C.

6.5 Training the ANN

The second step in predicting the M_R from the |E*| is training the neural network. The ANN was trained using the neural network toolbox in MatLAB®. Once the ANN is trained, the output file containing the ANN structure can be implemented in any

commonly available computer language. The inputs to the ANN were three M_R values at three different temperatures along with the reduced frequencies of 10 Hz at those three temperatures. The reduced frequencies are calculated at the reference temperature of 10°C. Since the frequency of an M_R pulse is difficult to determine (Loulizi, 2006), the frequency was selected to correspond with the loading pulse. Even if the M_R is equal to the |E*| at a frequency other than 10 Hz, the ANN will compensate for that in its transfer functions. As long as the inputs are calculated the same way, the results are not affected by the choice of 10 Hz. The ANN was trained to predict the four coefficients describing the sigmoidal function in Equation (2.8) that represents the dynamic modulus mastercurve.

The time-temperature superposition principle states that unit response functions (e.g., dynamic modulus) in thermorheologically simple materials, such as HMA, can be shifted in the time or frequency domain (i.e., the horizontal axis) to produce a single, continuous mastercurve as shown in Section 2.1. Since the loading frequency used in the M_R testing is a single frequency of 10 Hz, prediction of the |E*| at multiple frequencies requires additional information. The best candidate to handle this frequency issue is the mixture time-temperature shift factor in Equation (2.7). However, determination of the mixture shift factor requires the dynamic modulus data at multiple temperatures and frequencies, which is the information to be predicted from the ANN model.

In order to break this circle, it is proposed to use binder shift factors in place of mixture shift factors. Dongre *et al.* (2005) provided evidence that the mastercurves generated from binder and mixture shift factors are the virtually the same. Further evidence of this

correlation is shown in Figure 6.7. The binders shown in the study are binders used in a current FHWA pooled-fund study. The binder types are modified binders labeled as PG70-22, CRTB (Crumb Rubber Terminal Blend), SBS, and Elvaloy. The binder testing was done by FHWA for the project. The mixture testing was done at North Carolina State University. Figure 6.7 shows the shift factors from measurements at 5°, 25°, 40°, and 54°C for both mixtures and binders. Binder DSR testing was performed at 7°C, so minor extrapolation was applied to determine the shift factors at 5°C. As seen from the figure, the values are very close to the line of equality. In many cases, the values are almost numerically exact. Based on the observations of Dongre *et al.* and these results, it is reasonable to use binder shift factors to determine the mixture |E*| values at multiple frequencies from the single frequency M_R data.

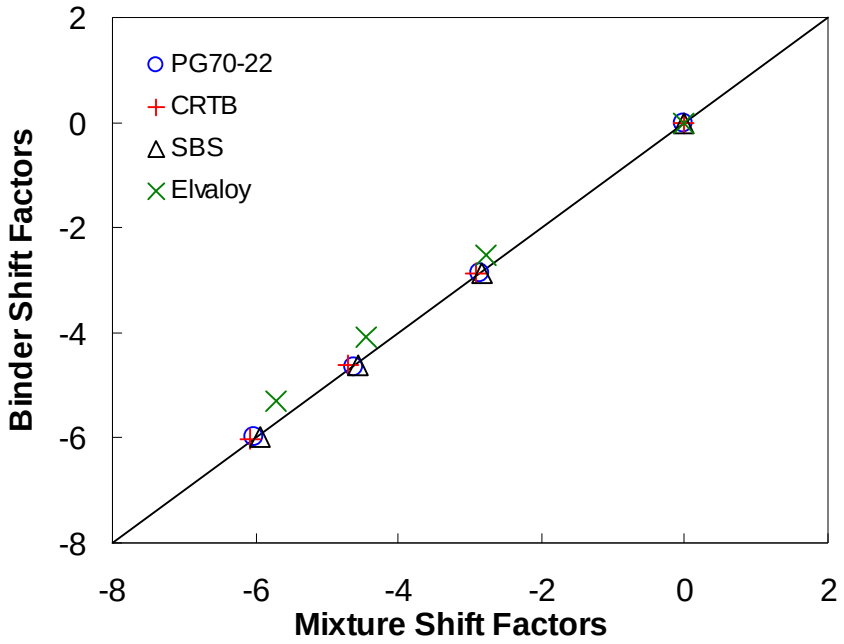

Figure 6.7 Line-of-equality graph for mixture and binder shift factors from FHWA study.

6.6 Verification of the ANN

The first step of verification is evaluating the predictive capabilities of the ANN using the data employed in the ANN training. As seen in Figure 6.8, the ANN results are around the line-of-equality. The prediction accuracy of the modified Witczak's model, which includes binder |G*| or shear modulus as an input (Bari and Witczak, 2007), is also shown in Figure 6.8. The comparisons in the figure are circular since the data used in evaluating the prediction accuracy were used in defining the models. The ANN shows less bias than the Witczak prediction. The Witczak prediction tends to over predict the modulus at high modulus values. The figure also shows how the nonlinear transfer functions can reduce the error for a training dataset when compared to the regression analysis used in the modified Witczak's model..

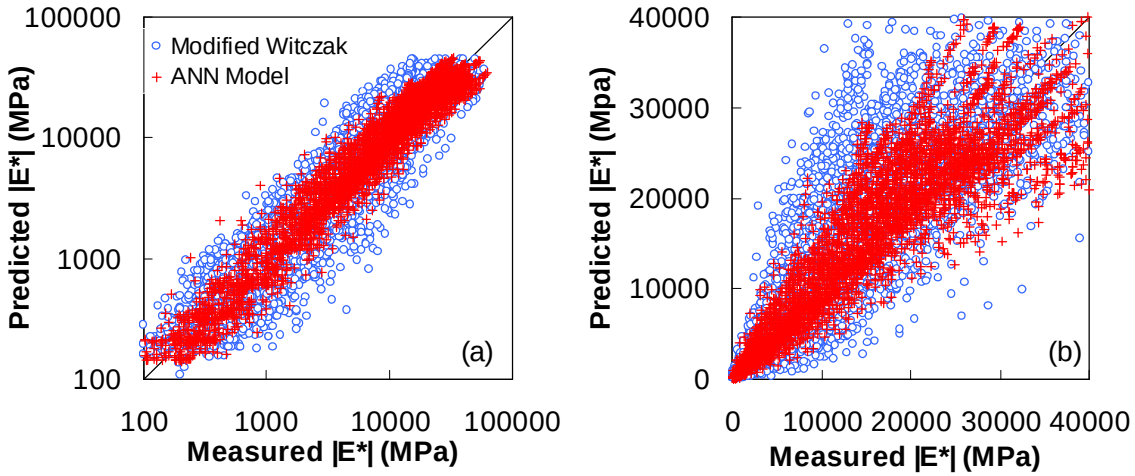

Figure 6.8 Line-of-equality graph of training data: (a) log-log and (b) arithmetic scales.

After the first verification, the ANN was further verified using two additional comparisons. The first comparison used a dataset of predicted M_R values and measured |E*| values composed of ten mixtures reserved from the Witczak's database. This dataset

was used to test the soundness of the ANN, assuming that the variability was similar to the variability of the training dataset. Also, this dataset provides the same framework as the ANN training dataset because the M_R values are predicted and not measured. The second dataset consists of measured M_R and |E*| values from the seven North Carolina mixtures. This dataset should yield the ultimate verification of the ANN model as well as show any differences between the Witczak and independent |E*| values, because the trained ANN is based on the Witczak data.

As seen in Figure 6.9, the ANN prediction for the first dataset is good considering the spread of data seen in Figure 6.8. In log-log scale, the variability is generally constant. In arithmetic scale, the variation is greater at large modulus values. It is noted that the comparison for the modified Witczak model is circular; i.e., the data shown in Figure 6.9 were used in developing the modified Witczak model. The ANN prediction is not circular because these data were not included in the ANN training set. The more accurate prediction of the ANN model compared to that of the modified Witczak model may be attributed to the superior ability of the ANN to describe the complex relationship between the M_R and |E*| values and/or the fact that the ANN model predicts the mixture property |E*| from another mixture property M_R, whereas the modified Witczak model predicts the mixture |E*| from component material properties.

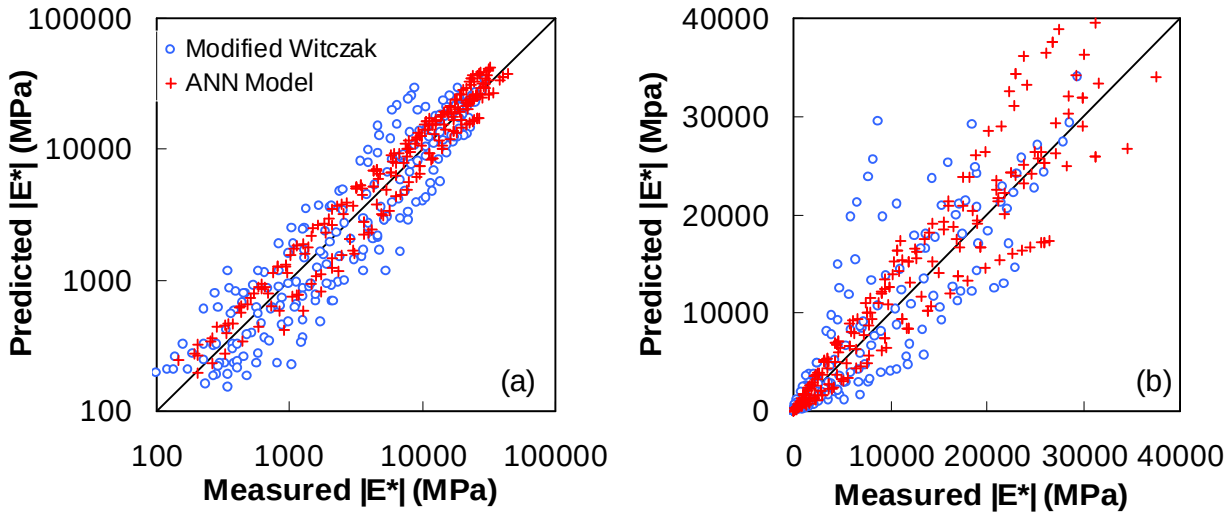

Figure 6.9. Line-of-equality graph of verification using Witczak data (a) log-log and (b) arithmetic scales.

The second verification of the ANN is performed using an independent source of data. Figure 6.10 shows the results of the prediction for the independent North Carolina database. Two observations can be made from this figure. First, predictions from both the ANN and the modified Witczak model show less variability than the training data shown in Figure 6.9. Because all the tests for the North Carolina database were performed by a single operator during a relatively short period (within a year), the independent database is expected to include more consistent quality data than the Witczak database that was developed by multiple operators over a much longer period. This additional consistency in the North Carolina database may be the reason for less variability seen in Figure 6.10 than that seen in Figure 6.9. The second observation is the slight underestimation of the |E*| values by the ANN model. It is assumed that this bias is the result of using two different databases. In training the ANN, the targeted |E*| values came from the Witczak database. The independent verification of the ANN used |E*| values measured for this study. The difference between the measurements of the Witczak |E*| and the |E*| of this

study is the difference in strain levels employed in the |E*| testing. The strain levels reported in the Witczak database are quite often greater than 100 microstrains (Bari 2005), whereas the North Carolina testing kept the strains below 75 microstrains. The lower strain level has a lower probability of damaging the specimen, and therefore a greater probability of larger |E*| values. This observation is supported by the fact that the modified Witczak model displays a similar underestimation of the |E*| values. Again, the different strain levels used in the Witczak and North Carolina databases explain this trend. One way to reduce this bias is to retrain the ANN model using the data from both the Witczak and North Carolina databases.

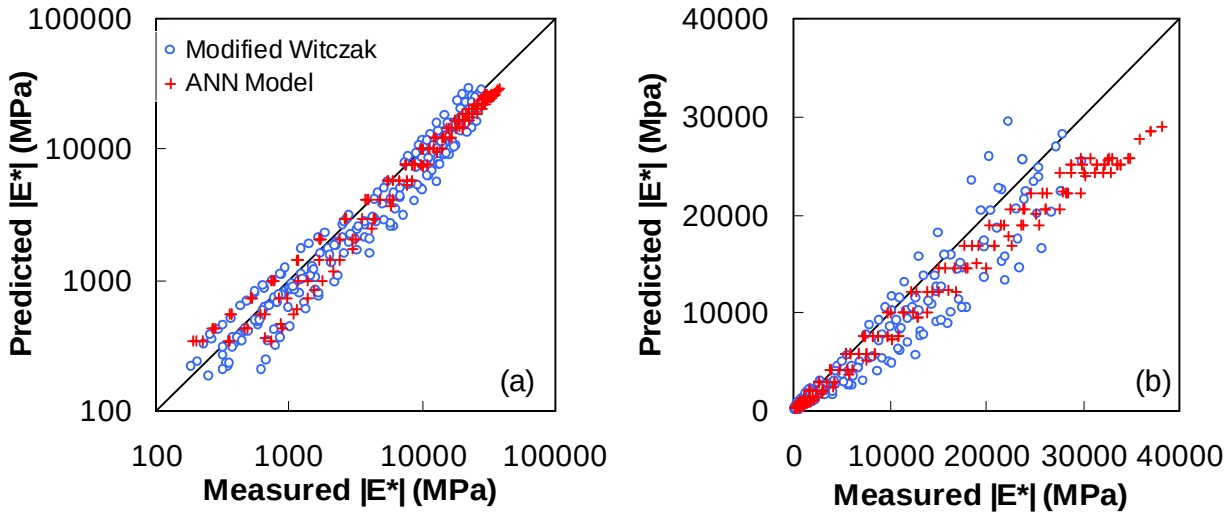

Figure 6.10. Line-of-equality graph of verification data (a) log-log and (b) arithmetic scales.

To determine if the level of accuracy, in the ANN model is adequate, as shown in Figure 6.10, the effect of the changes in the modulus on performance results has been evaluated using the MEPDG. The performance predictions based on the measured and predicted |E*| data calculated by the MEPDG are presented in Table 6.2. The measured |E*| values were obtained from the S12.5C mixture. The M_R values for the mixture were used to

predict the |E*| values. To characterize the predicted |E*| values, a linear regression was generated through the ANN data in Figure 6.10. The error was approximately 15%, similar to the error observed by measuring the |E*| with different geometries. Therefore, this comparison also allows the evaluation of the quality of data from different geometries as well as the predictions of the ANN. The measured and predicted |E*| values were used to predict the performance of both a thin and a thick pavement with different loading levels.

Table 6.2. MEPDG Performance Predictions Based on Measured and Predicted Data

Performance Criteria	Distress Target	Source of |E*|		ANN/Measured Ratio
		ANN	Measured	
10" Asphalt, 6" Aggregate Base AADTT = 8000				
Terminal IRI (in/mi)	172	120.9	118.4	1.02
AC Bottom Up Cracking (%):	25	7.6	5.6	1.36
Permanent Deformation (AC Only) (in):	0.25	0.13	0.12	1.08
4" Asphalt, 8" Aggregate Base AADTT = 300				
Terminal IRI (in/mi)	172	122.7	119.5	1.03
AC Bottom Up Cracking (%):	25	2.5	1.8	1.39
Permanent Deformation (AC Only) (in):	0.25	0.32	0.27	1.19

Note that the |E*| is a small strain measurement and provides a pavement response at similar levels. Performance evaluations concerning permanent deformation and cracking occur at high strain levels. Therefore, differences in the |E*| values – without including the changes in performance prediction model coefficients – may not provide an accurate evaluation. With this limitation in mind, the following comparisons are made. For both cases, the predicted |E*| values do not change the conclusions of the analysis. For example, the bottom up cracking ratio is large, but the values in both pavements are small compared to the failure criteria. In the thin pavement example, the pavement fails the permanent deformation criteria in both cases. The results imply that the IRI model is not

strongly influenced by the |E*| input. The predicted |E*| values provide similar performance results with consistent conclusions compared with those of the measured |E*| values.

6.7 Conclusions

The results show that using the M_R to predict the |E*| is possible using an ANN. Also, given the appropriate models, significant work and time can be saved by predicting a value instead of measuring it. A |E*| prediction methodology is developed using the ANN. This methodology uses the M_R values and binder time-temperature shift factors as inputs. The following three steps were conducted for verification: (1) prediction of the |E*| data in the Witczak database, which are used in the ANN training; (2) prediction of the |E*| data in the Witczak database, which are not used in the ANN training; and (3) prediction of the |E*| data from an independent database composed of seven North Carolina mixtures. In all three verification steps, the ANN model shows a better prediction accuracy than the modified Witczak model. A slight bias is observed in the third verification study that employs the independent North Carolina database. This bias, observed in both the ANN and modified Witczak models, may be due to the different strain levels used in the Witczak and North Carolina databases. Effects of this bias on the pavement performance are evaluated from limited MEPDG analyses and found to be insignificant. The developed ANN model is a reasonable method of populating the LTPP Materials database with |E*| values using M_R values, provided binder shift factor information is known.

As mentioned earlier, the ANN was created using a MatLAB® toolbox. Any standard programming language can use the output of the training session to recreate the neural network. For the pavement engineers, this provides an accessible product in which they provide the inputs, *i.e.* M_R values and reduced frequencies, and the program provides the sigmoidal shift factors. In this case, databases, such as the LTPP materials database, can be updated with |E*| at least as accurately as using other models.

CHAPTER 7 SUMMARY AND FUTURE RESEARCH

As mentioned in the Introduction, when applying mechanistic and mechanistic-empirical methods to pavment design and rehabilition, knowing the material property is important. As shown, the predictions in MEPDG are not significantly sensitive for a thin and thick pavement to variations in dynamic modulus as large as 15%. The preferred method for acquiring |E*|is measuring the material response using the standard axial specimen. The dynamic modulus should be measured for most projects when the road is built to have a database of the initial stiffness of the pavement. When this in not possible, i.e. an in-place pavement, another method such as IDT testing is an alternative. The second option allows for better rehabilitation design since one would know the |E*| at a few points along the road. The challenge would be acquiring the data fast enough, since testing takes time. For this reason, most moduli values are determined using falling-weight deflectometer (FWD). A third alternative is is to predict the |E*| from the M_R. This alternative is the most desireable for populating the LTPP materials database since binder information is more readily available.

The latter two options provide viable methods for populating the LTPP materials database. To balance accuracy with expediency, both require some testing to adequately characterize the mixtures for predicting pavement performance with the MEPDG. With the additional pavement performance predictions, an estimate of the accuracy of MEPDG performance predictions can be made by comparing predictions to field observations collected for LTPP pavement sections.

REFERENCES

AASHTO TP-31 *Standard Test Method for Determining the Resilient Modulus of Bituminous Mixtures by Indirect Tension* (1996). AASHTO, Washington D.C.

AASHTO TP-62 Standard Method of Test for Determining Dynamic Modulus of Hot-Mix Asphalt Concrete Mixtures (2004). AASHTO, Washington D.C.

ASTM D 4123 *Standard Test Method for Indirect Tension Test for Resilient Modulus of Bituminous Mixture* (1982). ASTM International, West Conshohocken, PA,

Bari, J (2005). *Development of a New Revised Version of Witczak E* Predictive Models for Hot Mix Asphalt Mixtures.* Ph D Thesis, Arizona State University, Tempe, AZ.

Bari, J and M. Witczak (2007). New Predictive Models for the Viscosity and Complex Shear Modulus of Asphalt Binders for Use with the Mechanistic-Empirical Pavement Design Guide. In *Transportation Research Board: 86th Annual Meeting Compendium of Papers*, TRB, National Research Council, Washington, D.C.

Barksdale, R. D., J. Alba, N. P. Khosla, R. Kim, P. C. Lambe, and M. S. Rahman (June 1997). *NCHRP Web Document 14: Laboratory Determination of Resilient Modulus for Flexible Pavement Design*. NCHRP Program 1-28 Project, TRB, National Research Council, Washington, D.C.

Christensen Jr., D. W., T. K. Pellinen, and R. F. Bonaquist. (2003). Hirsch Model for Estimating the Modulus of Asphalt Concrete. *Journal of the Association of Asphalt Paving Technologists* (*AAPT*), Vol. 72.

Dongre, R., L. Myers, J. D'Angelo, C. Paugh, and J. Gudimettla (2005). Field Evaluation of Witczak and Hirsch Models for Predicting the Dynamic Modulus of Hot-Mix Asphalt. *Journal of the Association of Asphalt Paving Technologists*, Vol. 74, pp. 381-442.

Drescher A., D.E. Newcomb, and W. Zhang (1997). Interpretation of Indirect Tension Test Based on Viscoelasticity. In *Transportation Research Record: Journal of the Transportation Research Board, No. 1590*, TRB, National Research Council, Washington, D.C., pp. 45-52.

Fairhurst, C. E., Y. R. Kim, and N. P. Khosla (October 1990). *Resilient Modulus Testing of Asphalt Specimens in Accordance with ASTM D 4123-82*. Proceedings, RILEM Fourth International Symposium, Budapest, Hungry.

Hondros, G. (1959). Evaluation of Poisson's Ratio and the Modulus of Materials of a Low Tensile Resistance by the Brazilian (Indirect Tensile) Test with Particular

Reference to Concrete. *Australian Journal of Applied Science*, Vol. 10, No. 3, pp. 243-268.

Hunter, A., G. Airey, and A. Collop (2004). Aggregate Orientation and Segregation in Laboratory-Compacted Asphalt Samples. In *Transportation Research Record: Journal of the Transportation Research Board, No. 1891*, TRB, National Research Council, Washington, D.C., pp. 8-15.

Kim, Y. R. and Y. C. Lee (1995). Interrelationships among Stiffnesses of Asphalt-Aggregate Mixtures. *Journal of the Association of Asphalt Paving Technologists*, Vol. 64, pp. 575-609.

Kim, Y. R., Y. Seo, M. King, and M. Momen (2004). Dynamic Modulus Testing of Asphalt Concrete in Indirect Tension Mode. In *Transportation Research Record: Journal of the Transportation Research Board, No. 1891*, TRB, National Research Council, Washington, D.C., pp. 163-173.

Kim, Y. R., S. Lee, Y. Seo, and O. El-Haggan (2005). *Impact of Price Reductions on the Long-Term Pavement Performance of HMA Mixes in North Carolina*. North Carolina Department of Transportation Final Report. Research Project No. HWY-2002-07.

Li, Y., and J. B. Metcalf (July/August 2005). Two-Step Approach to Prediction of Asphalt Concrete Modulus from Two-Phase Micromechanical Models. *Journal of Materials in Civil Engineering*, Vol. 17, No. 4, pp. 407-415.

Loulizi, A., G. W. Flintsch, I. L. Al-Qadi, and D. Mokarem (2006). Comparison between Resilient Modulus and Dynamic Modulus of Hot-Mix Asphalt as Material Properties for Flexible Pavement Design. In *TRB Annual Meeting 2006 CD-ROM*: *Journal of the Transportation Research Board, No. 2255,* TRB, National Research Council, Washington, D.C.

Mirza, M. W., R. A. Graul, J. L. Groeger, and A. Lopez (1997). Theoretical Evaluation of Poisson's Ratio and Elastic Modulus Using Indirect Tensile Test with Emphasis on Bituminous Mixtures. In *Transportation Research Record: Journal of the Transportation Research Board, No. 1590*, TRB, National Research Council, Washington, D.C. pp. 34-44.

Mirza, M. W., R. A. Graul, J. L. Groeger, and A. Lopez (2006). Evaluation of Testing Protocols for Dynamic Modulus of Hot-Mix Asphalt. In *Transportation Research Record: Journal of the Transportation Research Board, No. 1970,* TRB, National Research Council, Washington, D.C., pp. 126-132.

Park, S.W. and R.A. Schapery (1999). Methods of Interconversion between Linear Viscoelastic Material Functions. Part I – a Numerical Method Based on Prony Series. *International Journal of Solids and Structures*, Vol. 36, pp. 1653-1675.

Roque, R. and W. G. Buttlar (1992). The Development of a Measurement and Analysis System to Accurately Determine Asphalt Concrete Properties Using the Indirect Tensile Mode. *The Journal of the Association of Asphalt Paving Technologists*, Vol. 60, pp. 304-332.

Saadeh, S (2002). *Comparative Analysis of Axial and Shear Moduli of Asphalt Mixes*. Master Thesis, Washington State University, Pullman, WA.

SAS Institute Inc. (2004). *SAS OnlineDoc® 9.1.3*. SAS Institute Inc., Cary, NC.

Schwartz, C. W. Sensitivity of Predictive Models for the Dynamic Modulus of Aspahlt Concrete, white paper prepared for the Long Term Pavement Performance Program, Federal Highway Administration, U.S. Department of Transportation, Washington, D.C.

SHRP-LTPP Protocol P07, Test Method for Determining the Creep Compliance, Resilient Modulus, and Strength of Asphalt Materials Using the Indirect Tensile Test Device (August 2001). LAW PCS, SHRP, National Research Council, Washington, D.C.

Tashman, L. E. Masad, D. Little, and R. Lytton (2004). Internal Structure Analysis of Asphalt Mixes to Improve the Simulation of Superpave Gyratory Compaction to Field Conditions. *Journal of the Association of Asphalt Paving Technologists.* Vol 70, pp. 605-645.

Underwood, B. S., Y. R. Kim, and M. N. Guddati (2005). Characterization and Performance Prediction of ALF Mixtures Using a Viscoelastoplastic Continuum Damage Model. Submitted to the *Journal of Association of Asphalt Paving Technologists*,.

Vinson, T. S (1989). *Fundamentals of Resilient Modulus Testing*. Proceedings of the Workshop on Resilient Modulus Testing, Oregon State University, Corvallis, Oregon.

Witczak, M. W (January 2004). Laboratory Determination of Resilient Modulus for Flexible Pavement. *NCHRP Research Results Digest*, No. 285. TRB, National Research Council, Washington, D.C.

Xu, B., R. S. Ranjithan, and Y. R. Kim (2002). New Relationships Between Falling Weight Deflectometer Deflections and Asphalt Pavement Layer Condition Indicators. In *Transportation Research Record: Journal of the Transportation Research Board, No. 1806*, TRB, National Research Council, Washington, D.C., pp.48-56.

Zhang, W (1996). *Viscoelastic Analysis of Diametrical Compression Test on Asphalt Concrete*. Ph. D. Dissertation, University of Minnesota, Minneapolis, MN.

Zhang, W., A. Drescher, And D. E. Newcomb (1997). Viscoelastic Analysis of Diametrical Compression of Asphalt Concrete. *Journal of Engineering Mechanics*, Vol. 123, pp. 596-603.

APPENDIX A DYNAMIC MODULUS DATA

A.1 Mixture Sigmoidal and Shift Factor Coefficients

Table A.1

	Mixture	Sigmoidal Coefficients				Shift Factors		
		a	b	c	d	a_1	a_2	a_3
Axial	S12.5C	2.044669	2.488376	1.951166	0.512443	0.000683	-0.16253	0.919948
	S12.5C-AV+2	1.986494	2.586147	1.901819	0.515423	0.000934	-0.17406	0.953549
	S12.5C-AV-2	2.018849	2.590057	1.995269	0.516639	0.000682	-0.15861	0.861768
	S12.5C-AC+1	1.676709	2.896986	1.895851	0.494786	0.000825	-0.170077	0.914055
	S12.5C-AC-1	2.250625	2.374951	2.020612	0.488145	0.000793	-0.168306	0.926656
	S12.5CM	2.500876	2.095267	1.638537	0.490938	0.000632	-0.166693	0.873433
	S12.5FE	1.769719	2.753742	1.945557	0.515966	0.000661	-0.157656	0.846027
	S12.5F	1.957131	2.624962	2.118853	0.513554	0.000915	-0.176118	1.000702
	B25.0C	1.997727	2.551977	2.023047	0.594048	0.000805	-0.162505	0.896254
IDT	S12.5C	2.373155	2.112485	1.886832	0.678727	0.000769	-0.157041	0.930516
	S12.5C-AV+2	2.039487	2.48537	1.84858	0.475245	0.000973	-0.173364	0.907035
	S12.5C-AV+2 Slab	2.347533	2.094682	1.730307	0.609049	0.000787	-0.162825	0.921306
	S12.5C-AV-2	2.473963	2.02156	1.890154	0.622401	0.000739	-0.160514	0.943953
	S12.5C-AC+1	2.126996	2.316107	1.758575	0.615916	0.001264	-0.180201	0.988167
	S12.5C-AC-1	2.37779	2.172179	2.023028	0.554675	0.000935	-0.16431	0.88008
	S12.5CM	2.444128	2.042913	1.684486	0.579766	0.000675	-0.160453	0.913901
	S12.5FE	1.820922	2.757234	1.935167	0.519584	0.000786	-0.160663	0.846053
	S12.5F	2.055404	2.483069	2.10817	0.552521	0.000748	-0.159598	0.909225
	B25.0C	2.717084	1.794979	1.80222	0.681913	0.001167	-0.172266	0.88456
	S12.5FE-AV+3	2.732508	1.797971	1.536977	0.640441	0.000521	-0.155534	0.835576
	S12.5FE-AV+3 Slab	1.978501	2.526673	1.673439	0.500727	0.000926	-0.165553	0.8771
Prism	S12.5C	2.036595	2.531957	2.003515	0.502241	0.000715	-0.169097	0.921334
	S12.5C-AV+2 Slab	1.696742	2.839284	2.029391	0.489489	0.000714	-0.167155	0.88696
	S12.5FE	2.044806	2.454112	1.872072	0.54516	0.000783	-0.167034	0.934974
	S12.5FE-AV+3 Slab	1.738379	2.780385	1.895498	0.512745	0.000734	-0.165977	0.868306
	B25.0C	2.23839	2.291789	1.969988	0.621249	0.000898	-0.168496	0.959314

A.2 Axial Specimen Data

Table A.2 S12.5C Axial Data

Temperature (°C)	Replicate	Parameters	Frequency (Hz)							
			25	10	5	1	0.5	0.1	0.05	0.01
-10	1	|E*| (MPa)	38098	37033	36089	33713	32537	29731	28425	25172
		Phase Angle (°)	5.7	5.4	6.0	6.7	7.5	8.7	9.2	11.0
		Microstrain	41	43	43	42	42	40	42	36
	2	|E*| (MPa)	28547	27396	26501	24504	23408	21291	20115	17488
		Phase Angle (°)	7.1	7.2	7.4	8.6	8.9	10.8	11.2	11.8
		Microstrain	54	57	58	58	58	56	60	52
	3	|E*| (MPa)	29594	28420	27436	25017	24067	21637	20527	18276
		Phase Angle (°)	9.0	9.2	9.2	10.5	11.1	12.2	13.8	16.5
		Microstrain	52	55	56	57	56	55	58	49
	4	|E*| (MPa)	33363	32376	31442	29178	28044	25457	23940	20980
		Phase Angle (°)	7.2	7.4	7.8	8.9	9.4	11.7	11.5	13.3
		Microstrain	51	50	50	49	49	48	51	44
	Average	Average |E*|	32400	31307	30367	28103	27014	24529	23252	20479
		Std. dev. |E*|	4325	4380	4375	4286	4213	3948	3851	3468
10	1	|E*| (MPa)	22244	20022	18396	14581	12949	9429	8076	5398
		Phase Angle (°)	12.9	13.8	15.0	18.4	20.7	25.2	29.2	36.3
		Microstrain	49	50	49	47	46	44	39	34
	2	|E*| (MPa)	17391	15716	14463	11501	10203	7588	6436	4564
		Phase Angle (°)	13.8	14.7	15.7	19.0	21.0	26.0	30.7	27.2
		Microstrain	63	64	63	60	58	55	50	43
	3	|E*| (MPa)	18892	16815	14913	11996	10546	7844	6828	4629
		Phase Angle (°)	15.6	16.5	17.9	21.4	23.5	28.9	33.4	35.2
		Microstrain	57	59	61	57	56	53	48	43
	4	|E*| (MPa)	20294	18349	16754	13356	11820	8660	7267	4955
		Phase Angle (°)	14.0	15.0	16.3	19.4	22.3	27.3	32.2	37.3
		Microstrain	56	56	55	51	50	48	45	40
	Average	Average |E*|	19705	17725	16132	12858	11380	8380	7152	4886
		Std. dev. |E*|	2067	1874	1806	1391	1257	836	703	381
35	1	|E*| (MPa)	5672	4234	3325	1821	1399	836	1024	436
		Phase Angle (°)	28.3	31.4	33.0	35.0	36.5	34.9	41.2	30.9
		Microstrain	40	42	42	38	36	27	6	79
	2	|E*| (MPa)	5343	4060	3181	1761	1349	776	627	477
		Phase Angle (°)	31.4	33.4	35.7	39.0	41.1	40.4	40.2	36.9
		Microstrain	43	44	44	39	37	39	39	29
	3	|E*| (MPa)	5559	4163	3231	1738	1290	721	572	386
		Phase Angle (°)	31.4	32.2	34.5	36.7	38.2	36.2	37.3	34.6
		Microstrain	40	43	43	40	39	42	42	36
	4	|E*| (MPa)	5539	4087	3204	1729	1318	783	640	
		Phase Angle (°)	31.7	32.1	33.8	36.4	38.8	36.1	36.5	
		Microstrain	37	42	43	40	38	39	38	
	Average	Average |E*|	5528	4136	3235	1762	1339	779	716	433
		Std. dev. |E*|	136	79	63	41	46	47	207	45
54	1	|E*| (MPa)	1383	1039	757	479	439	445		
		Phase Angle (°)	37.8	34.7	33.8	31.3	29.9	34.6		
		Microstrain	52	38	48	28	18	6		
	2	|E*| (MPa)	957	735	511	303	259	230		
		Phase Angle (°)	38.9	34.9	34.7	31.6	30.4	29.2		
		Microstrain	82	57	84	65	56	28		
	3	|E*| (MPa)	1306	1026	707	412	346	278		
		Phase Angle (°)	38.5	34.5	34.1	31.1	30.0	28.4		
		Microstrain	60	41	61	48	42	23		
	4	|E*| (MPa)	1264	942	699	464	443	415		
		Phase Angle (°)	39.4	36.1	34.2	31.2	30.4	24.1		
		Microstrain	44	35	44	29	21	16		
	Average	Average |E*|	1227	935	669	414	372	342		
		Std. dev. |E*|	187	140	108	80	87	104		

Table A.3 S12.5C-AC-1 Axial Data

Temperature (°C)	Replicate	Parameters	Frequency (Hz)							
			25	10	5	1	0.5	0.1	0.05	0.01
-10	1	|E*| (MPa)	38222	37015	35686	33316	32175	29663	28499	25367
		Phase Angle (°)	7.2	6.5	7.3	8.6	8.7	10.5	11.7	13.9
		Microstrain	44	44	44	43	42	41	40	36
	2	|E*| (MPa)	40179	38832	37863	35953	34561	31068	29811	26828
		Phase Angle (°)	7.2	7.1	7.0	7.9	8.8	10.1	11.5	12.0
		Microstrain	42	42	41	40	39	39	38	34
	3	|E*| (MPa)	41982	41262	40197	37673	35600	33722	31702	28862
		Phase Angle (°)	8.0	8.2	8.8	9.4	10.5	13.3	11.1	14.2
		Microstrain	40	39	39	38	38	36	36	32
	Average	Average |E*|	40128	39036	37915	35647	34112	31484	30004	27019
		Std. dev. |E*|	1880	2131	2256	2195	1756	2062	1610	1755
10	1	|E*| (MPa)	23745	21685	20129	16293	14925	11818	10406	7636
		Phase Angle (°)	12.3	12.8	14.1	17.1	19.0	22.7	24.2	29.9
		Microstrain	56	57	55	56	53	50	47	40
	2	|E*| (MPa)	24736	22747	20897	17050	15499	11947	10587	7651
		Phase Angle (°)	12.9	13.0	14.1	16.7	19.4	23.4	26.1	30.3
		Microstrain	53	54	53	54	51	49	47	40
	3	|E*| (MPa)	27958	24872	23075	18764	17282	13607	12123	8842
		Phase Angle (°)	14.6	15.5	16.6	19.3	21.6	27.4	28.9	34.2
		Microstrain	38	38	37	35	33	29	26	24
	Average	Average |E*|	25480	23101	21367	17369	15902	12457	11039	8043
		Std. dev. |E*|	2203	1623	1528	1266	1229	998	943	692
35	1	|E*| (MPa)	7910	6097	4897	2833	2196	1390	1144	773
		Phase Angle (°)	28.4	29.8	31.4	38.5	40.5	40.2	40.4	38.5
		Microstrain	26	29	30	27	26	26	26	30
	2	|E*| (MPa)	7782	6072	4959	2879	2293	1369	1104	740
		Phase Angle (°)	28.1	29.1	31.3	38.4	39.8	38.7	39.1	37.8
		Microstrain	29	31	30	27	25	26	27	31
	3	|E*| (MPa)	8788	6848	5587	3314	2629	1693	1442	982
		Phase Angle (°)	30.7	32.4	34.0	41.4	42.0	40.3	40.5	40.3
		Microstrain	26	27	27	23	22	21	20	23
	Average	Average |E*|	8160	6339	5148	3009	2373	1484	1230	831
		Std. dev. |E*|	547	441	382	265	227	181	184	131
54	1	|E*| (MPa)	2532	1654	1277	819	801	669		
		Phase Angle (°)	40.1	36.6	36.3	34.3	36.7	35.8		
		Microstrain	12	21	23	17	13	11		
	2	|E*| (MPa)	2108	1477	1153	726	649	519		
		Phase Angle (°)	37.6	36.2	35.4	33.5	32.2	29.0		
		Microstrain	20	25	26	19	16	15		
	3	|E*| (MPa)	2507	1762	1418	1026	889	653		
		Phase Angle (°)	39.6	37.2	36.7	32.8	32.0	29.5		
		Microstrain	17	21	21	14	14	20		
	Average	Average |E*|	2383	1631	1283	857	780	614		
		Std. dev. |E*|	238	144	132	153	121	83		

Table A.4 S12.5C-AC+1 Axial Data

Temperature (°C)	Replicate	Parameters	Frequency (Hz)							
			25	10	5	1	0.5	0.1	0.05	0.01
-10	1	|E*| (MPa)	32063	31389	30501	28106	26561	23717	22385	19240
		Phase Angle (°)	5.6	5.8	6.7	8.4	9.0	10.1	11.7	13.4
		Microstrain	52	52	51	51	51	51	51	48
	2	|E*| (MPa)	30854	30001	28892	26213	25230	22585	21233	18451
		Phase Angle (°)	6.3	6.4	6.9	9.3	8.6	10.4	10.8	13.1
		Microstrain	54	54	54	54	54	54	54	50
	3	|E*| (MPa)	39967	38796	37889	33608	31911	29022	28082	24865
		Phase Angle (°)	15.6	15.0	15.6	17.2	17.3	18.8	21.4	23.4
		Microstrain	42	42	41	42	43	42	41	37
	Average	Average |E*|	34295	33395	32427	29309	27900	25108	23900	20852
		Std. dev. |E*|	4950	4728	4798	3842	3536	3436	3667	3498
10	1	|E*| (MPa)	18230	16437	14859	10996	9573	6519	5337	3202
		Phase Angle (°)	13.9	14.8	17.2	22.5	25.0	31.6	34.7	40.3
		Microstrain	59	60	60	67	66	72	74	76
	2	|E*| (MPa)	17829	15925	14348	10915	9553	6667	5503	3498
		Phase Angle (°)	14.0	15.0	16.3	21.1	23.7	29.0	32.7	37.8
		Microstrain	74	77	77	84	83	88	90	87
	3	|E*| (MPa)	20467	17962	16052	11992	10443	7514	6317	3957
		Phase Angle (°)	21.6	22.6	24.0	29.1	32.2	37.6	41.4	47.1
		Microstrain	51	53	53	55	54	52	51	53
	Average	Average |E*|	18842	16775	15086	11301	9856	6900	5719	3553
		Std. dev. |E*|	1422	1059	874	600	508	537	524	381
35	1	|E*| (MPa)	4145	2944	2225	1110	836	476	383	264
		Phase Angle (°)	34.3	35.7	37.4	41.1	40.6	37.8	36.3	33.5
		Microstrain	38	45	49	53	52	56	60	68
	2	|E*| (MPa)	3852	2735	2076	1046	794	451	366	256
		Phase Angle (°)	32.8	33.4	34.9	37.9	37.8	33.8	32.7	28.5
		Microstrain	57	66	71	74	73	79	80	90
	3	|E*| (MPa)	4605	3304	2510	1243	951	595	516	267
		Phase Angle (°)	39.4	39.1	40.9	44.7	44.7	40.5	38.4	35.7
		Microstrain	35	42	46	47	50	45	42	57
	Average	Average |E*|	4201	2994	2270	1133	860	507	422	262
		Std. dev. |E*|	379	288	220	101	82	77	83	6
54	1	|E*| (MPa)	866	530	393	232	202	160		
		Phase Angle (°)	38.6	34.8	32.6	28.4	26.8	23.5		
		Microstrain	32	62	72	61	51	48		
	2	|E*| (MPa)	839	544	423	265	243	209		
		Phase Angle (°)	37.4	34.0	32.2	28.3	25.9	22.0		
		Microstrain	45	65	71	54	42	37		
	3	|E*| (MPa)	880	570	431	268	225	178		
		Phase Angle (°)	42.8	37.9	37.8	32.9	30.0	23.0		
		Microstrain	33	46	26	39	36	22		
	Average	Average |E*|	862	548	415	255	223	182		
		Std. dev. |E*|	21	21	20	20	20	25		

Table A.5 S12.5C- AV-2 Axial Data

Temperature (°C)	Replicate	Parameters	Frequency (Hz)							
			25	10	5	1	0.5	0.1	0.05	0.01
-10	1	|E*| (MPa)	35709	34569	33488	30903	29705	26803	25444	22339
		Phase Angle (°)	5.5	5.3	5.7	6.1	7.1	8.9	9.5	10.2
		Microstrain	45	46	46	46	46	45	47	41
	2	|E*| (MPa)	40867	38937	37058	33877	32235	29029	27638	23790
		Phase Angle (°)	4.8	4.6	4.8	5.6	6.5	6.6	9.2	10.8
		Microstrain	42	42	41	40	40	40	39	35
	3	|E*| (MPa)	41825	40600	39055	36539	34788	31096	29480	26294
		Phase Angle (°)	7.1	8.2	7.6	9.2	10.4	11.6	12.8	15.4
		Microstrain	40	40	40	39	39	39	39	35
	4	|E*| (MPa)	35577	34421	33670	30901	29923	26562	25511	22334
		Phase Angle (°)	6.7	6.7	6.9	7.4	8.8	9.4	10.9	12.0
		Microstrain	47	47	47	46	45	46	45	41
	Average	Average |E*|	38494	37132	35818	33055	31663	28373	27018	23689
		Std. dev. |E*|	3316	3120	2711	2713	2377	2128	1931	1867
10	1	|E*| (MPa)	21581	19398	17782	14175	12561	9085	8003	5623
		Phase Angle (°)	12.2	12.6	13.7	17.0	18.7	24.2	26.7	22.8
		Microstrain	52	52	51	48	47	46	41	35
	2	|E*| (MPa)	27043	24025	21814	17216	15267	11489	9785	6652
		Phase Angle (°)	15.4	15.4	16.6	20.3	22.4	26.6	29.0	32.1
		Microstrain	46	48	47	49	48	47	46	41
	3	|E*| (MPa)	24886	22221	20383	15803	14337	10412	8929	5972
		Phase Angle (°)	14.3	14.4	15.4	17.2	22.6	26.7	29.5	34.5
		Microstrain	53	56	55	58	55	56	55	51
	4	|E*| (MPa)	22241	20138	18562	14582	13121	9791	8364	5649
		Phase Angle (°)	12.8	13.4	14.5	17.5	20.1	24.5	28.0	31.8
		Microstrain	60	61	60	63	60	60	59	54
	Average	Average |E*|	23937	21445	19635	15444	13821	10194	8770	5974
		Std. dev. |E*|	2515	2094	1816	1369	1216	1020	776	479
35	1	|E*| (MPa)	5439	4074	3175	1736	1319	753	608	424
		Phase Angle (°)	29.8	31.3	33.2	34.7	36.1	34.2	34.1	30.8
		Microstrain	43	45	44	40	38	41	40	33
	2	|E*| (MPa)	6936	5017	3969	2123	1667	950	755	512
		Phase Angle (°)	32.5	33.6	35.4	41.0	41.1	37.8	36.8	32.3
		Microstrain	30	34	34	33	31	32	32	35
	3	|E*| (MPa)	6086	4495	3487	1838	1447	822	675	464
		Phase Angle (°)	31.9	33.0	34.5	39.6	41.0	37.7	37.1	34.8
		Microstrain	38	41	43	42	40	43	44	49
	4	|E*| (MPa)	6686	5067	3986	2156	1657	984	840	607
		Phase Angle (°)	29.5	31.1	33.4	39.3	39.7	39.5	36.2	34.1
		Microstrain	29	30	31	29	29	27	26	27
	Average	Average |E*|	6287	4663	3654	1963	1522	877	720	502
		Std. dev. |E*|	668	470	394	208	169	108	100	79
54	1	|E*| (MPa)	1272	938	678	390	336	263		
		Phase Angle (°)	38.0	34.5	33.9	30.6	28.5	24.4		
		Microstrain	62	48	63	51	43	24		
	2	|E*| (MPa)	1667	1107	868	537	482	373		
		Phase Angle (°)	39.4	37.2	35.3	32.9	33.0	26.1		
		Microstrain	21	27	28	20	16	15		
	3	|E*| (MPa)	1630	1079	824	510	457	379		
		Phase Angle (°)	40.6	37.4	36.1	35.3	32.9	32.3		
		Microstrain	24	33	36	28	22	20		
	4	|E*| (MPa)	1684	1131	864	549	497	413		
		Phase Angle (°)	39.0	35.9	34.9	31.8	30.8	27.9		
		Microstrain	23	32	34	26	21	18		
	Average	Average |E*|	1563	1064	808	496	443	357		
		Std. dev. |E*|	196	86	89	72	73	65		

Table A.6 S12.5C-AV+2 Axial Data

Temperature (°C)	Replicate	Parameters	Frequency (Hz)							
			25	10	5	1	0.5	0.1	0.05	0.01
-10	1	|E*| (MPa)	34779	33338	32635	30065	29068	26062	24824	21950
		Phase Angle (°)	7.6	7.0	7.0	8.5	9.0	10.6	13.1	14.7
		Microstrain	49	49	48	47	47	47	46	42
	2	|E*| (MPa)	36929	35323	34308	31848	30459	26953	26111	23119
		Phase Angle (°)	8.8	8.8	9.0	10.7	11.2	12.7	14.7	16.5
		Microstrain	45	46	46	45	45	45	44	40
	3	|E*| (MPa)	35722	34423	33571	31322	29893	26982	25861	22662
		Phase Angle (°)	7.8	8.9	8.5	9.6	10.1	11.9	11.8	14.5
		Microstrain	47	47	47	46	46	45	44	41
	Average	Average |E*|	35810	34361	33505	31078	29807	26665	25599	22577
		Std. dev. |E*|	1078	994	839	916	700	523	683	589
10	1	|E*| (MPa)	18291	16351	14911	11624	10382	7404	6339	4214
		Phase Angle (°)	12.6	12.9	14.6	18.6	19.5	25.0	27.9	37.5
		Microstrain	73	75	74	79	76	79	78	72
	2	|E*| (MPa)	21496	19127	17644	13862	12361	9170	7871	5353
		Phase Angle (°)	14.7	15.5	17.1	21.0	23.1	28.4	30.6	37.0
		Microstrain	62	65	63	66	64	64	63	57
	3	|E*| (MPa)	21146	19063	17394	13646	12083	8996	7674	5172
		Phase Angle (°)	14.0	14.8	16.2	19.8	22.1	27.5	30.3	35.6
		Microstrain	63	65	64	67	65	65	64	59
	Average	Average |E*|	20311	18180	16650	13044	11609	8524	7295	4913
		Std. dev. |E*|	1758	1584	1511	1235	1071	973	834	612
35	1	|E*| (MPa)	4981	3698	2890	1507	1129	646	519	342
		Phase Angle (°)	29.2	30.7	32.5	36.9	38.2	33.9	34.0	30.6
		Microstrain	43	49	51	52	51	55	57	67
	2	|E*| (MPa)	5358	3990	3159	1667	1280	731	587	376
		Phase Angle (°)	32.2	33.3	35.4	42.1	42.8	41.4	40.6	37.4
		Microstrain	44	46	47	46	45	49	50	61
	3	|E*| (MPa)	4976	3697	2858	1569	1227	757	626	470
		Phase Angle (°)	31.7	32.6	34.1	39.4	39.9	38.1	37.3	36.0
		Microstrain	45	49	52	50	47	47	47	49
	Average	Average |E*|	5105	3795	2969	1581	1212	712	577	396
		Std. dev. |E*|	219	169	165	81	77	58	55	67
54	1	|E*| (MPa)	1211	814	615	375	323	259		
		Phase Angle (°)	37.0	34.4	33.4	29.5	27.8	22.5		
		Microstrain	33	44	48	38	32	30		
	2	|E*| (MPa)	1284	817	616	379	344	287		
		Phase Angle (°)	41.6	38.4	37.2	35.8	34.8	33.1		
		Microstrain	25	42	47	37	30	26		
	3	|E*| (MPa)	1247	844	656	459	468	396		
		Phase Angle (°)	39.0	35.9	34.7	32.3	30.4	25.2		
		Microstrain	29	41	45	31	22	19		
	Average	Average |E*|	1247	825	629	404	378	314		
		Std. dev. |E*|	37	16	23	47	78	73		

Table A.7 S12.5CM Axial Data

Temperature (°C)	Replicate	Parameters	Frequency (Hz)							
			25	10	5	1	0.5	0.1	0.05	0.01
-10	1	|E*| (MPa)	31087	29818	28909	26454	25224	22895	21647	19212
		Phase Angle (°)	7.5	6.9	7.3	8.3	9.2	10.8	11.8	13.9
		Microstrain	54	54	54	54	54	53	53	48
	2	|E*| (MPa)	34827	33032	32195	29246	28121	24802	23869	21063
		Phase Angle (°)	8.9	8.8	8.7	10.7	11.3	13.4	14.6	15.9
		Microstrain	48	49	49	49	48	49	48	44
	3	|E*| (MPa)	44572	42272	40060	36639	36206	32225	31489	28107
		Phase Angle (°)	11.4	10.4	11.6	13.1	14.1	13.5	15.9	17.4
		Microstrain	37	38	39	39	38	38	36	33
	Average	Average |E*|	36829	35040	33721	30780	29850	26640	25668	22794
		Std. dev. |E*|	6962	6466	5730	5263	5692	4929	5162	4694
10	1	|E*| (MPa)	18635	16782	15356	12225	10959	8229	7186	5150
		Phase Angle (°)	13.0	13.6	14.8	18.2	19.7	23.6	25.5	27.7
		Microstrain	71	73	72	75	72	71	69	59
	2	|E*| (MPa)	20339	18327	16724	13264	11785	8940	7732	5625
		Phase Angle (°)	14.4	15.6	16.4	19.7	21.7	25.5	29.0	30.6
		Microstrain	59	59	60	65	62	56	57	44
	3	|E*| (MPa)	24077	21626	19421	15252	13634	10764	9263	6819
		Phase Angle (°)	18.3	19.1	20.2	23.4	25.4	28.7	31.8	34.0
		Microstrain	49	50	52	57	53	47	47	45
	Average	Average |E*|	21017	18912	17167	13580	12126	9311	8060	5865
		Std. dev. |E*|	2783	2474	2068	1538	1370	1308	1077	860
35	1	|E*| (MPa)	4958	3722	3009	1741	1421	966	852	674
		Phase Angle (°)	29.3	30.4	31.7	35.1	36.2	35.2	34.7	33.5
		Microstrain	45	49	49	45	40	37	34	34
	2	|E*| (MPa)	5507	4163	3379	1959	1602	1085	952	752
		Phase Angle (°)	31.6	32.5	33.9	38.1	39.6	37.1	36.5	34.3
		Microstrain	39	44	44	40	36	33	31	31
	3	|E*| (MPa)	5633	4220	3400	2002	1679	1172	1040	837
		Phase Angle (°)	32.4	32.6	34.7	39.6	40.8	40.6	39.3	37.8
		Microstrain	37	43	43	39	34	30	28	27
	Average	Average |E*|	5366	4035	3263	1901	1568	1074	948	754
		Std. dev. |E*|	359	273	220	140	132	103	94	82
54	1	|E*| (MPa)	1545	1152	946	742	746	733		
		Phase Angle (°)	34.6	32.2	31.2	29.6	30.4	32.1		
		Microstrain	26	32	32	19	14	10		
	2	|E*| (MPa)	1637	1223	1018	781	732	773		
		Phase Angle (°)	35.7	32.8	31.5	30.7	31.2	36.0		
		Microstrain	26	30	30	20	17	12		
	3	|E*| (MPa)	1616	1142	914	680	615	506		
		Phase Angle (°)	37.4	34.4	33.6	34.1	31.9	33.0		
		Microstrain	22	31	32	23	21	20		
	Average	Average |E*|	1600	1172	960	734	698	671		
		Std. dev. |E*|	48	44	53	51	72	144		

Table A.8 S12.F Axial Data

Temperature (°C)	Replicate	Parameters	Frequency (Hz)							
			25	10	5	1	0.5	0.1	0.05	0.01
-10	1	|E*| (MPa)	43564	41970	40865	38351	36539	33331	32183	28480
		Phase Angle (°)	7.5	7.1	7.4	8.6	8.8	10.4	12.5	12.7
		Microstrain	38	39	38	37	37	37	35	32
	2	|E*| (MPa)	36663	35171	34503	31926	30840	28403	26768	23943
		Phase Angle (°)	7.0	6.4	6.9	8.2	8.5	10.1	9.8	12.2
		Microstrain	45	46	45	45	44	43	43	38
	3	|E*| (MPa)	36785	35692	34724	32579	31235	28932	27414	24407
		Phase Angle (°)	6.0	6.2	6.3	6.6	7.9	9.1	11.3	11.1
		Microstrain	45	45	45	44	44	42	42	38
	4	|E*| (MPa)	33007	32138	31285	29912	28952	26541	25282	22793
		Phase Angle (°)	6.1	5.3	5.9	7.7	8.5	9.2	10.4	13.0
		Microstrain	51	50	50	48	47	46	45	40
	Average	Average |E*|	37505	36243	35344	33192	31892	29302	27912	24906
		Std. dev. |E*|	4403	4127	4002	3622	3255	2875	2984	2477
10	1	|E*| (MPa)	25551	23111	21045	16816	15033	11204	9700	6675
		Phase Angle (°)	13.3	14.3	14.8	18.6	20.9	24.8	29.6	33.0
		Microstrain	52	53	53	55	53	52	51	46
	2	|E*| (MPa)	22849	20614	19182	15388	13907	10628	9234	6624
		Phase Angle (°)	13.1	13.2	14.1	17.9	19.7	25.2	26.9	34.5
		Microstrain	57	60	58	60	57	55	53	46
	3	|E*| (MPa)	23219	20976	19316	15642	14016	10617	9234	6413
		Phase Angle (°)	11.5	12.1	14.1	16.9	19.2	23.8	25.8	31.7
		Microstrain	57	59	58	59	56	55	53	48
	4	|E*| (MPa)	20847	19035	17606	14168	12731	9555	8308	5671
		Phase Angle (°)	12.1	12.4	13.9	17.8	19.9	24.4	26.9	32.9
		Microstrain	63	65	63	65	62	61	59	54
	Average	Average |E*|	23116	20934	19287	15504	13922	10501	9119	6346
		Std. dev. |E*|	1928	1678	1406	1086	942	688	584	464
35	1	|E*| (MPa)	6587	4961	3905	2102	1626	941	755	507
		Phase Angle (°)	29.4	30.3	32.6	38.5	40.5	37.7	37.5	35.0
		Microstrain	33	37	38	37	35	38	39	45
	2	|E*| (MPa)	6307	4755	3798	2055	1597	918	733	472
		Phase Angle (°)	30.1	31.7	33.9	40.8	42.3	40.4	40.6	39.8
		Microstrain	35	38	39	38	36	39	40	49
	3	|E*| (MPa)	6723	5110	4062	2249	1753	1024	804	523
		Phase Angle (°)	29.5	28.8	31.5	38.0	39.4	37.7	37.8	36.2
		Microstrain	31	36	37	35	33	35	36	44
	4	|E*| (MPa)	5853	4373	3406	1785	1354	751	586	373
		Phase Angle (°)	30.6	31.6	34.5	40.6	42.3	39.2	38.4	34.9
		Microstrain	37	41	43	43	42	48	50	62
	Average	Average |E*|	6368	4800	3793	2048	1583	908	719	469
		Std. dev. |E*|	384	320	280	193	167	114	94	67
54	1	|E*| (MPa)								
		Phase Angle (°)								
		Microstrain								
	2	|E*| (MPa)	1569	1046	770	446	379	276		
		Phase Angle (°)	37.8	37.0	36.1	33.4	30.5	27.0		
		Microstrain	23	34	39	32	34	42		
	3	|E*| (MPa)	1716	1091	835	500	423	322		
		Phase Angle (°)	39.0	36.3	33.8	30.9	28.5	24.8		
		Microstrain	18	32	35	28	30	36		
	4	|E*| (MPa)	1378	918	674	398	336	251		
		Phase Angle (°)	40.2	36.7	35.8	31.7	29.5	25.4		
		Microstrain	30	39	44	36	38	46		
	Average	Average |E*|	1554	1018	760	448	379	283		
		Std. dev. |E*|	169	90	81	51	43	36		

Table A.9 S12.5FE Axial Data

Temperature (°C)	Replicate	Parameters	Frequency (Hz)							
			25	10	5	1	0.5	0.1	0.05	0.01
-10	1	|E*| (MPa)	30875	29645	28667	26114	24970	22227	20982	18119
		Phase Angle (°)	7.3	7.5	7.7	8.7	9.3	10.5	11.8	15.6
		Microstrain	51	53	54	54	54	54	57	50
	2	|E*| (MPa)	30305	29305	28425	26122	24988	22520	21187	18376
		Phase Angle (°)	6.0	6.3	6.8	7.9	8.6	10.6	10.8	13.9
		Microstrain	55	55	55	55	55	54	58	50
	3	|E*| (MPa)	31000	29573	28523	26060	24747	22028	20677	17734
		Phase Angle (°)	8.0	7.8	8.4	9.6	10.2	11.3	12.4	14.5
		Microstrain	54	55	55	55	55	55	59	52
	Average	Average |E*|	30727	29508	28538	26099	24901	22258	20949	18076
		Std. dev. |E*|	370	179	122	34	134	247	257	323
10	1	|E*| (MPa)	17902	16045	14496	11163	9707	6813	5641	3529
		Phase Angle (°)	14.8	15.7	17.0	20.6	23.5	29.4	33.9	39.4
		Microstrain	64	64	63	61	61	61	58	56
	2	|E*| (MPa)	18144	16265	14857	11504	9948	7065	5834	3684
		Phase Angle (°)	13.6	14.9	16.9	20.0	23.1	28.9	33.8	37.8
		Microstrain	61	62	62	60	60	59	56	54
	3	|E*| (MPa)	18674	16835	15186	11752	10241	7160	5962	3778
		Phase Angle (°)	15.3	16.1	17.3	20.9	23.7	29.4	29.5	38.2
		Microstrain	60	60	60	59	58	58	54	52
	Average	Average |E*|	18240	16382	14846	11473	9966	7013	5812	3664
		Std. dev. |E*|	395	408	345	296	267	179	161	126
35	1	|E*| (MPa)	4219	3035	2312	1222	926	539	439	336
		Phase Angle (°)	33.5	33.7	34.9	35.9	36.9	34.6	34.1	31.2
		Microstrain	48	56	59	58	54	57	55	42
	2	|E*| (MPa)	4456	3201	2450	1290	970	535	430	300
		Phase Angle (°)	33.3	33.7	36.4	36.0	38.2	35.7	35.1	31.5
		Microstrain	43	53	56	55	51	57	56	46
	3	|E*| (MPa)	4277	3027	2306	1199	909	530	434	327
		Phase Angle (°)	34.6	34.6	35.6	36.9	38.1	35.2	34.9	33.0
		Microstrain	46	57	59	58	55	58	56	43
	Average	Average |E*|	4317	3088	2356	1237	935	535	434	321
		Std. dev. |E*|	123	98	82	47	32	4	4	19
54	1	|E*| (MPa)	892	649	474	282	246	190		
		Phase Angle (°)	38.4	34.8	33.4	29.9	28.9	24.6		
		Microstrain	63	52	65	48	39	36		
	2	|E*| (MPa)	1016	640	483	288	252	201		
		Phase Angle (°)	37.3	34.3	32.6	28.3	26.8	21.9		
		Microstrain	28	52	60	50	41	38		
	3	|E*| (MPa)	924	603	462	286	256	213		
		Phase Angle (°)	37.5	33.9	32.0	28.7	26.8	24.0		
		Microstrain	36	57	63	50	40	36		
	Average	Average |E*|	944	631	473	285	251	202		
		Std. dev. |E*|	64	24	11	3	5	11		

Table A.10 B25.0C Axial Data

Temperature (°C)	Replicate	Parameters	Frequency (Hz)							
			25	10	5	1	0.5	0.1	0.05	0.01
-10	1	|E*| (MPa)	35251	33986	33474	30874	29473	26710	25573	22917
		Phase Angle (°)	9.2	9.0	9.9	10.0	11.3	13.1	13.7	15.8
		Microstrain	41	40	40	39	39	38	40	33
	2	|E*| (MPa)	34188	32778	31888	29346	28567	25541	24397	21612
		Phase Angle (°)	8.0	8.1	8.3	9.9	10.0	12.1	11.9	14.9
		Microstrain	49	50	49	49	48	48	50	43
	3	|E*| (MPa)	36266	35001	34025	31954	31185	27963	26738	23899
		Phase Angle (°)	7.2	7.6	5.9	8.7	9.6	10.6	12.2	15.4
		Microstrain	47	46	46	45	44	44	46	38
	Average	Average |E*|	35235	33922	33129	30725	29742	26738	25569	22809
		Std. dev. |E*|	1039	1113	1109	1310	1329	1211	1171	1147
10	1	|E*| (MPa)	22644	20993	18813	15374	13199	9777	8123	4995
		Phase Angle (°)	15.0	16.0	17.1	20.6	24.3	30.3	38.5	44.6
		Microstrain	43	41	41	38	38	36	33	32
	2	|E*| (MPa)	20582	18488	16863	13068	11476	7962	6545	
		Phase Angle (°)	14.6	15.7	16.9	20.9	24.6	30.9	35.9	
		Microstrain	65	67	66	70	69	74	75	
	3	|E*| (MPa)	21295	19030	17364	13314	11571	8052	6576	4016
		Phase Angle (°)	14.5	15.6	16.4	20.9	24.2	30.2	35.3	41.8
		Microstrain	62	65	64	69	68	73	75	76
	Average	Average |E*|	21507	19504	17680	13919	12082	8597	7081	4506
		Std. dev. |E*|	1047	1318	1012	1266	969	1023	903	692
35	1	|E*| (MPa)	5426	3755	2855	1404	1045	584	469	376
		Phase Angle (°)	34.3	35.0	36.5	38.8	39.0	35.4	35.9	34.1
		Microstrain	35	41	43	44	42	46	46	34
	2	|E*| (MPa)	4435	3103	2319	1123	829	436	344	229
		Phase Angle (°)	35.0	36.0	37.8	39.1	38.6	36.1	34.7	30.4
		Microstrain	55	64	69	77	80	91	100	107
	3	|E*| (MPa)	5243	3576	2796	1393	1099	652	550	417
		Phase Angle (°)	35.4	35.3	36.1	37.2	36.4	32.7	32.6	28.5
		Microstrain	40	50	52	56	52	55	53	55
	Average	Average |E*|	5035	3478	2657	1307	991	557	454	341
		Std. dev. |E*|	527	337	294	159	143	111	104	99
54	1	|E*| (MPa)	1142	743	568	354	327	301		
		Phase Angle (°)	38.7	34.8	32.5	27.4	25.7	22.6		
		Microstrain	28	43	48	37	29	25		
	2	|E*| (MPa)	949	585	424	232	202	157		
		Phase Angle (°)	41.4	37.3	35.1	30.8	28.6	25.2		
		Microstrain	37	58	68	61	51	48		
	3	|E*| (MPa)	1195	768	574	355	319	289		
		Phase Angle (°)	39.5	35.6	33.4	29.8	28.8	24.1		
		Microstrain	31	45	51	40	32	26		
	Average	Average |E*|	1096	699	522	314	283	249		
		Std. dev. |E*|	129	99	85	71	70	80		

A.3 Prism Specimen Data

Table A.11 S12.5C Prism Data

Temperature (°C)	Replicate	Parameters	Frequency (Hz)							
			25	10	5	1	0.5	0.1	0.05	0.01
-10	1	|E*| (MPa)	36052	35439	34487	31562	30387	27735	25830	23506
		Phase Angle (°)	10.2	10.3	10.7	11.8	12.0	13.7	14.6	17.9
		Microstrain	48	46	46	45	45	44	47	39
	2	|E*| (MPa)	32680	32146	31132	28734	27610	25053	23757	21228
		Phase Angle (°)	7.9	7.9	8.6	9.9	9.8	11.6	13.1	15.3
		Microstrain	53	51	51	50	49	48	51	43
	3	|E*| (MPa)	32883	32385	31360	29222	28261	25516	24063	20908
		Phase Angle (°)	8.5	8.4	9.1	10.1	10.5	13.0	13.1	14.0
		Microstrain	51	50	50	49	48	48	50	44
	4	|E*| (MPa)	32593	31272	30472	27955	27270	24261	23024	19861
		Phase Angle (°)	7.1	7.1	7.1	8.5	9.3	10.4	11.1	12.5
		Microstrain	52	52	52	51	50	50	53	46
	5	|E*| (MPa)	35000	33785	32761	30123	28780	26130	24659	21648
		Phase Angle (°)	9.2	9.4	9.8	11.1	11.6	12.9	13.8	18.1
		Microstrain	49	48	48	48	47	46	49	42
	Average	Average |E*|	33842	33005	32042	29519	28462	25739	24267	21430
		Std. dev. |E*|	1586	1632	1601	1386	1224	1308	1054	1335
10	1	|E*| (MPa)	21727	19882	18332	14585	13107	9953	8562	6045
		Phase Angle (°)	16.3	17.7	18.9	22.2	24.1	28.7	31.4	36.4
		Microstrain	53	52	50	47	45	41	37	34
	2	|E*| (MPa)	20155	18475	16890	13565	12143	9253	8072	5522
		Phase Angle (°)	14.5	15.7	17.5	20.0	21.7	26.1	30.0	37.4
		Microstrain	58	56	54	50	48	45	40	37
	3	|E*| (MPa)	20780	19175	17584	14236	12625	9709	8312	5806
		Phase Angle (°)	15.3	15.8	17.0	20.2	22.3	26.7	29.2	36.3
		Microstrain	54	53	52	48	47	42	39	35
	4	|E*| (MPa)	19772	17908	16430	12935	11505	8570	7290	4850
		Phase Angle (°)	13.4	14.6	15.5	18.4	21.1	26.0	30.6	36.7
		Microstrain	57	57	56	53	51	48	44	42
	5	|E*| (MPa)	21680	19545	17978	14299	12565	9311	7995	5314
		Phase Angle (°)	15.7	16.6	17.9	21.3	24.2	29.4	33.6	42.1
		Microstrain	52	52	51	48	47	44	40	38
	Average	Average |E*|	20823	18997	17443	13924	12389	9359	8046	5508
		Std. dev. |E*|	881	802	779	667	601	527	478	461

Table A.11 S12.5C Prism Data (continued)

Temperature (°C)	Replicate	Parameters	Frequency (Hz)							
			25	10	5	1	0.5	0.1	0.05	0.01
35	1	|E*| (MPa)	5734	4303	3410	1899	1486	894	736	674
		Phase Angle (°)	30.2	31.7	33.6	37.4	39.5	38.9	39.2	33
		Microstrain	42	47	47	45	43	44	45	34.2
	2	|E*| (MPa)	5762	4387	3543	1970	1536	904	734	572
		Phase Angle (°)	30.2	31.7	33.6	36.4	37.7	36.6	36.1	33
		Microstrain	44	47	46	43	41	43	45	28.7
	3	|E*| (MPa)	5543	4133	3240	1784	1413	892	753	366
		Phase Angle (°)	34.8	35.9	37.2	39.1	40.7	38.7	38.2	29
		Microstrain	34	40	40	39	36	34	33	39.3
	4	|E*| (MPa)	5177	3746	2914	1554	1190	717	601	510
		Phase Angle (°)	32.5	33.1	34.2	35.5	36.9	34.7	34.9	34
		Microstrain	36	44	45	45	43	43	41	23.8
	5	|E*| (MPa)	5827	4292	3407	1834	1409	828	665	540
		Phase Angle (°)	34.9	35.4	37.3	40.4	41.2	39.4	39.3	36.375
		Microstrain	48	51	51	52	52	59	65	49.351
	Average	Average |E*|	5609	4172	3303	1808	1407	847	698	532
		Std. dev. |E*|	263	255	242	158	133	79	64	112
54	1	|E*| (MPa)	1545	1152	946	742	746	733		
		Phase Angle (°)	34.6	32.2	31.2	29.6	30.4	32.1		
		Microstrain	26	32	32	19	14	10		
	2	|E*| (MPa)	1339	1003	506	320	282	229		
		Phase Angle (°)	37.6	34.3	29.5	24.7	22.6	19.2		
		Microstrain	54	44	65	52	36	36		
	3	|E*| (MPa)	1001	624	473	301	269	219		
		Phase Angle (°)	34.8	31.8	29.8	24.4	21.7	17.9		
		Microstrain	25	55	69	55	38	37		
	4	|E*| (MPa)	1176	785	597	372	325			
		Phase Angle (°)	37.0	33.7	31.8	27.6	25.5			
		Microstrain	42	66	82	78	76			
	5	|E*| (MPa)	1412	896	671	413	363	308		
		Phase Angle (°)	40.8	36.7	34.2	29.4	27.7	24.5		
		Microstrain	36	58	73	70	68	66		
	Average	Average |E*|	1295	892	639	430	397	372		
		Std. dev. |E*|	212	202	189	180	198	244		

Table A.12 S12.5C Prism – Slab Data

Temperature (°C)	Replicate	Parameters	Frequency (Hz)							
			25	10	5	1	0.5	0.1	0.05	0.01
-10	1	|E*| (MPa)	31823	29834	29320	27151	25825	23304	22182	19122
		Phase Angle (°)	4.5	3.4	4.6	5.3	5.2	8.2	8.1	11.8
		Microstrain	53	55	54	53	53	52	50	48
	2	|E*| (MPa)	32024	31023	30517	27774	26771	24054	22367	19761
		Phase Angle (°)	6.6	6.1	7.2	7.7	8.4	10.3	9.6	13.6
		Microstrain	54	53	52	52	51	50	50	46
	3	|E*| (MPa)	30317	29417	29090	26548	25552	23061	21888	18866
		Phase Angle (°)	6.4	5.2	6.0	7.2	7.7	8.9	9.9	10.8
		Microstrain	57	56	54	54	53	53	51	49
	Average	Average |E*|	31388	30092	29643	27158	26049	23473	22146	19250
		Std. dev. |E*|	933	833	766	613	640	518	241	461
10	1	|E*| (MPa)	18644	17185	15336	12151	10708	7676	6510	4195
		Phase Angle (°)	10.0	12.4	13.5	16.1	18.8	24.0	27.7	32.4
		Microstrain	34	43	46	45	44	43	41	41
	2	|E*| (MPa)	19654	17303	15915	12418	10860	7816	6552	4280
		Phase Angle (°)	14.1	15.5	16.5	20.1	21.8	27.9	30.1	36.0
		Microstrain	37	45	44	44	43	42	41	41
	3	|E*| (MPa)	18922	17004	15486	12030	10684	7713	6576	4244
		Phase Angle (°)	12.5	13.8	14.5	18.1	20.2	25.6	29.4	37.1
		Microstrain	38	45	46	46	44	43	41	41
	Average	Average |E*|	19073	17164	15579	12200	10751	7735	6546	4240
		Std. dev. |E*|	522	151	300	198	95	73	34	42
35	1	|E*| (MPa)	4309	3218	2471	1317	977	553	426	281
		Phase Angle (°)	32.3	33.6	34.9	37.6	38.5	38.4	39.5	41.3
		Microstrain	36	44	46	44	42	41	43	36
	2	|E*| (MPa)	4595	3425	2596	1388	1050	601	497	411
		Phase Angle (°)	33.3	35.2	37.5	40.3	42.1	42.9	44.6	49.7
		Microstrain	36	42	44	42	39	37	37	25
	3	|E*| (MPa)		3324	2586	1393	1065	619	495	352
		Phase Angle (°)		33.8	35.8	37.5	39.6	39.2	41.4	47.6
		Microstrain		42	43	42	39	36	37	29
	Average	Average |E*|	4452	3322	2551	1366	1031	591	472	348
		Std. dev. |E*|	202	104	69	42	47	34	41	65
54	1	|E*| (MPa)	1015	614	458	278	242	202		
		Phase Angle (°)	47.7	39.2	37.0	29.8	29.9	32.1		
		Microstrain	14	39	53	45	43	41		
	2	|E*| (MPa)	981	580	435	274	241	196		
		Phase Angle (°)	48.5	40.7	36.9	31.2	30.2	31.7		
		Microstrain	15	42	56	46	43	42		
	3	|E*| (MPa)	998	600	446	276	240	200		
		Phase Angle (°)	46.5	39.1	36.9	31.8	30.4	34.8		
		Microstrain	15	39	54	45	43	41		
	Average	Average |E*|	998	598	446	276	241	199		
		Std. dev. |E*|	17	17	11	2	1	3		

Table A.13 S12.5FE Prism Data

Temperature (°C)	Replicate	Parameters	Frequency (Hz)							
			25	10	5	1	0.5	0.1	0.05	0.01
-10	1	|E*| (MPa)	28921	27976	27100	25114	24208	21694	20282	17916
		Phase Angle (°)	7.9	8.0	8.4	9.2	10.2	11.3	12.7	16.8
		Microstrain	60	59	58	57	56	56	60	51
	2	|E*| (MPa)	30964	30045	29137	27175	25858	23434	21816	18929
		Phase Angle (°)	5.0	5.0	5.4	6.3	7.5	9.0	9.7	9.6
		Microstrain	55	54	54	53	53	52	51	48
	3	|E*| (MPa)	30152	29124	28176	26090	24926	22511	21274	18595
		Phase Angle (°)	5.5	4.9	5.4	6.4	6.7	8.9	9.6	12.3
		Microstrain	57	56	56	55	54	54	52	49
	Average	Average |E*|	30012	29048	28138	26127	24997	22547	21124	18480
		Std. dev. |E*|	1029	1036	1019	1031	827	871	778	517
10	1	|E*| (MPa)	16933	15272	13845	10723	9277	6659	5599	3643
		Phase Angle (°)	14.9	16.0	17.3	20.8	23.4	29.7	33.6	38.5
		Microstrain	68	67	66	64	63	62	57	56
	2	|E*| (MPa)	19162	17380	15792	12392	10912	7842	6563	4199
		Phase Angle (°)	12.4	13.1	13.9	17.7	20.2	25.4	30.3	35.4
		Microstrain	59	59	58	55	54	53	51	56
	3	|E*| (MPa)	17980	15884	14374	11117	9519	6706	5491	3373
		Phase Angle (°)	12.8	13.7	15.0	18.8	21.6	27.9	32.4	37.5
		Microstrain	63	64	64	61	62	61	61	70
	Average	Average |E*|	18025	16179	14670	11411	9903	7069	5884	3738
		Std. dev. |E*|	1115	1085	1007	872	883	670	590	421
35	1	|E*| (MPa)	4144	2983	2309	1254	985	619	539	674
		Phase Angle (°)	34.0	34.1	35.7	36.5	37.7	36.0	35.4	33.5
		Microstrain	45	55	55	57	52	50	45	34
	2	|E*| (MPa)	4268	3114	2393	1243	951	545	445	304
		Phase Angle (°)	31.2	31.7	33.0	33.5	34.1	30.9	29.9	25.3
		Microstrain	60	68	71	77	78	90	96	87
	3	|E*| (MPa)	4227	3049	2360	1259	972	578	482	366
		Phase Angle (°)	31.4	32.2	33.2	33.8	34.5	31.4	31.4	29.5
		Microstrain	51	60	61	61	57	53	51	39
	Average	Average |E*|	4213	3049	2354	1252	970	581	488	448
		Std. dev. |E*|	63	66	42	8	17	37	48	198
54	1	|E*| (MPa)	1545	1152	946	742	746	733		
		Phase Angle (°)	34.6	32.2	31.2	29.6	30.4	32.1		
		Microstrain	26	32	32	19	14	10		
	2	|E*| (MPa)	1027	663	506	320	282	229		
		Phase Angle (°)	34.9	31.1	29.5	24.7	22.6	19.2		
		Microstrain	26	53	65	52	36	36		
	3	|E*| (MPa)	1001	624	473	301	269	219		
		Phase Angle (°)	34.8	31.8	29.8	24.4	21.7	17.9		
		Microstrain	25	55	69	55	38	37		
	Average	Average |E*|	1191	813	642	454	432	394		
		Std. dev. |E*|	307	294	264	249	271	294		

Table A.14 S12.5FE Prism – Slab Data

Temperature (°C)	Replicate	Parameters	Frequency (Hz)							
			25	10	5	1	0.5	0.1	0.05	0.01
-10	1	|E*| (MPa)	29878	28687	27724	25608	24406	21891	20573	17488
		Phase Angle (°)	6.1	5.3	6.5	7.2	8.1	10.2	10.1	13.7
		Microstrain	57	57	57	56	56	55	54	52
	2	|E*| (MPa)	30222	30075	28664	26403	25295	22436	21043	18146
		Phase Angle (°)	5.7	5.8	6.3	6.9	7.9	9.4	10.7	13.8
		Microstrain	56	54	55	54	54	54	53	51
	3	|E*| (MPa)	29361	28418	27830	25090		21350	20060	17375
		Phase Angle (°)	7.1	8.1	8.4	8.5		13.0	13.4	15.9
		Microstrain	58	58	57	57		57	28	53
	Average	Average |E*|	29821	29060	28073	25700	24851	21892	20558	17670
		Std. dev. |E*|	433	889	515	661	629	543	492	416
10	1	|E*| (MPa)	16605	14707	13093	9802	8389	5741	4661	2823
		Phase Angle (°)	14.5	16.1	17.2	21.0	23.9	29.9	33.5	40.5
		Microstrain	54	65	67	70	71	72	72	83
	2	|E*| (MPa)	19049	16555	15149	11522	9949	7032	5795	3606
		Phase Angle (°)	15.2	14.7	16.3	20.0	22.7	28.0	31.3	38.3
		Microstrain	35	46	47	48	47	47	46	48
	3	|E*| (MPa)	16605	14662	12880	9756	8346	5705	4708	2897
		Phase Angle (°)	13.7	15.9	16.9	20.5	23.5	28.6	31.9	36.6
		Microstrain	43	52	55	57	56	58	57	60
	Average	Average |E*|	17420	15308	13708	10360	8894	6159	5054	3109
		Std. dev. |E*|	1411	1080	1253	1007	913	756	642	433
35	1	|E*| (MPa)	3276	2362	1799	921	695	401	327	238
		Phase Angle (°)	34.3	34.8	35.8	36.8	37.4	34.8	36.2	40.3
		Microstrain	65	77	80	64	59	56	56	43
	2	|E*| (MPa)	3894	2819	2109	1102	849	497	396	312
		Phase Angle (°)	35.7	35.5	36.2	37.3	38.4	36.5	39.1	45.7
		Microstrain	36	49	53	53	49	45	46	33
	3	|E*| (MPa)	3288	2336	1827	915	706	421	355	
		Phase Angle (°)	36.5	35.8	36.5	33.0	37.7	36.1	36.9	
		Microstrain	45	58	61	64	58	53	52	
	Average	Average |E*|	3486	2505	1912	979	750	440	360	275
		Std. dev. |E*|	353	271	172	107	86	51	35	52
54	1	|E*| (MPa)	678	420	318	207	180	150		
		Phase Angle (°)	39.2	34.3	31.7	27.8	27.2	36.9		
		Microstrain	18	52	74	61	57	54		
	2	|E*| (MPa)	802	491	367	242	210	173		
		Phase Angle (°)	40.1	34.8	33.2	28.2	27.8	32.9		
		Microstrain	16	47	65	52	49	48		
	3	|E*| (MPa)	823	463	351	231	211	182		
		Phase Angle (°)	43.6	36.0	33.9	29.6	29.8	40.0		
		Microstrain	15	50	68	55	49	44		
	Average	Average |E*|	768	458	345	226	200	168		
		Std. dev. |E*|	78	36	25	18	17	16		

Table A.15 B25.0C Prism Data

Temperature (°C)	Replicate	Parameters	Frequency (Hz)							
			25	10	5	1	0.5	0.1	0.05	0.01
-10	1	|E*| (MPa)	33860	33129	32215	30125	29007	26277	25312	22015
		Phase Angle (°)	5.1	5.3	5.1	6.2	7.4	8.4	9.8	12.2
		Microstrain	52	50	49	48	47	46	44	42
	2	|E*| (MPa)	34763	33818	33180	30770	29674	27113	25632	22735
		Phase Angle (°)	7.5	7.6	8.1	8.7	10.0	11.7	13.2	14.0
		Microstrain	50	49	48	47	46	45	43	40
	3	|E*| (MPa)	33037	32084	31138	29198	28253	25555	24692	21469
		Phase Angle (°)	5.8	5.8	6.4	7.2	8.2	9.7	11.3	13.8
		Microstrain	52	51	51	49	48	48	45	43
	Average	Average |E*|	33887	33010	32178	30031	28978	26315	25212	22073
		Std. dev. |E*|	863	873	1021	790	711	780	478	635
10	1	|E*| (MPa)	21268	19319	17717	13773	12113	8630	7215	4529
		Phase Angle (°)	13.0	13.9	15.5	18.8	22.5	28.4	33.0	39.1
		Microstrain	55	53	52	49	49	48	47	52
	2	|E*| (MPa)	21819	19650	17997	13926	12247	8889	7193	4470
		Phase Angle (°)	14.5	15.9	17.7	21.4	24.6	30.5	34.3	41.0
		Microstrain	40	49	49	49	48	46	47	53
	3	|E*| (MPa)	20665	18556	16769	13274	11475	8057	6695	4140
		Phase Angle (°)	13.4	14.8	17.3	20.1	23.3	28.9	34.7	41.0
		Microstrain	44	52	53	52	51	51	50	57
	Average	Average |E*|	21251	19175	17494	13658	11945	8525	7034	4380
		Std. dev. |E*|	578	561	644	341	413	426	294	210
35	1	|E*| (MPa)	5044	3617	2699	1394	1059	630	539	442
		Phase Angle (°)	33.1	33.4	34.2	35.2	33.7	30.1	29.2	25.6
		Microstrain	43	51	54	55	52	49	45	32
	2	|E*| (MPa)	5494	3830	2872	1482	1136	676	568	445
		Phase Angle (°)	29.9	34.8	36.2	36.4	36.1	31.7	30.4	27.0
		Microstrain	60	74	81	84	81	85	83	83
	3	|E*| (MPa)	4950	3499	2681	1360	1027	609	512	424
		Phase Angle (°)	34.9	34.5	35.9	36.6	36.8	32.5	31.0	27.1
		Microstrain	44	53	54	56	54	50	48	34
	Average	Average |E*|	5163	3649	2751	1412	1074	638	540	437
		Std. dev. |E*|	291	168	105	63	56	35	28	11
54	1	|E*| (MPa)	1234	757	584	396	358	332		
		Phase Angle (°)	34.6	32.7	29.5	23.3	22.4	17.3		
		Microstrain	22	45	55	42	29	24		
	2	|E*| (MPa)	1484	864	662	477	457	423		
		Phase Angle (°)	37.8	33.9	29.8	23.7	22.5	17.2		
		Microstrain	18	41	49	35	22	19		
	3	|E*| (MPa)	1179	695	539	355	345	298		
		Phase Angle (°)	38.3	33.8	30.9	25.0	22.3	16.9		
		Microstrain	25	52	61	47	30	27		
	Average	Average |E*|	1299	772	595	409	387	351		
		Std. dev. |E*|	162	85	62	62	61	64		

A.4 IDT Specimen Data

Table A.16 S12.5C IDT Data

Temperature (°C)	Replicate	Parameters	Frequency (Hz)							
			25	10	5	1	0.5	0.1	0.05	0.01
-10	1	|E*| (MPa)	33655	32584	31941	29269	27869	25035	23731	20625
		Horiz. Phase (°)	-4.0	-2.9	-1.7	0.6	-0.3	3.5	8.6	6.0
		Vert. Phase (°)	4.6	5.1	4.6	6.0	6.6	8.4	9.4	12.5
		Poisson's Ratio	0.17	0.18	0.20	0.20	0.21	0.21	0.23	0.22
		Horiz. Microstrain	67	70	71	71	72	72	79	68
		Vert. Microstrain	-167	-170	-169	-168	-170	-169	-179	-155
	2	|E*| (MPa)	31535	30925	30043	27745	26648	23958	22625	19535
		Horiz. Phase (°)	-4.1	-2.7	-2.2	-0.6	-1.3	1.3	6.7	3.7
		Vert. Phase (°)	1.4	1.5	1.6	2.6	3.0	4.7	5.7	8.8
		Poisson's Ratio	0.03	0.05	0.05	0.04	0.05	0.05	0.06	0.04
		Horiz. Microstrain	53	57	57	54	55	55	59	49
		Vert. Microstrain	-178	-179	-180	-175	-176	-175	-185	-160
	3	|E*| (MPa)	28448	27248	26476	24263	23366	20923	19932	17036
		Horiz. Phase (°)	9.2	12.5	16.6	13.9	16.0	21.0	28.3	24.0
		Vert. Phase (°)	2.4	2.5	2.3	3.1	3.8	5.4	6.5	9.5
		Poisson's Ratio	-0.16	-0.17	-0.16	-0.17	-0.16	-0.17	-0.14	-0.18
		Horiz. Microstrain	27	27	29	26	28	27	34	24
		Vert. Microstrain	-194	-198	-198	-196	-195	-195	-206	-181
	4	|E*| (MPa)	33377	32699	31926	28998	27971	24637	23794	20866
		Horiz. Phase (°)	4.4	7.0	7.8	7.2	8.4	6.3	13.9	2.2
		Vert. Phase (°)	4.1	3.8	4.1	5.0	6.3	7.1	8.3	10.5
		Poisson's Ratio	0.00	0.00	0.00	-0.02	-0.03	-0.05	-0.02	-0.05
		Horiz. Microstrain	24	24	24	22	22	20	23	18
		Vert. Microstrain	-87	-88	-87	-86	-85	-85	-89	-76
	Average	Average |E*|	31754	30864	30096	27569	26463	23638	22520	19515
		Std. dev. |E*|	2396	2543	2573	2302	2151	1864	1807	1751
10	1	|E*| (MPa)	20601	18353	16630	12787	11069	7807	6357	4007
		Horiz. Phase (°)	5.1	8.5	10.6	15.2	17.8	24.9	32.5	33.7
		Vert. Phase (°)	12.5	13.4	15.0	19.1	22.7	29.2	34.2	39.4
		Poisson's Ratio	0.26	0.28	0.31	0.36	0.39	0.43	0.45	0.47
		Horiz. Microstrain	88	93	97	103	108	114	111	110
		Vert. Microstrain	-188	-194	-196	-195	-198	-198	-190	-185
	2	|E*| (MPa)	19654	17769	16102	12424	10810	7646	6292	3943
		Horiz. Phase (°)	5.7	9.0	11.0	15.5	18.6	25.8	33.1	33.7
		Vert. Phase (°)	8.7	9.9	11.3	15.1	18.5	24.4	29.1	34.1
		Poisson's Ratio	0.08	0.12	0.13	0.16	0.17	0.20	0.20	0.20
		Horiz. Microstrain	64	70	72	74	76	80	76	73
		Vert. Microstrain	-189	-192	-192	-189	-190	-189	-179	-174
	3	|E*| (MPa)	17216	15262	13725	10674		6493	5334	3391
		Horiz. Phase (°)	27.6	30.1	33.0	38.9		49.2	58.0	67.4
		Vert. Phase (°)	10.1	11.2	12.5	16.7		26.0	30.8	36.9
		Poisson's Ratio	-0.07	-0.05	-0.04	-0.07		-0.04	-0.03	0.00
		Horiz. Microstrain	45	49	52	45		51	50	52
		Vert. Microstrain	-206	-212	-213	-205		-207	-196	-190
	4	|E*| (MPa)	20224	18146	16380	12606	11050	7849	6459	4153
		Horiz. Phase (°)	12.6	15.5	17.9	23.3	24.5	32.3	42.4	39.9
		Vert. Phase (°)	10.7	12.2	13.0	16.6	19.4	25.1	29.1	35.3
		Poisson's Ratio	0.08	0.10	0.09	0.11	0.12	0.11	0.10	0.07
		Horiz. Microstrain	34	38	38	38	39	37	34	32
		Vert. Microstrain	-103	-109	-109	-107	-105	-103	-97	-95
	Average	Average |E*|	19424	17382	15710	12123	10976	7449	6111	3873
		Std. dev. |E*|	1523	1434	1340	977	144	643	522	333

Table A.16 S12.5C IDT Data (continued)

Temperature (°C)	Replicate	Parameters	Frequency (Hz)							
			25	10	5	1	0.5	0.1	0.05	0.01
35	1	|E*| (MPa)	5550	3947	2981	1484	1173	789	689	
		Horiz. Phase (°)	21.8	22.7	24.3	24.9	25.2	24.3	29.1	
		Vert. Phase (°)	31.1	32.2	32.9	33.6	34.3	31.6	31.5	
		Poisson's Ratio	0.52	0.61	0.65	0.72	0.76	0.93	1.06	
		Horiz. Microstrain	69	94	116	139	141	137	143	
		Vert. Microstrain	-111	-140	-166	-190	-186	-164	-160	
	2	|E*| (MPa)	5090	3458	2662	1247	950	568	470	341
		Horiz. Phase (°)	28.1	30.1	31.8	29.6	30.2	28.2	33.0	21.0
		Vert. Phase (°)	26.0	28.3	29.3	30.1	31.0	27.5	27.6	25.3
		Poisson's Ratio	0.22	0.25	0.28	0.28	0.30	0.28	0.29	0.31
		Horiz. Microstrain	57	77	87	99	104	95	97	71
		Vert. Microstrain	-131	-170	-181	-206	-211	-198	-200	-145
	3	|E*| (MPa)	4545	3230	2341	1158	876	537	439	308
		Horiz. Phase (°)	27.6	30.0	31.9	30.6	30.9	28.6	32.8	25.1
		Vert. Phase (°)	25.4	27.1	28.2	28.1	29.3	25.8	25.6	24.3
		Poisson's Ratio	0.28	0.28	0.29	0.30	0.30	0.28	0.31	0.26
		Horiz. Microstrain	71	89	101	109	112	100	107	73
		Vert. Microstrain	-149	-186	-209	-224	-228	-209	-215	-157
	4	|E*| (MPa)	8088	3151	1659	1284	790	663	538	
		Horiz. Phase (°)	355.6	27.9	31.8	36.8	37.4	41.7	48.3	
		Vert. Phase (°)	12.5	28.2	29.8	32.7	30.6	31.0	30.0	
		Poisson's Ratio	0.14	0.40	0.39	0.39	0.38	0.41	0.31	
		Horiz. Microstrain	14	55	60	60	64	69	45	
		Vert. Microstrain	-35	-99	-110	-109	-118	-123	-91	
	Average	Average |E*|	5818	3446	2411	1293	948	639	534	325
		Std. dev. |E*|	1568	358	566	138	164	114	111	23

Table A.17 S12.5C-AC-1 IDT Data

Temperature (°C)	Replicate	Parameters	Frequency (Hz)							
			25	10	5	1	0.5	0.1	0.05	0.01
-10	1	|E*| (MPa)	35237	33745	32817	30444	29543	26452	25658	22988
		Horiz. Phase (°)	-9.4	-8.0	-6.5	-3.7	-6.4	-2.4	5.8	1.9
		Vert. Phase (°)	2.4	3.7	4.0	5.0	5.1	6.8	7.3	9.9
		Poisson's Ratio	0.00	-0.01	-0.02	0.00	-0.01	-0.01	0.00	0.04
		Horiz. Microstrain	24	23	22	24	23	23	25	27
		Vert. Microstrain	-86	-86	-85	-86	-85	-87	-88	-90
	2	|E*| (MPa)	33736	32395	31886	29680	28560	25836	24843	21831
		Horiz. Phase (°)	-1.5	-0.5	1.0	2.9	2.7	5.2	8.8	4.8
		Vert. Phase (°)	-1.3	-0.6	-0.9	-0.1	0.5	1.7	2.7	4.9
		Poisson's Ratio	0.00	0.01	0.01	0.01	0.01	0.00	0.00	0.01
		Horiz. Microstrain	24	25	25	24	24	23	23	24
		Vert. Microstrain	-87	-88	-88	-87	-86	-85	-84	-86
	3	|E*| (MPa)	35097	33726	32783	30968	29525	27109	26027	23088
		Horiz. Phase (°)	-2.4	0.5	1.9	1.8	3.0	3.6	10.1	5.9
		Vert. Phase (°)	-0.1	0.1	1.3	0.9	1.9	3.4	3.8	4.8
		Poisson's Ratio	0.13	0.12	0.11	0.14	0.13	0.12	0.13	0.13
		Horiz. Microstrain	32	32	31	32	32	31	31	32
		Vert. Microstrain	-85	-87	-87	-86	-86	-83	-83	-84
	Average	Average |E*|	34690	33289	32495	30364	29209	26466	25509	22636
		Std. dev. |E*|	829	774	528	648	563	637	606	699
10	1	|E*| (MPa)	22978	21281	19616	15777	14159	10974	9412	6765
		Horiz. Phase (°)	-3.8	-1.0	2.4	5.6	8.2	14.9	20.1	23.4
		Vert. Phase (°)	9.7	10.6	11.3	14.5	16.8	21.8	23.9	30.7
		Poisson's Ratio	0.05	0.06	0.05	0.08	0.07	0.12	0.11	0.16
		Horiz. Microstrain	24	24	23	27	26	30	28	31
		Vert. Microstrain	-77	-77	-74	-80	-79	-82	-78	-78
	2	|E*| (MPa)	21198	19700	18388	15361	13704	10129	8840	6028
		Horiz. Phase (°)	5.4	5.7	6.7	13.5	14.9	18.6	24.2	28.8
		Vert. Phase (°)	5.6	5.6	6.7	10.0	11.8	16.5	19.0	24.4
		Poisson's Ratio	-0.09	-0.04	-0.03	0.00	0.00	-0.03	-0.01	-0.01
		Horiz. Microstrain	11	16	16	18	18	15	15	15
		Vert. Microstrain	-53	-65	-66	-65	-64	-59	-56	-56
	3	|E*| (MPa)	21808	20719	19492	15861	14468	11027	9579	6858
		Horiz. Phase (°)	2.5	8.0	9.5	15.2	15.8	21.1	28.1	29.6
		Vert. Phase (°)	6.1	7.1	8.6	10.8	13.1	17.2	20.0	25.8
		Poisson's Ratio	-0.03	0.01	0.04	0.09	0.09	0.08	0.08	0.08
		Horiz. Microstrain	13	18	19	22	21	19	18	17
		Vert. Microstrain	-52	-62	-63	-65	-62	-56	-53	-50
	Average	Average |E*|	21994	20567	19165	15666	14110	10710	9277	6550
		Std. dev. |E*|	904	801	676	267	384	504	388	455
35	1	|E*| (MPa)	7587	5699	4550	2531	2008	1183	999	784
		Horiz. Phase (°)	18.1	22.6	24.7	30.9	31.6	31.4	31.1	28.6
		Vert. Phase (°)	28.0	26.5	28.8	34.1	35.6	34.8	34.5	34.6
		Poisson's Ratio	0.16	0.27	0.30	0.34	0.37	0.32	0.33	0.49
		Horiz. Microstrain	15	32	37	48	49	42	33	43
		Vert. Microstrain	-37	-67	-74	-94	-92	-83	-65	-71
	2	|E*| (MPa)	4863	3831	3098	1747	1374	812	642	452
		Horiz. Phase (°)	47.3	21.6	22.9	27.3	26.1	25.1	33.8	37.2
		Vert. Phase (°)	20.5	23.3	23.5	27.6	28.8	25.4	25.3	24.1
		Poisson's Ratio	-0.08	-0.02	-0.01	-0.01	-0.02	-0.03	-0.04	0.03
		Horiz. Microstrain	8	14	16	16	16	18	20	30
		Vert. Microstrain	-37	-55	-60	-60	-60	-72	-80	-100
	3	|E*| (MPa)	7415	6569	6495	3850	3271	2278	1879	1583
		Horiz. Phase (°)	38.7	22.3	26.3	33.7	33.5	33.2	38.5	46.2
		Vert. Phase (°)	17.8	20.3	18.3	22.5	22.9	20.0	21.2	26.9
		Poisson's Ratio	0.24	0.40	0.51	0.58	0.60	0.76	0.82	1.24
		Horiz. Microstrain	12	20	21	21	20	24	27	41
		Vert. Microstrain	-27	-36	-33	-32	-30	-32	-34	-42
	Average	Average |E*|	6622	5366	4714	2709	2218	1424	1173	940
		Std. dev. |E*|	1526	1399	1705	1063	966	763	637	582

Table A.18 S12.5C-AC+1 IDT Data

Temperature (°C)	Replicate	Parameters	Frequency (Hz)							
			25	10	5	1	0.5	0.1	0.05	0.01
-10	1	|E*| (MPa)	25723	24810	24347	22172	20999	18683	17386	14783
		Horiz. Phase (°)	-0.5	4.0	5.6	7.1	8.7	11.0	18.5	18.0
		Vert. Phase (°)	2.1	2.5	2.8	4.6	5.5	7.4	8.2	11.7
		Poisson's Ratio	-0.18	-0.17	-0.16	-0.15	-0.15	-0.15	-0.16	-0.12
		Horiz. Microstrain	14	15	16	17	17	17	17	22
		Vert. Microstrain	-108	-111	-111	-112	-113	-114	-116	-124
	2	|E*| (MPa)	28995	27320	26097	23887	23447	21844	21818	
		Horiz. Phase (°)	-0.3	0.5	2.1	4.8	4.8	7.1	12.5	
		Vert. Phase (°)	2.4	3.4	3.1	3.5	3.9	4.8	5.7	
		Poisson's Ratio	0.11	0.10	0.09	0.10	0.11	0.14	0.18	
		Horiz. Microstrain	38	38	38	40	40	40	42	
		Vert. Microstrain	-105	-109	-111	-112	-110	-106	-102	
	3	|E*| (MPa)	29933	28794	28082	25558	24451	21675	20319	17232
		Horiz. Phase (°)	-4.3	-3.0	-3.2	-0.5	-0.6	2.5	6.5	5.2
		Vert. Phase (°)	0.0	0.3	0.7	1.7	2.9	4.7	5.9	9.3
		Poisson's Ratio	0.21	0.19	0.21	0.21	0.21	0.22	0.24	0.25
		Horiz. Microstrain	45	44	46	46	47	48	50	54
		Vert. Microstrain	-104	-106	-107	-108	-108	-109	-111	-119
	Average	Average |E*|	28217	26975	26175	23872	22966	20734	19841	16008
		Std. dev. |E*|	2210	2014	1869	1693	1776	1778	2254	1732
10	1	|E*| (MPa)	15001	13152	11647	8626	7508	4856	3901	2268
		Horiz. Phase (°)	9.4	15.3	20.7	30.5	34.6	44.5	51.6	54.2
		Vert. Phase (°)	11.6	12.9	14.5	20.2	24.8	31.6	35.1	41.1
		Poisson's Ratio	-0.16	-0.11	-0.11	-0.07	-0.03	-0.02	0.00	0.04
		Horiz. Microstrain	10	18	19	26	30	33	36	47
		Vert. Microstrain	-74	-95	-102	-116	-119	-126	-131	-154
	2	|E*| (MPa)	14668	13296	11940	8708	7549	5110	4107	2511
		Horiz. Phase (°)	21.8	20.2	21.8	28.0	31.3	38.1	43.8	44.3
		Vert. Phase (°)	9.5	11.9	13.7	19.0	22.8	28.4	31.9	35.6
		Poisson's Ratio	-0.03	0.07	0.10	0.18	0.18	0.22	0.23	0.27
		Horiz. Microstrain	20	33	38	50	51	56	59	70
		Vert. Microstrain	-80	-100	-106	-123	-125	-128	-132	-148
	3	|E*| (MPa)	16901	14819	13288	9864	8517	5717	4632	2758
		Horiz. Phase (°)	8.1	9.3	10.9	15.8	19.6	24.7	30.9	30.6
		Vert. Phase (°)	10.5	10.7	12.6	18.6	21.4	27.1	30.6	35.6
		Poisson's Ratio	0.22	0.26	0.27	0.32	0.34	0.36	0.39	0.41
		Horiz. Microstrain	32	44	47	57	60	63	66	78
		Vert. Microstrain	-73	-95	-101	-113	-116	-119	-122	-139
	Average	Average |E*|	15524	13755	12291	9066	7858	5228	4213	2512
		Std. dev. |E*|	1205	924	875	693	572	442	377	245
35	1	|E*| (MPa)	2893	1908	1398	683	535	333	284	204
		Horiz. Phase (°)	40.3	37.8	36.9	37.2	35.3	38.8	47.1	61.9
		Vert. Phase (°)	30.6	31.6	31.7	32.3	31.2	28.3	28.7	38.1
		Poisson's Ratio	-0.15	-0.10	-0.06	-0.05	-0.07	-0.14	-0.15	-0.09
		Horiz. Microstrain	7	17	26	33	32	25	26	43
		Vert. Microstrain	-48	-87	-111	-140	-142	-152	-166	-216
	2	|E*| (MPa)	4050	2775	2051	1036	828	524	452	352
		Horiz. Phase (°)	19.5	21.1	19.8	24.7	24.1	20.8	24.8	28.4
		Vert. Phase (°)	31.9	29.8	31.0	32.5	31.7	27.9	27.4	29.8
		Poisson's Ratio	0.46	0.43	0.45	0.47	0.53	0.57	0.60	0.74
		Horiz. Microstrain	24	41	51	64	68	77	86	117
		Vert. Microstrain	-41	-71	-88	-107	-109	-118	-128	-158
	3	|E*| (MPa)	3762	2523	1835	911	716	446	408	324
		Horiz. Phase (°)	27.6	24.5	25.8	28.0	26.7	26.0	30.4	33.3
		Vert. Phase (°)	31.4	31.1	32.0	33.2	32.7	29.6	29.6	33.0
		Poisson's Ratio	0.36	0.42	0.44	0.47	0.49	0.52	0.61	0.77
		Horiz. Microstrain	24	49	63	80	82	96	103	142
		Vert. Microstrain	-46	-86	-109	-134	-135	-154	-152	-187
	Average	Average |E*|	3568	2402	1762	877	693	434	381	293
		Std. dev. |E*|	602	446	333	179	148	96	88	78

Table A.19 S12.5C-AV-2 IDT Data

Temperature (°C)	Replicate	Parameters	Frequency (Hz)							
			25	10	5	1	0.5	0.1	0.05	0.01
-10	1	|E*| (MPa)	29800	28656	28116	25913	25301	22572	21233	18645
		Horiz. Phase (°)	25.7	10.8	23.7	25.8	23.5	25.1	31.0	46.8
		Vert. Phase (°)	1.4	1.4	1.5	2.9	3.2	5.5	5.8	7.3
		Poisson's Ratio	-0.17	-0.17	-0.14	-0.15	-0.09	-0.12	-0.15	-0.14
		Horiz. Microstrain	13	12	15	15	19	17	15	16
		Vert. Microstrain	-90	-93	-94	-94	-94	-93	-93	-96
	2	|E*| (MPa)	30424	29188	28488	26058	25209	22698	21630	18968
		Horiz. Phase (°)	6.2	0.3	2.5	2.2	4.0	10.9	7.4	15.1
		Vert. Phase (°)	2.8	3.2	3.1	5.1	6.0	8.2	8.0	9.9
		Poisson's Ratio	-0.19	-0.19	-0.19	-0.20	-0.19	-0.20	-0.19	-0.18
		Horiz. Microstrain	10	11	11	10	11	10	11	12
		Vert. Microstrain	-88	-91	-92	-92	-92	-90	-90	-93
	3	|E*| (MPa)	33985	32708	31547	29609	28225	25876	24780	21543
		Horiz. Phase (°)	7.6	10.0	9.9	12.0	13.4	16.6	15.5	21.6
		Vert. Phase (°)	2.8	3.3	4.0	5.2	6.0	8.2	8.3	10.4
		Poisson's Ratio	0.02	0.01	0.01	0.04	0.03	0.05	0.06	0.05
		Horiz. Microstrain	25	25	25	27	26	27	27	28
		Vert. Microstrain	-85	-87	-89	-88	-88	-86	-85	-89
	Average	Average |E*|	31403	30184	29384	27193	26245	23715	22548	19719
		Std. dev. |E*|	2258	2202	1883	2093	1716	1872	1943	1588
10	1	|E*| (MPa)	19280	17314	16004	12996	11329	8408	7362	5216
		Horiz. Phase (°)	17.5	26.9	27.5	44.9	48.5	55.0	56.9	61.3
		Vert. Phase (°)	7.6	8.8	9.8	14.5	16.1	20.2	21.8	27.0
		Poisson's Ratio	-0.21	-0.21	-0.18	-0.09	-0.13	-0.14	-0.11	-0.07
		Horiz. Microstrain	6	7	9	17	14	13	15	16
		Vert. Microstrain	-58	-72	-77	-81	-82	-81	-81	-75
	2	|E*| (MPa)	21361	18332	16758	12797	11332	8614	7411	5118
		Horiz. Phase (°)	8.3	20.7	22.6	28.2	32.8	38.8	42.4	52.0
		Vert. Phase (°)	12.7	13.8	14.6	19.6	21.1	27.1	29.1	33.5
		Poisson's Ratio	-0.10	-0.08	-0.06	-0.05	-0.05	-0.04	-0.02	-0.02
		Horiz. Microstrain	10	15	17	20	20	20	22	21
		Vert. Microstrain	-52	-70	-76	-83	-84	-81	-83	-78
	3	|E*| (MPa)	20440	18043	16640	13046	11657	8499	7286	4787
		Horiz. Phase (°)	22.8	19.6	22.0	29.9	35.4	41.7	41.4	49.7
		Vert. Phase (°)	8.7	9.6	10.0	15.0	17.3	23.2	25.5	29.5
		Poisson's Ratio	-0.09	-0.09	-0.06	-0.03	-0.02	-0.02	0.03	0.02
		Horiz. Microstrain	11	14	18	21	22	22	26	25
		Vert. Microstrain	-55	-71	-77	-82	-82	-83	-86	-85
	Average	Average |E*|	20360	17896	16467	12946	11439	8507	7353	5040
		Std. dev. |E*|	1043	524	406	132	188	103	63	225

Table A.19 S12.5C-AV-2 IDT Data (continued)

Temperature (°C)	Replicate	Parameters	Frequency (Hz)							
			25	10	5	1	0.5	0.1	0.05	0.01
35	1	|E*| (MPa)	5697	4201	3221	1761	1383	829	807	1062
		Horiz. Phase (°)	41.7	48.0	44.4	51.5	55.9	50.1	48.4	58.8
		Vert. Phase (°)	26.8	28.5	29.7	34.6	35.1	33.4	33.9	32.2
		Poisson's Ratio	-0.07	-0.01	0.03	0.09	0.08	0.02	0.09	0.56
		Horiz. Microstrain	8	16	23	30	28	23	24	34
		Vert. Microstrain	-36	-60	-75	-87	-82	-80	-70	-53
	2	|E*| (MPa)	6580	4643	3455	1818	1466	907	782	656
		Horiz. Phase (°)	37.4	38.4	38.9	42.7	45.6	41.2	39.7	44.0
		Vert. Phase (°)	32.4	30.5	32.3	37.0	37.1	35.6	34.5	33.9
		Poisson's Ratio	0.17	0.23	0.25	0.29	0.29	0.29	0.31	0.48
		Horiz. Microstrain	14	27	35	43	40	38	39	50
		Vert. Microstrain	-35	-61	-76	-89	-83	-79	-78	-84
	3	|E*| (MPa)	6171	4530	3502	1838	1401	788	638	438
		Horiz. Phase (°)	34.9	38.4	39.9	44.5	47.1	43.3	40.4	46.3
		Vert. Phase (°)	27.8	28.1	29.5	34.8	35.2	32.7	31.0	28.7
		Poisson's Ratio	0.08	0.16	0.20	0.22	0.24	0.15	0.15	0.17
		Horiz. Microstrain	14	25	32	38	38	34	35	46
		Vert. Microstrain	-41	-63	-76	-86	-85	-87	-91	-115
	Average	Average |E*|	6149	4458	3393	1805	1416	841	743	719
		Std. dev. |E*|	442	230	151	40	43	60	91	317
54	1	|E*| (MPa)		956	722	454	390	333		
		Horiz. Phase (°)		41.1	37.3	36.8	36.4	35.5		
		Vert. Phase (°)		28.7	26.5	23.1	20.5	18.7		
		Poisson's Ratio		0.20	0.27	0.28	0.12	0.00		
		Horiz. Microstrain		37	57	56	24	11		
		Vert. Microstrain		-88	-120	-118	-65	-41		
	2	|E*| (MPa)	1633	1048	782	508	493	659		
		Horiz. Phase (°)	40.5	39.8	36.6	33.9	33.5	29.7		
		Vert. Phase (°)	35.1	31.2	30.1	26.8	27.8	25.7		
		Poisson's Ratio	0.30	0.36	0.39	0.50	0.50	0.73		
		Horiz. Microstrain	22	46	63	69	35	19		
		Vert. Microstrain	-45	-87	-116	-113	-57	-26		
	3	|E*| (MPa)	1938	1270	1006	687	700	841		
		Horiz. Phase (°)	55.2	42.4	40.1	38.5	40.8	26.9		
		Vert. Phase (°)	31.4	29.2	28.2	25.0	22.7	10.4		
		Poisson's Ratio	0.06	0.24	0.34	0.39	0.22	-0.04		
		Horiz. Microstrain	10	30	45	44	16	4		
		Vert. Microstrain	-31	-67	-88	-81	-37	-16		
	Average	Average |E*|	1786	1092	837	550	528	611		
		Std. dev. |E*|	215	161	150	122	158	257		

Table A.20 S12.5C-AV+2 IDT Data

Temperature (°C)	Replicate	Parameters	Frequency (Hz)							
			25	10	5	1	0.5	0.1	0.05	0.01
-10	1	|E*| (MPa)	28527	27315	26575	24330	23576	21020	20196	17597
		Horiz. Phase (°)	-3.4	3.6	2.8	4.2	5.7	7.0	13.7	12.6
		Vert. Phase (°)	1.9	1.9	2.2	2.9	3.6	5.4	6.1	9.2
		Poisson's Ratio	-0.02	-0.03	-0.03	-0.03	-0.02	-0.04	-0.03	-0.02
		Horiz. Microstrain	27	26	26	27	27	26	26	28
		Vert. Microstrain	-101	-104	-105	-106	-105	-105	-104	-108
	2	|E*| (MPa)	31091	29633	29102	27085	25977	23585	22536	19629
		Horiz. Phase (°)	-13.6	-7.8	-5.0	0.4	1.1	3.0	7.7	6.8
		Vert. Phase (°)	1.6	1.1	1.8	3.9	3.8	5.4	5.7	8.8
		Poisson's Ratio	0.07	0.07	0.08	0.06	0.06	0.06	0.05	0.06
		Horiz. Microstrain	31	32	33	31	31	30	30	31
		Vert. Microstrain	-94	-98	-98	-96	-96	-94	-94	-97
	3	|E*| (MPa)	33487	32156	31287	28794	28108	26605		
		Horiz. Phase (°)	5.2	6.9	5.8	9.0	9.4	11.5		
		Vert. Phase (°)	2.7	3.6	3.7	5.1	5.5	6.1		
		Poisson's Ratio	0.07	0.07	0.07	0.07	0.08	0.09		
		Horiz. Microstrain	29	29	30	30	30	29		
		Vert. Microstrain	-88	-90	-91	-91	-90	-85		
	4	|E*| (MPa)	31538	29994	29497	27477	26366	23687	22325	19400
		Horiz. Phase (°)	3.6	2.2	0.4	6.4	7.0	7.9	13.2	11.8
		Vert. Phase (°)	3.5	2.9	3.3	5.2	5.9	8.3	9.4	12.0
		Poisson's Ratio	0.02	0.02	0.01	0.03	0.03	0.02	0.01	0.02
		Horiz. Microstrain	27	28	27	28	28	27	27	29
		Vert. Microstrain	-92	-95	-95	-94	-94	-93	-93	-97
	Average	Average |E*|	31161	29775	29115	26921	26007	23724	21685	18875
		Std. dev. |E*|	2041	1982	1942	1876	1867	2282	1294	1113
10	1	|E*| (MPa)	15978	13692	12428	9374	8418	6113	5205	3480
		Horiz. Phase (°)	-3.3	6.1	9.0	18.7	22.2	26.3	35.3	37.5
		Vert. Phase (°)	9.7	10.8	11.4	16.3	18.6	24.5	27.1	32.8
		Poisson's Ratio	-0.07	-0.07	-0.04	-0.02	0.00	0.00	0.03	0.07
		Horiz. Microstrain	15	21	24	28	30	28	30	33
		Vert. Microstrain	-70	-93	-98	-108	-108	-100	-99	-101
	2	|E*| (MPa)	18903	17173	15397	11645	10486	7866	6739	4487
		Horiz. Phase (°)	-5.5	3.9	8.5	15.9	20.9	24.7	32.1	37.2
		Vert. Phase (°)	9.9	10.3	12.6	17.4	19.9	25.5	28.3	34.5
		Poisson's Ratio	-0.04	-0.02	0.02	0.03	0.05	0.07	0.09	0.12
		Horiz. Microstrain	15	20	23	26	27	26	26	29
		Vert. Microstrain	-62	-75	-80	-87	-86	-78	-76	-78
	3	|E*| (MPa)	14968	13952	12938	10183	9101	6534	5667	3708
		Horiz. Phase (°)	14.3	17.9	18.9	23.7	26.2	31.5	37.2	40.1
		Vert. Phase (°)	10.5	7.0	8.9	12.0	15.3	18.6	23.7	27.4
		Poisson's Ratio	-0.08	0.19	0.26	0.38	0.43	0.44	0.49	0.48
		Horiz. Microstrain	12	22	26	31	33	35	37	36
		Vert. Microstrain	-58	-53	-56	-58	-57	-60	-60	-60
	4	|E*| (MPa)	20232	18041	16330	13038	11589	8556	7497	5058
		Horiz. Phase (°)	13.5	13.2	14.6	19.4	20.2	28.8	35.5	34.5
		Vert. Phase (°)	10.6	10.9	12.2	17.3	19.4	21.9	25.1	30.0
		Poisson's Ratio	-0.05	-0.02	-0.04	0.01	0.02	0.03	0.04	0.07
		Horiz. Microstrain	14	19	20	24	24	25	26	27
		Vert. Microstrain	-58	-74	-79	-83	-84	-84	-84	-82
	Average	Average |E*|	17520	15714	14273	11060	9899	7267	6277	4183
		Std. dev. |E*|	2460	2216	1887	1619	1418	1138	1037	725

Table A.20 S12.5C-AV+2 IDT Data (continued)

Temperature (°C)	Replicate	Parameters	Frequency (Hz)							
			25	10	5	1	0.5	0.1	0.05	0.01
35	1	|E*| (MPa)	5391	4128	3178	1693	1344	810	686	496
		Horiz. Phase (°)	23.4	21.2	25.8	29.9	29.8	30.9	35.5	39.3
		Vert. Phase (°)	25.2	28.1	30.4	34.5	34.9	33.9	33.4	37.0
		Poisson's Ratio	0.24	0.38	0.42	0.44	0.44	0.43	0.45	0.52
		Horiz. Microstrain	13	28	35	43	42	48	51	72
		Vert. Microstrain	-30	-52	-63	-74	-72	-83	-87	-115
	2	|E*| (MPa)	5329	3784	2866	1553	1240	808	669	475
		Horiz. Phase (°)	22.8	25.1	24.2	27.8	28.7	30.0	37.1	44.7
		Vert. Phase (°)	28.9	28.2	29.3	34.3	34.6	33.9	33.3	38.2
		Poisson's Ratio	0.05	0.07	0.10	0.11	0.13	0.17	0.19	0.29
		Horiz. Microstrain	9	17	22	26	26	30	34	54
		Vert. Microstrain	-29	-52	-63	-72	-70	-76	-82	-111
	3	|E*| (MPa)	6003	4168	3163	1631	1260	727	590	412
		Horiz. Phase (°)	37.6	32.8	32.5	36.1	36.7	35.0	36.6	34.6
		Vert. Phase (°)	30.1	29.9	32.2	36.3	36.5	33.0	32.8	30.8
		Poisson's Ratio	0.15	0.22	0.28	0.29	0.31	0.30	0.32	0.40
		Horiz. Microstrain	13	29	40	49	48	48	52	72
		Vert. Microstrain	-35	-66	-84	-100	-97	-99	-103	-131
	4	|E*| (MPa)	5292	3645	3779	2675	2214	1337	1123	817
		Horiz. Phase (°)	30.4	29.9	32.4	36.7	35.4	31.0	36.3	27.0
		Vert. Phase (°)	30.4	29.2	33.1	32.5	34.3	29.7	28.9	27.9
		Poisson's Ratio	-0.01	0.04	0.19	0.49	0.58	0.62	0.72	0.83
		Horiz. Microstrain	10	21	28	39	39	40	44	58
		Vert. Microstrain	-36	-69	-67	-65	-59	-59	-60	-74
	Average	Average |E*|	5504	3931	3247	1888	1515	920	767	550
		Std. dev. |E*|	335	257	383	527	468	280	241	181
54	1	|E*| (MPa)								
		Horiz. Phase (°)								
		Vert. Phase (°)								
		Poisson's Ratio								
		Horiz. Microstrain								
		Vert. Microstrain								
	2	|E*| (MPa)								
		Horiz. Phase (°)								
		Vert. Phase (°)								
		Poisson's Ratio								
		Horiz. Microstrain								
		Vert. Microstrain								
	3	|E*| (MPa)		931	717	435	386	315		
		Horiz. Phase (°)		37.9	33.7	30.6	30.6	31.4		
		Vert. Phase (°)		31.0	30.3	25.4	22.3	19.6		
		Poisson's Ratio		0.20	0.26	0.31	0.25	0.13		
		Horiz. Microstrain		36	55	62	31	17		
		Vert. Microstrain		-87	-119	-125	-68	-45		
	4	|E*| (MPa)	1269	826	636	394	304			
		Horiz. Phase (°)	27.1	28.5	27.7	24.4	16.0			
		Vert. Phase (°)	33.3	30.0	28.8	24.3	17.9			
		Poisson's Ratio	0.09	0.19	0.23	0.27	0.20			
		Horiz. Microstrain	16	42	60	65	21			
		Vert. Microstrain	-45	-102	-135	-137	-48			
	Average	Average |E*|	1269	878	677	415	345	315		
		Std. dev. |E*|		74	57	29	58			

Table A.21 S12.5C-AV+2 IDT - Slab Data

Temperature (°C)	Replicate	Parameters	Frequency (Hz)							
			25	10	5	1	0.5	0.1	0.05	0.01
-10	1	|E*| (MPa)	28204	27127	26411	24092	23033	20679	19880	16950
		Horiz. Phase (°)	-1.7	1.6	3.4	5.8	11.6	11.7	12.8	15.1
		Vert. Phase (°)	5.8	6.8	7.1	8.3	8.5	10.0	12.4	14.3
		Poisson's Ratio	0.01	0.03	0.02	0.04	0.04	0.05	0.06	0.05
		Horiz. Microstrain	25	27	26	27	27	27	28	27
		Vert. Microstrain	-86	-90	-88	-90	-89	-88	-86	-87
	2	|E*| (MPa)	27275	26397	25669	23414	22560	19705	18999	16093
		Horiz. Phase (°)	3.7	5.6	7.9	8.2	11.5	14.5	15.3	18.0
		Vert. Phase (°)	3.8	5.4	5.1	5.9	6.6	7.4	10.6	12.8
		Poisson's Ratio	0.13	0.14	0.14	0.15	0.15	0.13	0.15	0.13
		Horiz. Microstrain	36	38	37	39	39	38	37	37
		Vert. Microstrain	-97	-101	-98	-100	-99	-100	-97	-98
	3	|E*| (MPa)	26251	25670	24906	22869	21630	19529	18337	15814
		Horiz. Phase (°)	6.2	11.0	13.0	13.6	20.0	17.0	22.4	24.7
		Vert. Phase (°)	3.8	5.2	5.5	5.7	7.1	9.0	10.8	12.0
		Poisson's Ratio	0.02	0.02	0.03	0.04	-0.01	0.04	0.01	0.01
		Horiz. Microstrain	28	29	29	30	27	30	27	27
		Vert. Microstrain	-95	-99	-98	-99	-98	-97	-96	-96
	Average	Average |E*|	27243	26398	25662	23458	22408	19971	19072	16286
		Std. dev. |E*|	977	728	753	613	714	619	774	592
10	1	|E*| (MPa)	17696	15191	13934	10639	9291	6705	5749	3828
		Horiz. Phase (°)	4.2	5.8	13.2	16.7	23.8	31.9	30.4	42.8
		Vert. Phase (°)	12.4	15.0	16.6	20.3	23.2	28.9	33.2	39.8
		Poisson's Ratio	-0.02	-0.02	0.01	0.00	-0.01	0.01	0.02	0.05
		Horiz. Microstrain	13	18	21	22	21	21	20	20
		Vert. Microstrain	-51	-69	-74	-79	-77	-73	-70	-65
	2	|E*| (MPa)	15688	14420	12967	10112	8767	6215	5206	3259
		Horiz. Phase (°)	16.3	17.1	19.8	22.2	30.1	35.3	40.8	48.1
		Vert. Phase (°)	10.9	13.8	15.5	18.6	21.1	26.5	31.6	37.4
		Poisson's Ratio	0.04	0.07	0.08	0.12	0.09	0.08	0.08	0.07
		Horiz. Microstrain	19	26	29	33	30	28	28	26
		Vert. Microstrain	-63	-78	-85	-90	-88	-85	-83	-80
	3	|E*| (MPa)	15888	13911	12691	9755	8516	6142	5107	3291
		Horiz. Phase (°)	11.9	17.2	19.6	27.6	34.6	38.5	44.0	54.5
		Vert. Phase (°)	11.8	13.8	15.4	19.0	21.8	26.7	31.3	37.9
		Poisson's Ratio	-0.10	-0.07	-0.05	-0.01	-0.02	-0.01	-0.01	0.01
		Horiz. Microstrain	12	17	20	24	22	23	22	22
		Vert. Microstrain	-59	-77	-83	-89	-87	-83	-82	-78
	Average	Average |E*|	16424	14507	13197	10169	8858	6354	5354	3459
		Std. dev. |E*|	1106	644	653	445	395	306	346	319
35	1	|E*| (MPa)	4275	3106	2360	1251	991	637	590	479
		Horiz. Phase (°)	32.6	44.9	37.7	44.4	48.2	50.5	53.8	69.3
		Vert. Phase (°)	34.2	34.2	35.4	38.2	39.1	37.3	38.4	38.0
		Poisson's Ratio	-0.12	-0.05	-0.02	0.04	0.05	-0.02	0.04	0.24
		Horiz. Microstrain	4	9	13	18	18	14	14	20
		Vert. Microstrain	-23	-37	-48	-58	-59	-52	-46	-45
	2	|E*| (MPa)	4546	3032	2423	1288	1014	673	643	491
		Horiz. Phase (°)	31.8	33.0	34.2	41.6	49.3	52.8	63.2	80.8
		Vert. Phase (°)	34.2	35.0	36.8	42.7	45.9	46.9	51.4	67.5
		Poisson's Ratio	0.17	0.11	0.17	0.17	0.14	0.09	0.16	0.32
		Horiz. Microstrain	12	17	22	25	24	18	18	24
		Vert. Microstrain	-31	-46	-54	-62	-62	-54	-46	-48
	3	|E*| (MPa)	4090	2846	2177	1145	879	508	415	278
		Horiz. Phase (°)	33.1	36.9	39.9	46.2	51.9	56.3	61.9	71.5
		Vert. Phase (°)	33.7	32.7	35.4	41.2	43.6	44.4	47.7	58.7
		Poisson's Ratio	0.13	0.14	0.16	0.20	0.22	0.22	0.23	0.46
		Horiz. Microstrain	10	18	23	30	32	32	32	52
		Vert. Microstrain	-26	-47	-58	-70	-73	-74	-73	-87
	Average	Average |E*|	4304	2995	2320	1228	961	606	549	416
		Std. dev. |E*|	229	134	127	74	72	87	119	120

Table A.22 S12.CM IDT Data

Temperature (°C)	Replicate	Parameters	Frequency (Hz)							
			25	10	5	1	0.5	0.1	0.05	0.01
-10	1	|E*| (MPa)	32144	29993	28847	26187	25144	22567	21154	18596
		Horiz. Phase (°)	4.4	6.8	7.8	10.3	7.8	11.5	16.4	15.7
		Vert. Phase (°)	3.7	2.8	3.0	3.5	4.4	6.2	6.6	9.6
		Poisson's Ratio	0.06	0.06	0.07	0.08	0.07	0.09	0.09	0.10
		Horiz. Microstrain	28	31	31	33	32	34	34	34
		Vert. Microstrain	-89	-94	-96	-98	-97	-97	-98	-96
	2	|E*| (MPa)	30842	29534	28802	26070	24696	21910	20617	17834
		Horiz. Phase (°)	0.9	1.7	1.9	4.7	4.4	7.2	11.5	9.6
		Vert. Phase (°)	2.1	1.7	1.4	3.4	4.1	5.6	6.1	9.0
		Poisson's Ratio	0.12	0.13	0.14	0.16	0.16	0.17	0.17	0.19
		Horiz. Microstrain	36	38	39	42	42	43	44	47
		Vert. Microstrain	-98	-102	-103	-105	-106	-107	-108	-114
	3	|E*| (MPa)	30057	29132	28124	25587	24432	22078	20993	18173
		Horiz. Phase (°)	-2.7	0.9	0.0	2.5	-0.1	3.4	7.9	7.6
		Vert. Phase (°)	0.9	2.8	2.2	2.3	3.4	4.7	5.4	7.5
		Poisson's Ratio	0.04	0.03	0.03	0.04	0.04	0.05	0.05	0.05
		Horiz. Microstrain	30	30	31	32	32	32	32	34
		Vert. Microstrain	-100	-100	-102	-103	-103	-103	-102	-107
	4	|E*| (MPa)	28187	27000	26497	24208	23333	20879	19591	16983
		Horiz. Phase (°)	10.1	12.3	13.7	13.8	14.1	15.8	22.2	18.9
		Vert. Phase (°)	1.5	1.8	2.3	3.3	3.7	5.5	5.7	8.2
		Poisson's Ratio	-0.09	-0.09	-0.07	-0.05	-0.06	-0.06	-0.07	-0.06
		Horiz. Microstrain	22	22	23	25	24	25	23	25
		Vert. Microstrain	-105	-106	-106	-108	-107	-107	-107	-112
	Average	Average |E*|	30308	28915	28067	25513	24401	21858	20589	17897
		Std. dev. |E*|	1655	1324	1098	908	770	710	702	684
10	1	|E*| (MPa)		14718	13384	10085	9273	6570	5631	3716
		Horiz. Phase (°)		2.9	11.5	19.9	23.4	23.1	39.3	30.6
		Vert. Phase (°)		8.9	9.2	13.8	15.5	19.6	21.8	25.1
		Poisson's Ratio		-0.20	-0.20	-0.27	-0.16	-0.19	-0.16	-0.20
		Horiz. Microstrain		9	9	4	13	10	12	9
		Vert. Microstrain		-80	-84	-89	-88	-82	-84	-79
	2	|E*| (MPa)	18986	16190	15243	11740	10329	7373	6321	4168
		Horiz. Phase (°)	6.5	8.5	10.4	16.5	17.6	23.0	29.3	26.3
		Vert. Phase (°)	8.3	9.7	12.1	14.8	17.6	21.1	23.4	27.5
		Poisson's Ratio	0.10	0.12	0.16	0.19	0.18	0.17	0.19	0.18
		Horiz. Microstrain	23	31	33	38	38	35	36	35
		Vert. Microstrain	-64	-84	-85	-92	-92	-88	-85	-87
	3	|E*| (MPa)	17812	16202	14663	11696	10384	7575	6425	4336
		Horiz. Phase (°)	0.3	6.5	9.5	14.2	14.8	19.5	24.3	21.8
		Vert. Phase (°)	8.4	8.9	10.3	13.1	15.7	20.5	22.9	25.9
		Poisson's Ratio	-0.04	0.02	0.03	0.07	0.07	0.06	0.04	0.04
		Horiz. Microstrain	15	23	26	30	29	26	25	24
		Vert. Microstrain	-64	-81	-85	-89	-88	-83	-80	-80
	4	|E*| (MPa)	16195	14717	13564	10655	9480	6875	5878	3953
		Horiz. Phase (°)	4.4	14.0	20.9	29.4	29.3	32.8	41.4	37.4
		Vert. Phase (°)	9.7	10.3	11.6	15.0	16.9	20.7	22.2	26.4
		Poisson's Ratio	-0.19	-0.14	-0.13	-0.05	-0.03	-0.08	-0.08	-0.10
		Horiz. Microstrain	8	14	15	23	24	19	18	17
		Vert. Microstrain	-70	-86	-89	-96	-95	-89	-86	-86
	Average	Average |E*|	17664	15457	14213	11044	9867	7098	6064	4043
		Std. dev. |E*|	1402	853	889	813	572	459	373	269

Table A.22 S12.5CM IDT Data (continued)

Temperature (°C)	Replicate	Parameters	Frequency (Hz)							
			25	10	5	1	0.5	0.1	0.05	0.01
35	1	|E*| (MPa)	4571	3480	2687	1476	1168	725	619	444
		Horiz. Phase (°)	17.6	20.7	24.3	32.8	29.0	27.6	31.3	36.5
		Vert. Phase (°)	21.9	24.1	25.3	28.8	29.1	25.9	25.4	25.2
		Poisson's Ratio	-0.07	-0.02	0.00	-0.02	-0.05	-0.09	-0.07	-0.01
		Horiz. Microstrain	8	14	16	17	15	14	16	26
		Vert. Microstrain	-35	-53	-60	-64	-62	-68	-74	-99
	2	|E*| (MPa)	4833	3321	2506	1315	1067	732	663	568
		Horiz. Phase (°)	51.4	37.0	36.9	41.5	40.3	40.8	50.2	58.5
		Vert. Phase (°)	32.0	30.3	31.5	35.2	35.0	32.8	32.0	34.0
		Poisson's Ratio	-0.16	-0.07	-0.03	-0.03	-0.06	-0.11	-0.06	0.04
		Horiz. Microstrain	5	12	16	19	16	13	17	25
		Vert. Microstrain	-32	-55	-65	-75	-71	-70	-73	-82
	3	|E*| (MPa)	5207	3892	3046	1692	1377	895	773	582
		Horiz. Phase (°)	25.7	21.0	22.6	28.5	28.2	27.2	31.1	29.4
		Vert. Phase (°)	25.6	25.4	26.6	30.4	31.0	29.8	28.8	31.8
		Poisson's Ratio	0.11	0.20	0.24	0.24	0.23	0.18	0.16	0.15
		Horiz. Microstrain	11	23	29	31	29	29	28	34
		Vert. Microstrain	-30	-54	-64	-68	-66	-70	-71	-88
	4	|E*| (MPa)	4263	3292	2556	1475	1179	765	662	499
		Horiz. Phase (°)	22.8	29.0	28.8	36.8	35.8	34.5	37.7	40.9
		Vert. Phase (°)	26.4	25.3	26.3	30.3	30.7	28.7	28.0	28.6
		Poisson's Ratio	-0.07	0.07	0.11	0.15	0.10	0.04	0.00	0.00
		Horiz. Microstrain	8	21	27	30	26	24	22	28
		Vert. Microstrain	-36	-63	-75	-77	-75	-80	-81	-100
	Average	Average |E*|	4719	3496	2699	1490	1198	779	679	523
		Std. dev. |E*|	401	276	244	155	129	79	65	64

Table A.23 S12.5F IDT Data

Temperature (°C)	Replicate	Parameters	Frequency (Hz)							
			25	10	5	1	0.5	0.1	0.05	0.01
-10	1	|E*| (MPa)	32049	37301	34698	28100	32227		23943	19360
		Horiz. Phase (°)	3.8	5.8	7.2	9.4	15.4		16.7	19.1
		Vert. Phase (°)	2.9	5.0	5.0	5.1	5.3		7.8	7.1
		Poisson's Ratio	0.04	0.11	0.10	0.06	0.09		0.03	0.02
		Horiz. Microstrain	28	29	29	30	28		27	29
		Vert. Microstrain	-92	-80	-84	-95	-80		-89	-99
	2	|E*| (MPa)	34726	32931	32177	29910	29118	26947	25616	22520
		Horiz. Phase (°)	10.4	13.0	15.9	15.5	19.5	20.7	21.3	24.2
		Vert. Phase (°)	5.5	6.0	6.2	7.3	7.9	9.2	11.4	11.9
		Poisson's Ratio	0.10	0.09	0.09	0.10	0.10	0.08	0.08	0.06
		Horiz. Microstrain	30	30	31	31	31	29	28	28
		Vert. Microstrain	-85	-89	-89	-89	-88	-84	-84	-86
	3	|E*| (MPa)	30854	30132	29467	27538	26567	23989	22997	20247
		Horiz. Phase (°)	6.9	5.3	8.4	7.7	11.3	13.9	15.2	18.8
		Vert. Phase (°)	3.3	4.6	5.3	5.2	6.3	6.7	8.7	9.9
		Poisson's Ratio	-0.02	-0.02	-0.02	-0.01	-0.01	-0.02	-0.02	-0.02
		Horiz. Microstrain	25	25	25	25	25	24	24	25
		Vert. Microstrain	-95	-96	-97	-95	-95	-93	-93	-95
	Average	Average |E*|	32543	33454	32114	28516	29304	25468	24185	20709
		Std. dev. |E*|	1983	3613	2616	1239	2835	2092	1326	1630
10	1	|E*| (MPa)	23065	19905	18407	14554	13063	9906	8534	5967
		Horiz. Phase (°)	4.6	14.8	19.7	24.0	30.3	34.4	39.8	43.1
		Vert. Phase (°)	14.9	16.3	17.6	21.1	22.8	28.5	32.4	37.3
		Poisson's Ratio	-0.06	-0.02	0.01	0.06	0.06	0.05	0.05	0.04
		Horiz. Microstrain	11	17	21	25	25	23	24	22
		Vert. Microstrain	-50	-67	-72	-78	-76	-74	-75	-70
	2	|E*| (MPa)	22766	20194	18724	15626	14465	10714	9482	6336
		Horiz. Phase (°)	13.5	22.0	21.6	31.9	35.0	41.9	43.7	57.6
		Vert. Phase (°)	12.7	13.7	15.0	17.2	20.3	25.6	30.2	37.7
		Poisson's Ratio	-0.13	-0.06	-0.05	0.09	0.10	0.04	0.11	0.04
		Horiz. Microstrain	9	15	17	25	24	21	24	20
		Vert. Microstrain	-50	-65	-69	-72	-69	-68	-68	-65
	3	|E*| (MPa)	20103	18192	16794	13376	12008	8753	7659	5071
		Horiz. Phase (°)	14.7	15.4	17.9	21.8	30.5	36.9	42.9	49.8
		Vert. Phase (°)	10.8	13.2	13.8	16.9	18.6	24.1	28.5	34.9
		Poisson's Ratio	-0.08	-0.05	-0.05	-0.02	-0.03	-0.03	0.00	0.00
		Horiz. Microstrain	12	17	19	21	21	21	23	23
		Vert. Microstrain	-57	-74	-79	-83	-82	-83	-83	-82
	Average	Average |E*|	21978	19430	17975	14519	13179	9791	8558	5791
		Std. dev. |E*|	1631	1082	1035	1126	1232	985	912	651

Table A.23 S12.5F IDT Data (continued)

Temperature (°C)	Replicate	Parameters	Frequency (Hz)							
			25	10	5	1	0.5	0.1	0.05	0.01
35	1	|E*| (MPa)	6574	4716	3692	2017	1558	938	778	531
		Horiz. Phase (°)	19.8	28.2	31.1	37.4	43.0	41.3	42.5	49.2
		Vert. Phase (°)	28.6	30.0	32.2	37.1	38.2	36.6	38.1	39.6
		Poisson's Ratio	0.06	0.09	0.12	0.18	0.17	0.18	0.19	0.33
		Horiz. Microstrain	11	21	27	33	30	31	32	52
		Vert. Microstrain	-34	-60	-72	-79	-76	-75	-77	-102
	2	|E*| (MPa)	6420	4902	3802	2053	1595	905	728	508
		Horiz. Phase (°)	32.2	36.0	37.8	43.0	47.3	47.9	51.4	61.0
		Vert. Phase (°)	27.5	28.9	32.1	36.7	37.1	34.9	36.2	39.2
		Poisson's Ratio	0.04	0.15	0.18	0.23	0.23	0.16	0.14	0.27
		Horiz. Microstrain	11	23	29	34	33	30	30	49
		Vert. Microstrain	-36	-60	-71	-78	-75	-77	-80	-104
	3	|E*| (MPa)	6210	4843	3652	1967	1476	842	670	447
		Horiz. Phase (°)	30.9	32.1	35.0	43.0	44.2	44.3	49.9	61.8
		Vert. Phase (°)	28.1	29.5	31.6	37.6	37.9	36.3	37.4	40.1
		Poisson's Ratio	0.06	0.09	0.08	0.11	0.11	0.10	0.11	0.19
		Horiz. Microstrain	14	20	24	29	29	29	32	49
		Vert. Microstrain	-42	-60	-72	-80	-80	-83	-88	-117
	Average	Average |E*|	6401	4820	3716	2012	1543	895	725	495
		Std. dev. |E*|	183	95	78	43	61	49	54	44
54	1	|E*| (MPa)	1647	1146	883	548	507	483		
		Horiz. Phase (°)	40.2	36.2	36.8	33.5	39.0	36.7		
		Vert. Phase (°)	36.6	34.0	33.1	30.0	27.9	28.4		
		Poisson's Ratio	0.06	0.21	0.30	0.37	0.29	0.26		
		Horiz. Microstrain	13	33	50	54	26	15		
		Vert. Microstrain	-40	-78	-103	-102	-53	-32		
	2	|E*| (MPa)	1946	1056	804	475	403	331		
		Horiz. Phase (°)	41.1	35.5	35.6	33.3	36.2	46.6		
		Vert. Phase (°)	34.2	33.8	32.2	28.1	25.7	22.9		
		Poisson's Ratio	0.32	0.32	0.38	0.42	0.34	0.22		
		Horiz. Microstrain	19	43	62	67	35	20		
		Vert. Microstrain	-38	-86	-115	-118	-67	-46		
	3	|E*| (MPa)	1391	940	693	417	343	279		
		Horiz. Phase (°)	42.8	37.5	40.0	37.4	35.4	48.9		
		Vert. Phase (°)	35.6	33.3	32.9	28.6	25.2	24.6		
		Poisson's Ratio	0.16	0.24	0.25	0.31	0.17	0.17		
		Horiz. Microstrain	21	43	59	66	31	22		
		Vert. Microstrain	-53	-96	-129	-134	-77	-54		
	Average	Average |E*|	1661	1048	793	480	418	364		
		Std. dev. |E*|	278	103	96	66	83	106		

Table A.24 S12.5FE IDT Data

Temperature (°C)	Replicate	Parameters	Frequency (Hz)							
			25	10	5	1	0.5	0.1	0.05	0.01
-10	1	|E*| (MPa)	34970	33524	31765	29817	28764	25629	24512	20997
		Horiz. Phase (°)	-7.1	-5.8	-5.2	-3.9	-3.9	-0.7	3.3	0.5
		Vert. Phase (°)	3.2	0.9	1.3	2.6	2.8	5.3	5.4	9.4
		Poisson's Ratio	0.18	0.16	0.16	0.18	0.19	0.19	0.20	0.19
		Horiz. Microstrain	39	39	40	42	43	43	44	45
		Vert. Microstrain	-95	-98	-100	-102	-103	-103	-103	-107
	2	|E*| (MPa)	37857	36763	35701	32750	31072	28069	26517	22662
		Horiz. Phase (°)	-1.8	2.4	4.5	4.9	8.1	8.6	14.9	10.0
		Vert. Phase (°)	4.1	3.6	3.7	5.3	6.0	8.0	8.8	11.7
		Poisson's Ratio	0.10	0.10	0.11	0.11	0.09	0.11	0.12	0.08
		Horiz. Microstrain	30	30	31	30	30	30	31	27
		Vert. Microstrain	-85	-86	-86	-86	-86	-85	-84	-79
	3	|E*| (MPa)	33690	32493	31766	29050	27862	24963	23733	20334
		Horiz. Phase (°)	-2.8	-1.0	1.4	2.8	3.3	5.8	10.6	9.3
		Vert. Phase (°)	2.3	2.8	3.3	4.1	4.8	6.3	7.9	11.0
		Poisson's Ratio	0.11	0.11	0.11	0.10	0.11	0.11	0.11	0.10
		Horiz. Microstrain	35	35	35	34	34	34	33	31
		Vert. Microstrain	-97	-98	-97	-96	-96	-96	-93	-88
	4	|E*| (MPa)	37328	37461	35952	33107	31666	29113	27539	24772
		Horiz. Phase (°)	-10.4	-6.5	0.3	5.8	6.4	5.9	16.1	17.8
		Vert. Phase (°)	2.3	3.4	3.5	4.4	5.3	7.0	7.6	11.2
		Poisson's Ratio	-0.17	-0.16	-0.16	-0.17	-0.15	-0.13	-0.13	-0.11
		Horiz. Microstrain	12	12	13	12	14	15	15	16
		Vert. Microstrain	-86	-85	-87	-87	-90	-87	-88	-87
	5	|E*| (MPa)	31961	30789	30324	27665	26763	23921	22570	19227
		Horiz. Phase (°)	-3.6	-4.7	-5.3	0.0	2.2	3.5	10.3	10.0
		Vert. Phase (°)	0.2	0.0	-0.1	0.8	1.5	3.2	3.9	7.0
		Poisson's Ratio	-0.15	-0.15	-0.14	-0.13	-0.12	-0.13	-0.12	-0.12
		Horiz. Microstrain	13	14	14	15	16	15	16	16
		Vert. Microstrain	-86	-88	-88	-89	-88	-88	-89	-89
	Average	Average |E*|	35161	34206	33102	30478	29225	26339	24974	21598
		Std. dev. |E*|	2470	2838	2558	2370	2092	2175	2031	2167

Table A.24 S12.5FE IDT Data (continued)

Temperature (°C)	Replicate	Parameters	Frequency (Hz)							
			25	10	5	1	0.5	0.1	0.05	0.01
10	1	|E*| (MPa)	22030	19003	17283	13200	11654	8167	6734	4256
		Horiz. Phase (°)	2.4	4.2	6.3	12.2	14.5	20.8	28.5	28.4
		Vert. Phase (°)	9.7	10.6	11.9	16.5	19.1	25.7	28.6	35.5
		Poisson's Ratio	0.16	0.18	0.19	0.22	0.24	0.27	0.27	0.29
		Horiz. Microstrain	21	29	32	36	37	38	38	37
		Vert. Microstrain	-54	-71	-76	-82	-81	-81	-80	-77
	2	|E*| (MPa)	23242	20193	18224	13662	11893	8073	6675	4021
		Horiz. Phase (°)	12.3	12.0	16.4	21.3	24.8	30.8	40.5	42.3
		Vert. Phase (°)	10.5	11.9	14.1	18.1	21.5	27.4	32.3	37.9
		Poisson's Ratio	0.10	0.11	0.13	0.17	0.19	0.20	0.23	0.24
		Horiz. Microstrain	26	30	33	38	38	39	43	47
		Vert. Microstrain	-74	-84	-87	-94	-92	-94	-97	-103
	3	|E*| (MPa)	20004	17784	16024	12481	10799	7548	6290	3921
		Horiz. Phase (°)	9.9	10.6	12.3	19.2	21.1	30.2	37.5	38.0
		Vert. Phase (°)	10.0	11.3	12.0	16.7	19.7	25.7	30.6	36.6
		Poisson's Ratio	0.06	0.09	0.09	0.12	0.13	0.13	0.16	0.17
		Horiz. Microstrain	29	33	34	37	37	37	40	41
		Vert. Microstrain	-90	-97	-99	-100	-100	-98	-101	-104
	4	|E*| (MPa)	25449	22648	20590	16106	13824	10147	8479	5480
		Horiz. Phase (°)	-2.5	8.5	18.7	28.7	33.0	42.4	50.5	58.5
		Vert. Phase (°)	11.9	12.6	13.7	19.1	21.9	27.7	33.0	39.9
		Poisson's Ratio	-0.14	-0.11	-0.09	-0.02	0.00	0.07	0.11	0.15
		Horiz. Microstrain	9	12	15	20	22	25	27	29
		Vert. Microstrain	-52	-66	-71	-77	-78	-75	-76	-74
	5	|E*| (MPa)	19238	17459	15936	12247	10595	7689	6299	3998
		Horiz. Phase (°)	-14.3	12.0	8.5	17.4	26.6	32.5	41.5	40.3
		Vert. Phase (°)	7.7	8.8	9.7	14.5	17.5	22.6	25.2	30.5
		Poisson's Ratio	-0.16	-0.13	-0.13	-0.10	-0.09	-0.05	-0.07	-0.07
		Horiz. Microstrain	7	11	11	14	15	17	16	16
		Vert. Microstrain	-51	-64	-67	-74	-74	-71	-72	-71
	Average	Average |E*|	21993	19417	17611	13539	11753	8325	6896	4335
		Std. dev. |E*|	2502	2105	1916	1542	1281	1051	909	652

Table A.24 S12.5FE IDT Data (continued)

Temperature (°C)	Replicate	Parameters	Frequency (Hz)							
			25	10	5	1	0.5	0.1	0.05	0.01
35	1	|E*| (MPa)	5636	4139	3012	1567	1254	844	768	752
		Horiz. Phase (°)	20.5	22.2	24.7	28.3	28.0	28.6	33.8	40.4
		Vert. Phase (°)	29.7	29.6	31.7	34.6	34.9	32.2	33.0	43.6
		Poisson's Ratio	0.32	0.39	0.40	0.43	0.46	0.51	0.60	1.10
		Horiz. Microstrain	16	26	36	44	44	39	40	52
		Vert. Microstrain	-31	-47	-65	-76	-74	-63	-60	-57
	2	|E*| (MPa)	5563	3807	2702	1370	1071	667	571	501
		Horiz. Phase (°)	29.9	27.4	26.9	26.4	27.0	27.1	31.4	26.9
		Vert. Phase (°)	31.1	30.4	31.4	30.9	31.3	28.3	28.1	26.5
		Poisson's Ratio	0.28	0.38	0.40	0.45	0.48	0.56	0.63	0.77
		Horiz. Microstrain	20	34	51	79	72	74	80	52
		Vert. Microstrain	-42	-62	-93	-136	-120	-115	-116	-68
	3	|E*| (MPa)	4418	3119	2298	1158	885	539	452	362
		Horiz. Phase (°)	31.4	28.0	28.9	31.2	32.3	34.0	41.0	42.5
		Vert. Phase (°)	30.9	31.1	32.8	32.8	33.0	30.6	30.3	29.9
		Poisson's Ratio	0.16	0.21	0.23	0.22	0.20	0.15	0.12	-0.04
		Horiz. Microstrain	21	37	49	53	49	44	41	16
		Vert. Microstrain	-54	-86	-110	-123	-116	-114	-111	-65
	4	|E*| (MPa)	11589	6705	4830	2833	2645			
		Horiz. Phase (°)	28.5	31.4	30.2	33.6	35.1			
		Vert. Phase (°)	40.7	33.8	34.4	37.5	38.3			
		Poisson's Ratio	0.33	0.29	0.30	0.32	0.43			
		Horiz. Microstrain	7	13	18	19	18			
		Vert. Microstrain	-13	-28	-36	-37	-31			
	5	|E*| (MPa)	4731	3528	2761	1426	1093	644	547	396
		Horiz. Phase (°)	30.7	33.0	34.6	39.8	41.6	43.3	52.1	58.9
		Vert. Phase (°)	29.5	28.7	30.0	34.3	34.8	32.3	31.8	36.4
		Poisson's Ratio	0.01	0.05	0.12	0.12	0.09	0.04	0.07	0.20
		Horiz. Microstrain	9	16	22	26	25	25	29	51
		Vert. Microstrain	-31	-51	-61	-71	-72	-81	-90	-120
	Average	Average |E*|	6387	4260	3121	1671	1390	673	585	503
		Std. dev. |E*|	2955	1417	989	666	714	126	133	176

Table A.25 S12.5FE-AV+3 IDT Data

Temperature (°C)	Replicate	Parameters	Frequency (Hz)							
			25	10	5	1	0.5	0.1	0.05	0.01
-10	1	|E*| (MPa)	33647	33105	31935	29633	28559	25830	24872	21469
		Horiz. Phase (°)	1.2	3.1	4.6	5.5	8.8	12.5	12.2	16.5
		Vert. Phase (°)	5.4	6.8	7.2	7.8	8.4	10.2	12.1	14.1
		Poisson's Ratio	0.21	0.22	0.22	0.21	0.22	0.23	0.24	0.24
		Horiz. Microstrain	34	36	35	35	35	34	34	35
		Vert. Microstrain	-80	-82	-81	-81	-80	-78	-77	-76
	2	|E*| (MPa)	31611	30456	29651	27331	26691	23983	22813	19706
		Horiz. Phase (°)	2.1	1.5	3.7	3.5	2.9	9.2	11.5	13.7
		Vert. Phase (°)	4.1	5.9	6.4	7.4	7.3	9.1	11.5	14.2
		Poisson's Ratio	-0.05	-0.05	-0.05	-0.04	-0.04	-0.04	-0.04	-0.04
		Horiz. Microstrain	18	19	19	19	19	19	18	19
		Vert. Microstrain	-78	-80	-79	-79	-77	-76	-75	-75
	3	|E*| (MPa)	31863	30903	29926	27416	26382	23621	22232	19256
		Horiz. Phase (°)	6.4	8.0	8.8	9.5	13.2	14.3	17.6	21.9
		Vert. Phase (°)	4.4	5.4	5.6	6.1	6.8	8.1	9.9	12.6
		Poisson's Ratio	0.12	0.12	0.12	0.11	0.13	0.11	0.11	0.12
		Horiz. Microstrain	29	30	30	29	31	29	29	29
		Vert. Microstrain	-80	-82	-81	-82	-82	-80	-80	-79
	4	|E*| (MPa)	32596		30614	28166	27123	24633	23172	19704
		Horiz. Phase (°)	0.8		3.4	4.2	7.4	10.1	12.7	13.2
		Vert. Phase (°)	4.2		5.8	6.1	6.5	8.1	11.1	13.0
		Poisson's Ratio	0.24		0.24	0.24	0.26	0.26	0.29	0.27
		Horiz. Microstrain	37		38	38	39	38	40	39
		Vert. Microstrain	-83		-84	-85	-84	-82	-83	-83
	Average	Average |E*|	32429	31488	30531	28137	27189	24517	23272	20034
		Std. dev. |E*|	913	1418	1019	1066	963	970	1135	980
10	1	|E*| (MPa)	21884	19350	17108	12521	11234	7870	6502	4186
		Horiz. Phase (°)	15.9	16.6	19.0	25.2	27.4	35.7	40.8	47.2
		Vert. Phase (°)	14.8	17.4	18.4	23.7	28.0	33.8	39.1	45.2
		Poisson's Ratio	0.19	0.21	0.20	0.17	0.24	0.24	0.25	0.26
		Horiz. Microstrain	20	26	28	30	32	32	32	31
		Vert. Microstrain	-47	-61	-67	-74	-72	-71	-70	-67
	2	|E*| (MPa)	21053	18193	16178	12262	10721	7534	6347	3994
		Horiz. Phase (°)	11.4	11.0	13.2	25.3	35.5	43.8	46.2	52.8
		Vert. Phase (°)	13.9	15.2	17.7	22.5	25.5	32.2	36.9	45.0
		Poisson's Ratio	-0.04	-0.04	-0.04	-0.01	0.03	0.01	0.06	0.09
		Horiz. Microstrain	11	14	16	19	20	19	21	22
		Vert. Microstrain	-45	-59	-64	-70	-69	-67	-66	-65
	3	|E*| (MPa)	18984	16941	15269	11796	10115	6910	5639	3479
		Horiz. Phase (°)	22.0	20.1	20.7	24.7	31.7	41.2	45.1	53.5
		Vert. Phase (°)	13.6	14.6	15.6	20.9	23.9	29.8	34.7	40.6
		Poisson's Ratio	0.02	0.08	0.09	0.15	0.14	0.14	0.15	0.16
		Horiz. Microstrain	14	22	24	29	28	29	29	30
		Vert. Microstrain	-48	-65	-70	-75	-75	-75	-76	-75
	4	|E*| (MPa)	20214	17606	15815	11976	10474	7253	5923	3702
		Horiz. Phase (°)	14.1	13.7	15.2	19.3	25.6	32.5	36.0	43.5
		Vert. Phase (°)	11.5	14.0	16.5	20.9	24.3	30.7	35.2	40.4
		Poisson's Ratio	0.21	0.24	0.24	0.28	0.29	0.32	0.32	0.35
		Horiz. Microstrain	20	30	33	38	38	39	39	40
		Vert. Microstrain	-47	-66	-72	-79	-77	-77	-78	-76
	Average	Average |E*|	20534	18022	16092	12139	10636	7392	6103	3840
		Std. dev. |E*|	1238	1022	773	319	470	408	394	313

Table A.25 S12.5FE-AV+3 IDT Data (continued)

Temperature (°C)	Replicate	Parameters	Frequency (Hz)							
			25	10	5	1	0.5	0.1	0.05	0.01
35	1	|E*| (MPa)	6066	4398	3076	1882	1680	1428	1395	1595
		Horiz. Phase (°)	36.6	31.4	36.4	40.3	44.7	49.6	58.8	74.5
		Vert. Phase (°)	35.0	35.1	36.2	38.7	38.2	32.1	33.9	45.8
		Poisson's Ratio	0.28	0.35	0.31	0.42	0.48	0.64	0.78	2.31
		Horiz. Microstrain	9	16	21	26	25	21	19	30
		Vert. Microstrain	-19	-31	-43	-46	-41	-30	-25	-23
	2	|E*| (MPa)			2533	1280	1042	697	656	651
		Horiz. Phase (°)			35.4	38.5	43.2	47.0	51.9	70.0
		Vert. Phase (°)			35.2	37.7	38.4	36.4	39.9	50.3
		Poisson's Ratio			0.26	0.29	0.30	0.32	0.39	0.95
		Horiz. Microstrain			23	30	30	27	26	35
		Vert. Microstrain			-50	-63	-62	-54	-47	-41
	3	|E*| (MPa)	4440	3128	2375	1292	1043	682	603	474
		Horiz. Phase (°)	48.4	40.9	40.7	42.8	48.5	54.5	62.1	79.5
		Vert. Phase (°)	35.7	33.4	35.2	38.3	39.4	37.8	39.9	53.8
		Poisson's Ratio	0.08	0.17	0.25	0.33	0.32	0.32	0.35	0.78
		Horiz. Microstrain	8	16	24	32	31	28	26	41
		Vert. Microstrain	-23	-39	-52	-63	-62	-55	-50	-53
	4	|E*| (MPa)	5131	3469	2570	1411	1179	997	1193	1973
		Horiz. Phase (°)	30.7	28.8	30.9	33.3	38.7	41.1	45.8	368.6
		Vert. Phase (°)	32.3	34.2	35.1	37.6	38.6	38.5	43.9	13.3
		Poisson's Ratio	0.46	0.42	0.42	0.50	0.53	0.85	1.33	3.97
		Horiz. Microstrain	14	22	29	38	37	36	33	39
		Vert. Microstrain	-24	-40	-52	-62	-59	-44	-33	-24
	Average	Average |E*|	5212	3665	2639	1466	1236	951	962	1173
		Std. dev. |E*|	816	657	304	284	303	349	393	725

Table A.26 S12.5FE-AV+3 IDT - Slab Data

Temperature (°C)	Replicate	Parameters	Frequency (Hz)							
			25	10	5	1	0.5	0.1	0.05	0.01
-10	1	|E*| (MPa)	29149	28422	27316	25139	23858	21229	19804	16808
		Horiz. Phase (°)	11.2	11.8	12.6	13.9	18.2	20.0	24.8	25.1
		Vert. Phase (°)	5.7	6.7	6.9	7.9	9.0	10.4	11.9	15.8
		Poisson's Ratio	0.07	0.10	0.09	0.12	0.11	0.13	0.10	0.12
		Horiz. Microstrain	27	31	31	34	33	34	33	34
		Vert. Microstrain	-82	-90	-90	-92	-92	-92	-92	-93
	2	|E*| (MPa)	28785	27753	26982	25060	23748	21705	20116	17093
		Horiz. Phase (°)	8.3	10.3	11.7	11.6	15.8	16.3	19.1	23.0
		Vert. Phase (°)	2.6	4.9	4.8	5.8	6.2	8.1	9.8	13.0
		Poisson's Ratio	0.06	0.07	0.08	0.09	0.09	0.10	0.11	0.12
		Horiz. Microstrain	33	34	36	37	37	38	39	42
		Vert. Microstrain	-104	-106	-107	-107	-108	-106	-109	-116
	3	|E*| (MPa)	21907	21232	20309	18430	17811	15766	14768	12689
		Horiz. Phase (°)	10.3	13.1	14.5	13.1	15.9	18.2	22.8	27.4
		Vert. Phase (°)	6.5	6.2	7.8	7.3	6.3	6.3	9.1	12.8
		Poisson's Ratio	-0.07	-0.06	-0.06	-0.01	0.01	0.08	0.09	0.13
		Horiz. Microstrain	20	21	21	23	23	23	23	24
		Vert. Microstrain	-91	-93	-94	-87	-81	-68	-65	-64
	4	|E*| (MPa)	27298	25713	25214	23054	21817	19178	17928	14994
		Horiz. Phase (°)	6.0	7.1	9.6	8.9	12.5	16.4	17.8	22.6
		Vert. Phase (°)	4.3	5.2	5.8	6.3	7.4	9.2	12.0	14.5
		Poisson's Ratio	0.15	0.13	0.15	0.19	0.18	0.20	0.20	0.20
		Horiz. Microstrain	36	37	37	41	41	42	43	44
		Vert. Microstrain	-93	-99	-97	-100	-100	-101	-101	-104
	Average	Average |E*|	26785	25780	24955	22921	21808	19470	18154	15396
		Std. dev. |E*|	3349	3243	3232	3145	2825	2702	2455	2030
10	1	|E*| (MPa)	15636	13816	12255	9156	7930	5345	4387	2616
		Horiz. Phase (°)	27.8	26.8	29.8	33.1	38.2	46.8	51.7	57.8
		Vert. Phase (°)	14.9	16.6	18.3	23.4	26.2	32.1	37.0	43.9
		Poisson's Ratio	-0.08	0.03	0.05	0.13	0.14	0.13	0.15	0.16
		Horiz. Microstrain	12	24	28	37	37	37	39	40
		Vert. Microstrain	-56	-78	-88	-99	-97	-99	-100	-102
	2	|E*| (MPa)	15776	14408	13035	9788	8536	5781	4737	2906
		Horiz. Phase (°)	24.8	23.6	26.5	31.2	36.6	44.5	48.6	52.6
		Vert. Phase (°)	12.0	14.9	16.1	21.8	24.9	30.8	35.9	43.2
		Poisson's Ratio	-0.03	0.08	0.12	0.20	0.22	0.23	0.28	0.30
		Horiz. Microstrain	19	32	38	50	53	60	69	76
		Vert. Microstrain	-75	-96	-105	-119	-122	-134	-145	-154
	3	|E*| (MPa)	15478	13696	12500	13123	12158	8527	6993	3840
		Horiz. Phase (°)	28.8	25.1	27.4	32.2	38.4	50.7	54.2	66.1
		Vert. Phase (°)	14.0	16.6	17.3	18.4	20.6	28.3	34.9	49.5
		Poisson's Ratio	-0.09	-0.05	-0.03	0.15	0.20	0.23	0.25	0.24
		Horiz. Microstrain	13	19	21	27	27	28	29	32
		Vert. Microstrain	-64	-80	-84	-68	-64	-63	-64	-70
	4	|E*| (MPa)	17723	15379	13619	10002	8588	5961	4794	3043
		Horiz. Phase (°)	20.5	25.8	26.8	33.0	39.9	48.0	51.8	65.1
		Vert. Phase (°)	19.5	21.4	24.0	27.7	32.0	38.2	43.9	51.2
		Poisson's Ratio	-0.08	0.00	0.02	0.11	0.08	0.10	0.12	0.20
		Horiz. Microstrain	11	19	22	31	29	30	33	37
		Vert. Microstrain	-54	-71	-77	-87	-86	-86	-88	-87
	Average	Average |E*|	16153	14324	12852	10517	9303	6403	5228	3101
		Std. dev. |E*|	1053	769	606	1774	1926	1439	1190	523

Table A.26 S12.5FE-AV+3 IDT - Slab Data (continued)

Temperature (°C)	Replicate	Parameters	Frequency (Hz)							
			25	10	5	1	0.5	0.1	0.05	0.01
35	1	|E*| (MPa)	3715	2429	1819	943	756	491	421	320
		Horiz. Phase (°)	52.0	46.4	39.1	46.7	50.1	57.5	63.6	81.4
		Vert. Phase (°)	39.6	37.3	38.3	42.1	44.3	45.0	48.9	65.8
		Poisson's Ratio	0.06	0.11	0.10	0.12	0.15	0.18	0.29	0.76
		Horiz. Microstrain	6	17	23	30	32	31	35	61
		Vert. Microstrain	-19	-47	-64	-83	-83	-75	-72	-82
	2	|E*| (MPa)	5581	3077	2893	1774	1386	1049	828	516
		Horiz. Phase (°)	40.1	38.6	40.2	43.7	49.3	53.6	57.0	71.6
		Vert. Phase (°)	28.3	34.0	37.2	37.5	44.0	44.8	52.1	65.9
		Poisson's Ratio	0.44	0.29	0.51	0.75	0.74	1.06	1.09	1.57
		Horiz. Microstrain	25	43	59	79	75	76	82	155
		Vert. Microstrain	-43	-89	-95	-106	-100	-85	-91	-142
	3	|E*| (MPa)	4251	3973	3035	1714	1272	661	593	349
		Horiz. Phase (°)	48.6	40.3	40.7	46.1	54.1	58.0	69.1	86.4
		Vert. Phase (°)	34.4	34.2	34.7	42.3	44.0	46.9	52.9	69.3
		Poisson's Ratio	0.01	0.30	0.35	0.51	0.48	0.38	0.44	0.69
		Horiz. Microstrain	6	15	22	31	32	32	30	52
		Vert. Microstrain	-22	-32	-41	-51	-53	-58	-53	-72
	4	|E*| (MPa)	3812	2676	1971	1016	811	504	449	353
		Horiz. Phase (°)	37.8	36.9	37.3	40.6	46.1	51.5	62.0	77.6
		Vert. Phase (°)	39.7	38.6	38.0	40.9	42.4	42.9	48.1	63.2
		Poisson's Ratio	0.33	0.40	0.38	0.44	0.47	0.49	0.60	1.23
		Horiz. Microstrain	13	27	34	47	49	47	48	78
		Vert. Microstrain	-27	-48	-63	-82	-82	-78	-72	-80
	Average	Average |E*|	4340	3039	2430	1362	1056	676	573	384
		Std. dev. |E*|	859	677	623	443	319	260	186	89

Table A.27 B25.0C IDT Data

Temperature (°C)	Replicate	Parameters	Frequency (Hz)							
			25	10	5	1	0.5	0.1	0.05	0.01
-10	1	|E*| (MPa)	38771	36701	35557	33375	32291	29441	27994	25259
		Horiz. Phase (°)	-14.6	-12.3	-11.2	-7.3	-8.1	-4.7	0.3	-1.8
		Vert. Phase (°)	4.2	4.7	4.4	5.8	6.1	8.0	9.1	11.9
		Poisson's Ratio	0.13	0.09	0.08	0.10	0.10	0.10	0.11	0.12
		Horiz. Microstrain	33	32	32	33	33	33	33	34
		Vert. Microstrain	-89	-93	-95	-94	-95	-93	-93	-92
	2	|E*| (MPa)	32069	31351	30212	28542	27197	24926	23785	21112
		Horiz. Phase (°)	-11.2	-8.1	-5.1	-2.3	-3.9	1.4	4.9	3.9
		Vert. Phase (°)	0.8	1.1	0.9	1.9	2.2	3.9	4.3	7.6
		Poisson's Ratio	0.01	0.02	0.01	0.01	0.00	0.03	0.03	0.05
		Horiz. Microstrain	28	29	28	29	28	30	31	32
		Vert. Microstrain	-98	-100	-101	-101	-103	-101	-102	-103
	3	|E*| (MPa)	29593	28986	28891	27161	26706	24970	24390	23485
		Horiz. Phase (°)	-4.5	-4.4	-2.6	-0.5	-1.5	1.5	5.9	5.9
		Vert. Phase (°)	0.3	0.8	1.0	1.9	2.2	3.4	3.3	6.7
		Poisson's Ratio	0.11	0.12	0.15	0.16	0.18	0.19	0.21	0.29
		Horiz. Microstrain	38	40	41	43	44	44	44	47
		Vert. Microstrain	-106	-109	-108	-109	-109	-104	-102	-97
	4	|E*| (MPa)	32339	31787	30728	28092	27200	25451	23644	20561
		Horiz. Phase (°)	-10.5	-10.6	-8.7	-5.8	-6.4	-3.6	-0.5	-1.9
		Vert. Phase (°)	2.5	3.0	4.0	4.7	6.1	7.8	8.9	12.4
		Poisson's Ratio	0.02	0.01	0.01	0.02	0.02	0.05	0.04	0.05
		Horiz. Microstrain	24	23	23	25	24	26	26	27
		Vert. Microstrain	-80	-81	-81	-85	-83	-82	-84	-85
	Average	Average |E*|	33193	32206	31347	29292	28348	26197	24953	22604
		Std. dev. |E*|	3919	3239	2911	2782	2639	2176	2053	2177
10	1	|E*| (MPa)	27898	22689	20426	15891	13900	9919	8208	5162
		Horiz. Phase (°)	-8.9	-0.3	2.3	6.8	13.4	23.1	31.4	34.3
		Vert. Phase (°)	13.8	13.5	15.1	20.0	23.4	30.9	36.7	44.6
		Poisson's Ratio	0.18	0.15	0.15	0.19	0.20	0.25	0.28	0.32
		Horiz. Microstrain	22	34	35	38	38	41	43	45
		Vert. Microstrain	-55	-86	-89	-91	-90	-90	-90	-90
	2	|E*| (MPa)	21001	18663	17202	13026	11554	8228	6799	4309
		Horiz. Phase (°)	7.0	-3.4	2.2	10.2	12.8	23.1	34.4	37.7
		Vert. Phase (°)	9.1	9.2	10.2	14.6	18.2	25.1	29.9	36.4
		Poisson's Ratio	0.05	0.01	0.03	0.04	0.03	0.10	0.11	0.16
		Horiz. Microstrain	21	19	22	24	23	27	27	29
		Vert. Microstrain	-68	-67	-72	-79	-77	-76	-76	-74
	3	|E*| (MPa)	19151	17186	15753	12521	10900	8511	7683	7084
		Horiz. Phase (°)	6.3	8.8	11.8	16.4	19.4	26.4	35.9	38.2
		Vert. Phase (°)	8.8	9.5	11.0	14.5	17.9	25.3	31.5	38.2
		Poisson's Ratio	0.12	0.15	0.18	0.23	0.26	0.36	0.47	0.94
		Horiz. Microstrain	22	29	33	38	40	41	43	45
		Vert. Microstrain	-59	-76	-81	-85	-86	-78	-73	-54
	4	|E*| (MPa)	21742	19518	17818	12611	11277	8080	6895	3852
		Horiz. Phase (°)	-0.6	3.6	5.5	11.4	15.1	25.2	33.0	33.7
		Vert. Phase (°)	11.8	14.7	16.3	21.3	24.0	31.7	36.1	45.2
		Poisson's Ratio	0.07	0.09	0.08	0.08	0.11	0.15	0.19	0.14
		Horiz. Microstrain	19	21	22	26	27	29	30	32
		Vert. Microstrain	-58	-60	-65	-76	-76	-75	-73	-82
	Average	Average |E*|	22448	19514	17800	13512	11908	8685	7396	5102
		Std. dev. |E*|	3793	2325	1953	1601	1355	842	670	1429

B25.0C IDT Data (continued)

Temperature (°C)	Replicate	Parameters	Frequency (Hz)							
			25	10	5	1	0.5	0.1	0.05	0.01
35	1	|E*| (MPa)	7362	4768	3397	1747	1411	972	1004	
		Horiz. Phase (°)	23.7	23.8	27.1	29.6	29.8	26.0	30.0	
		Vert. Phase (°)	36.2	34.5	34.8	35.2	33.8	32.3	31.4	
		Poisson's Ratio	0.38	0.39	0.41	0.47	0.50	0.55	0.68	
		Horiz. Microstrain	16	29	39	47	43	34	30	
		Vert. Microstrain	-30	-53	-69	-78	-71	-54	-42	
	2	|E*| (MPa)		4059	2884	1456	1125	689	604	497
		Horiz. Phase (°)		28.9	33.2	35.4	36.0	32.7	39.2	35.9
		Vert. Phase (°)		31.3	33.2	33.7	34.1	32.1	30.8	33.4
		Poisson's Ratio		0.13	0.13	0.17	0.17	0.17	0.19	0.24
		Horiz. Microstrain		16	23	30	31	28	28	31
		Vert. Microstrain		-42	-62	-76	-76	-70	-68	-69
	3	|E*| (MPa)	7400	5559	3930	1832	1443	898	784	780
		Horiz. Phase (°)	33.9	28.5	28.4	31.8	31.4	29.7	35.0	40.8
		Vert. Phase (°)	31.1	27.5	32.9	35.2	36.0	31.3	33.5	41.0
		Poisson's Ratio	0.55	0.74	0.77	0.72	0.76	0.75	0.80	1.18
		Horiz. Microstrain	16	28	41	50	52	46	47	52
		Vert. Microstrain	-25	-38	-54	-69	-68	-62	-61	-55
	4	|E*| (MPa)	4632	3198	3054	1979	1641	1149	1136	1565
		Horiz. Phase (°)	25.8	32.2	28.5	35.2	32.6	32.4	32.7	28.5
		Vert. Phase (°)	38.7	36.6	33.2	31.4	30.5	30.2	28.0	29.5
		Poisson's Ratio	0.09	0.15	0.35	0.61	0.63	0.82	0.77	1.69
		Horiz. Microstrain	13	19	27	36	34	49	28	33
		Vert. Microstrain	-37	-49	-51	-53	-49	-62	-37	-29
	Average	Average |E*|	6465	4396	3316	1754	1405	927	882	947
		Std. dev. |E*|	1587	1007	461	221	213	191	235	553

APPENDIX B RESILIENT MODULUS DATA

Table B.1 Resilient Modulus Values for Mixtures Tested

Mixture	Temperature (°C)	Resilient Modulus (Mpa)						
		1	2	3	4	5	Average	Predicted
S12.5C	5	20245	20780	22965	19481	18120	20318	20052
	25	5237	5593	5574	5025	5848	5456	5976
	40	1786	1790	1854	2474	2627	2106	1879
S12.5FE	5	22612	20301	23943	17908	18773	20707	20626
	25	6720	6373	6593	4579	4739	5801	5807
	40	1533	1790	2165	1937	1280	1741	1628
S12.5C-AC-1	5	22594	24363	25366			24108	22808
	25	11261	11794	8786			10614	8811
	40	3934	3371	3551			3619	3055
S12.5C-AC+1	5	17441	16223	15347			16337	14727
	25	4764	4532	7659			5652	3810
	40	1107	1000	2340			1482	1209
S12.5CM	5	17339	20161	17583			18361	17697
	25	7072	5407	5478			5986	5471
	40	1394	1710	1518			1541	1636
S12.5F	5	24593	20834	21615			22347	21179
	25	7907	6797	7416			7374	7062
	40	3414	2458	1936			2602	2246
B25.0C	5	22376	19759	21546			21227	21583
	25	6319	5913	6434			6222	6559
	40	1621	1729	1566			1639	2271

Table B.2 Resilient Modulus Predicted for Witczak Database

Mixture #	Temperature (°C)			Mixture #	Temperature (°C)		
	5	25	40		5	25	40
136	7988	2040	589	172	12045	3656	1142
137	7918	2032	702	173	11092	3192	1098
138	5659	1473	565	174	13050	3745	1248
139	6627	1635	559	175	10988	3170	1060
140	6325	1683	593	176	15169	5860	2254
141	6230	1189	379	177	15214	4450	1514
142	4542	1236	408	178	14632	5123	1517
143	5035	1081	458	179	16605	7848	2531
144	18413	6555	2256	180	10213	4050	1508
145	16830	5322	1469	181	6107	2179	726
146	15442	4760	1276	182	9035	3631	1018
147	16115	5916	1625	183	11625	4814	1435
148	14330	3975	998	184	9373	3778	1003
149	9898	2742	714	185	6711	2088	594
150	14319	3563	934	186	7784	2406	664
151	8881	2028	550	187	8861	3045	871
152	8658	2130	551	188	9732	3559	1283
153	10631	3525	883	189	9317	3407	1119
154	13167	4767	1289	190	8871	3127	951
155	10491	3489	974	191	8773	3237	1148
156	10784	3476	1358	192	20328	4281	841
157	6637	1996	659	193	11010	3199	792
158	8157	2646	1068	194	17148	3939	918
159	8280	2280	745	195	16453	4239	1029
160	14466	3872	1142	196	16953	5420	1462
161	14000	4613	1344	197	13571	3898	1101
162	13163	4606	1480	198	14573	4246	1118
163	13979	4455	1021	199	13398	3716	996
164	11248	2801	883	200	18193	4751	1022
165	13231	4073	1304	201	9799	1952	470
166	10717	2319	725	202	14353	3257	827
167	10260	2901	984	203	10739	3260	876
168	12971	3925	1240	204	14217	5029	1475
169	11621	3781	1270	205	15488	3986	1107
170	12204	3172	1403	206	20670	7471	1161
171	13145	3937	1296	207	32113	10440	2438

Table B.2 Resilient Modulus Predicted for Witczak Database

Mixture #	Temperature (°C)			Mixture #	Temperature (°C)		
	5	25	40		5	25	40
208	19632	6589	2214	244	16054	5772	1685
209	24310	9045	2230	245	26938	11648	3642
210	21224	6938	2070	246	27331	11576	2068
211	18054	5771	1399	247	25365	9976	2470
212	16212	5903	1758	248	34052	12121	2472
213	46481	18070	4391	249	16037	5859	1749
214	14134	5181	1554	250	23277	9362	2959
215	23426	7915	2020	251	32993	13455	3646
216	28424	8604	1620	252	29944	13661	2630
217	21961	10566	3777	253	22174	6986	1847
218	17255	6801	2059	254	31104	10135	1909
219	14062	3338	958	255	30251	12946	3508
220	12853	3628	1018	256	19826	8539	2015
221	28611	9127	1807	257	16546	5423	1558
222	32025	11107	3629	258	12674	2756	888
223	18133	8506	3301	259	17553	4542	1134
224	23417	8747	3415	260	17543	5026	1217
225	17436	7612	2249	261	7977	2222	778
226	25172	10856	3644	262	7207	2273	738
227	23882	5111	832	263	18900	5258	933
228	18208	5013	1296	264	10250	2488	648
229	20303	3780	875	265	11235	2432	724
230	28091	8081	1780	266	7583	2373	866
231	19245	5741	1478	267	10292	2360	656
232	20980	4858	1466	268	19921	5203	1528
233	22283	3416	1006	269	10535	1778	529
234	16874	6426	751	270	9378	2329	791
235	23265	8184	1729	271	9478	2277	681
236	12999	4563	1072	272	8142	2249	807
237	26992	11101	3069	273	8328	2353	815
238	21541	6601	1684	274	8363	1549	416
239	20176	6444	1328	275	12232	2803	746
240	31301	9339	1859	276	7872	1826	497
241	23741	8551	2415	277	10887	2945	885
242	25875	7637	1585	278	16920	5112	1063
243	21168	8831	2556	279	10857	3522	1223

Table B.2 Resilient Modulus Predicted for Witczak Database

Mixture #	Temperature (°C)			Mixture #	Temperature (°C)		
	5	25	40		5	25	40
280	13339	4692	1550	316	21480	6017	1731
281	11914	2168	664	317	14550	4367	1169
282	24020	7706	1777	318	12592	3605	998
283	14408	4311	1062	319	5892	1415	429
284	23763	8466	2287	320	22878	7993	2456
285	22274	14335	6864	321	18620	3060	680
286	23561	15596	7291	322	21980	4439	966
287	24525	24516	24512	323	22233	3926	976
288	29712	15410	5195	324	22302	5504	1123
289	30060	17791	8463	325	21527	5904	1373
290	19678	8153	2793	326	16287	6252	2209
291	18526	4082	696	327	22422	8151	2330
292	17046	7824	2180	328	24920	5619	1408
293	13514	4663	1438	329	22270	5391	1235
294	33876	8476	1866	330	31597	6287	1509
295	23833	10550	2822	331	23104	8587	2625
296	21488	6985	2431	332	11801	5552.7	1638.8
297	18670	3726	834	333	12884	10759	796.72
298	22812	5222	1101	334	13482	11824	744.52
299	18067	4303	1325	335	11594	5060.8	1575.3
300	17413	4523	1330	336	11526	5323.6	1623.6
301	27239	5938	1264	337	21069	5456.1	1308.6
302	18132	5136	1203	338	17146	3576.5	396.96
303	19183	7231	2574	339	13553	5647.4	1334.7
304	24643	11399	4568	340	21139	5298.8	1292.8
305	16848	2469	583	341	21193	5620.6	1384.6
306	18458	4110	921	342	12844	2369.7	571.67
307	19663	5022	1241	343	17193	6358.2	1593.9
308	21331	6341	1489	344	11085	2735.6	601.26
309	18957	4447	996	345	13285	2493	601.35
310	20596	6303	1929	346	12684	2464.2	633.3
311	4833	1392	536				
312	5480	1415	433				
313	19721	7585	2067				
314	20659	6618	1688				
315	11334	4373	1471				